UNIV RSITY OF R ADING
D PARTM NT OF MATH MATICS

THE USE OF ROBUST OBSERVERS IN THE SIMULATION OF GAS SUPPLY NETWORKS

by

SIMON M. STRING R

This thesis is submitted for the degree of
Doctor of Philosophy

NOV MB R 1993

For any gas network, it is desirable to have a reasonable estimate of the demand flows. However, flow meters are much more expensive than pressure sensors to install, and so it would be economical to be able to estimate the flow demands from pressure measurements alone. In this thesis, both model and observer based methods for estimating unmeasured flow demands in linear gas networks with sparse pressure telemetry are investigated.

Firstly, we introduce the basic gas network model in the form of a linear time invariant descriptor system, which requires the upstream pressure and all flow demands as inputs. Thus the basic model is useless for estimating the flow demands since these are needed to drive the model. Hence, we proceed to derive rearranged and augmented gas network models that contain the flow demands in their state vectors, and that are capable of flow demand estimation.

Acknowledgements

I would like to thank my academic supervisor, Dr Nancy Nichols, for my introduction to the mathematics of the real world; and thank British Gas for giving me the opportunity to work on such an interesting practical problem. I would also like to thank my industrial supervisors, Dr John Piggott, Dr Alan Lowdon, Dr Jim Mallinson and Mr Michael Gardiner, for their encouragement during my three years at Reading.

Finally, I would like to acknowledge both the Science and ngineering Research Council and British Gas for their financial support for the period of my studies.

Ch pter 1

Introduction

For any gas network, it is desirable to have a reasonable estimate of the demand flows. However, flow meters are much more expensive than pressure sensors to install, and so it would be economical to be able to estimate the flow demands from pressure measurements alone. In this thesis, both model and observer based methods for estimating unmeasured flow demands in linear gas networks with sparse pressure telemetry are investigated. Two techniques for constructing *robust* observers are employed: robust eigenstructure assignment [24], [25], and singular value assignment [34], [4].

The gas networks considered are linear and consist of a number of pipe sections with a gas source at the upstream end and flow demands at pipe junctions and at the downstream end. For example, for a three pipe network we would have

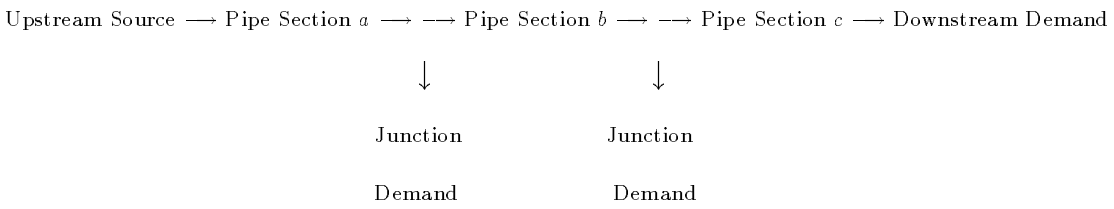

We assume the only measurements of the real gas network available are discrete pressure measurements at all sites of gas inflow (the upstream end) and outflow (the pipe junctions and downstream end). These measurement sites are the natural 'boundaries' of the network, where some data (pressure or flow demand) need to be specified to drive a network model.

In chapter 2 we introduce the basic gas network model from [34], based on two partial differential equations for modelling natural gas flow in high pressure pipelines, derived by mass and momentum balance arguments [19], [30]. Such a model, which we denote by 0, is in the form of a linear time invariant descriptor system

$$\_(\ +1) = \quad \_(\ ) + \quad \_(\ +1) + \quad \_(\ )$$

which results from linearising the original differential equations about a steady state and discretising the linearised equations using the -method [37]. All pressure and flow variables are thus perturbations away from that steady state. An 0 model requires the upstream pressure and all flow demands as inputs; thus an 0 model is useless for estimating the flow demands since these are needed to drive the model. Hence, we

trivial difference equations of the form

$$=$$

Obviously, if such a model were run, the estimates of the flow demands would not change. However, if the flow demands change slowly with time, then observers constructed upon such models can track the flow demands fairly well; although the above difference equation for the flows will contain some modelling error. Such trivial difference equations have been used previously for both leak detection [3] and state estimation [32]. xperimental and theoretical evidence is given to show how the two techniques, robust eigenstructure assignment and singular value assignment, reduce the effects of the above modelling error upon the observer state estimate. The 3 model is further developed by making use of the known time profiles for the flow demands to remove the modelling error introduced by the above trivial difference equations. The new trivial difference equations for the flow demands become

$$= \quad +$$

where the may be estimated from the telemetry from other demand flows.

$$-$$

$$- \qquad - \qquad -$$

$$-$$

to perturbations in the pressures. In chapter 9 a standard approach from [34] is explored but shown to be inadequate without a new approach to encoding information about the flow demand time profiles. We investigate a further model variation, denoted by 4, capable of estimating both flow demands and pressure measurement bias, but which uses trivial difference equations for the flow demands of the form

$$_{k+1} =$$

where the are estimated from other measured flow demands. This new way of incorporating information about the flow profiles allows the estimation of the measurement biases, as well as the flow demands themselves. However, the 4 models have time-varying system matrices and basic control theory for time-invariant systems does not always extend to time-varying systems [41], [26], [6], [7]. Our observer designs must also be modified [15].

In chapter 10 we examine the problem of measurement white noise. We avoid Kalman filters due to their unexceptional performance in [17], [40], [35], and instead examine two simple smoothing techniques, and derive two final model variations, 5 and 6, to deal with the problem of the sensitivity of the flow demand estimates. 5 and 6 models have only a single total flow demand perturbation state variable that is the sum of all the individual demand flow perturbation variables. Such models are less sensitive to pressure measurement noise.

Finally, in chapter 11 we make some final conclusions and suggest some proposals for future work.

Ch pter 2

he St nd rd System Model ($\mathcal{M}0$)

In this chapter, the standard underlying model, based directly on [34], is constructed for a simple linear network with demand flows. This initial model, which we denote as an $\mathcal{M}0$ model, actually assumes that all flow demands are measured and used as inputs to drive the model. Hence, obviously an $\mathcal{M}0$ model, itself, cannot be used for flow demand estimation.

2.1 The Linearised Differential Equations Governing Gas Pipe Dynamics

Firstly, we derive the linearised equations governing gas dynamics in a single section of pipe. For each section, from [34], we have the following two equations

$$_x(P^2) + \epsilon_1(1 - \tau P)Q|Q|^{\alpha-1} = 0, \tag{2.1}$$

the momentum balance equation ignoring time variations in Q, and

$$_t(P) + \epsilon_2(1 - \tau P)^2 \quad _x(Q) = 0, \tag{2.2}$$

the mass balance equation, where:

$P(x,t)$ is the gas pressure in bar

$Q(x,t)$ is the mass flow rate in m.s.c.m.h. (millions of standard cubic metres per hour)

x is distance along pipe in metres

is time in hours

are constants, and , are partial derivatives with respect to x and t respectively. is used in the linear expression for compressibility, = 1 , which is always positive.

We begin by modelling a straight section of pipe of length , with constant cross-sectional area.

For computational ease, we normalise the pipe section length, pressure and mass flow rate:

(2 3)

where and are positive constants which are chosen such that 1 The normalisation results in

(1) ( ) ( ) ( ) ( ) (2 4)

The normalised equations (2.1) and (2.2) are, therefore, to be solved for 0 1 and 0. The boundary and initial conditions are yet to be specified.

Our approach is to linearise about a mass flow rate and pressure profile in order to obtain two linear equations which approximate equations (2.1) and (2.2). Our mass flow rate and pressure profile are

( ) = (2 5)

( ) = ( ) (2 6)

where is a positive constant mass flow rate from = 0 to = 1, and ( ) is the constant pressure profile.

Substituting (2.5) and (2.6) into equation (2.1) gives

( ) + (1) = 0

which is equivalent to

The following boundary data are required at the ends of the pipe section:
at $x = 0$ we require

$$p(0,t) = P(0,t) - \mathcal{P}(0),$$

or

$$q(0,t) = -\epsilon_3 \quad _x(\Gamma p) \mid_{x=0} = Q(0,t) - \mathcal{Q},$$

and at $x = 1$, we require

$$p(1,t) = P(1,t) - \mathcal{P}(1),$$

or

$$q(1,t) = -\epsilon_3 \quad _x(\Gamma p) \mid_{x=1} = Q(1,t) - \mathcal{Q}.$$

2.2 The Finite Difference Approximation

ach of the pipe sections have nodes at either end and a number of regularly spaced internal nodes. For an arbitrary pipe section with $s+1$ nodes, we have

Nodes: 0—1—2—3.....s

←————Pipe section————→

Firstly, we introduce some notation. For any pipe section with $s+1$ nodes, we let our numerical approximations be

$$p_{i,k} \approx p(i\delta x, k\delta t),\ q_{i,k} \approx q(i\delta x, k\delta t),\ \Gamma_i \approx \Gamma(\mathcal{P}(i\delta x)),\ \Omega_i \approx \Omega(\mathcal{P}(i\delta x)),$$

where i = 0,1,2,3,....,s, δx is the spatial discretisation interval of the pipe and δt is the sample period with k=0,1,2,...

In our numerical model, we use a finite difference scheme based on the nodal *pressure perturbations only*; the perturbations in inline flows can then be calculated separately

from the computed pressure perturbation profile using a difference approximation based

For boundary conditions given at node in a general pipe section, we use the following theory.

Using equation (2.13) we derive the finite difference equation

$$(\Gamma \qquad \Gamma \qquad) = 2 \qquad (2\ 18)$$

for the boundary flow condition at the node = for any pipe section. From [37], approximating the derivative (Γ) by

$$(\Gamma\ )\ \ (\Gamma \qquad \Gamma \qquad)\ 2$$

involves a leading error on the right hand side of order ( ) . liminating Γ and Γ between equation (2.17), with = , equation gene9Γ finit9Γ differenc9Γ 7O6S8),

particular pipe sections.

Regarding the initial linearisation procedure, we linearise about different inline flows for all pipe sections. Hence, for our linear network, we linearise about a steady state where the flow demands at the junctions are not zero. In practice, a value for the steady flow, $\mathcal{Q}^z$, in each pipe section z may be suggested by, say, substituting the values of the pressure measurements at the opposite ends of the pipe section into equation (2.8) and solving for $\mathcal{Q}^z$. It may be the case that we have to make a best guess for a value for $\mathcal{Q}^z$.

Firstly, we use equation (2.8) to linearise for the upstream section (i.e. section a for the example network) by substituting in an assumed steady value for the inline flow, $\mathcal{Q}^{upstream\ section}$, and a value for $\mathcal{P}^{upstream\ section}(0)$, and generating a steady pressure profile using an iterative technique such as Newton's. In practice, a value for $\mathcal{P}^{upstream\ section}(0)$ is suggested by the upstream pressure measurement of that section.

Next, the same procedure is carried out for neighbouring sections downstream in turn, using different steady inline flows, $\mathcal{Q}^z$, for linearising each general pipe z, and using the calculated value for $\mathcal{P}^{z-1}(1)$ from the adjacent upstream section as the value for $\mathcal{P}^z(0)$ each time.

This means that at each pipe section junction we are linearising about a steady demand flow

$$\mathcal{Q}^{z/z+1} = \mathcal{Q}^z - \mathcal{Q}^{z+1}$$

where $\mathcal{Q}^z$ is the steady flow we linearised about in the upstream section z, and $\mathcal{Q}^{z+1}$ is the steady flow we linearised about in the downstream section $z+1$.

Now we examine how to link up the separate finite difference schemes for two general adjacent pipe sections, z and $z+1$, in a linear network. Pipe sections z and $z+1$ have, say, s^z+1 and $s^{z+1}+1$ nodes respectively (although one of these nodes is shared by both pipe sections).

Nodes: 0^z——1^z——2^z——3^z.....$(s^z)^z/0^{z+1}$——1^{z+1}——2^{z+1}——3^{z+1}.....$(s^{z+1})^{z+1}$

←————Section z————→ ←————Section $z+1$————→

For our 'internal boundary node' ( ) 0 , we derive a finite difference equation that links up the finite difference equations for the two pipe sections on either side, and +1.

We assume that at time level , we have a normalised flow demand, , out of the pipe junction, +1, where

$$= \quad +$$

is the demand flow out of the pipe junction +1 chosen for the linearisation, and is a perturbation away from that steady demand flow. Then to enforce continuity of mass flow at node ( ) 0 , we require

$$[\quad +(1 \quad) \quad]+[\quad +(1 \quad) \quad]+[\quad +(1 \quad) \quad]=0 \quad (2\ 22)$$

Rearranging both equation (2.19) for pipe and equation (2.21) for pipe +1, for etc., and substituting into equation (2.22) gives us the following finite difference equation for our internal boundary node ( ) 0 .

where we have defined

$$\Phi \quad = (\frac{}{2 \quad \Omega} + \frac{}{2 \quad \Omega})$$

and where, because and Γ Γ , at the junction we have denoted the pressure perturbation by , and denoted Γ by Γ Γ Γ . This equation is our 'connectivity equation', which is the actual finite difference equation we use

$$
\begin{bmatrix} & \\ & \end{bmatrix}
$$

$$
\begin{bmatrix} & \\ & \end{bmatrix}
$$

$$
= \begin{bmatrix} & & & \\ & \ddots & & \\ & & & \\ & & & \end{bmatrix}
$$

$$
\begin{bmatrix} & \\ & \end{bmatrix}
$$

$$
\begin{bmatrix} & \\ & \end{bmatrix}
$$

$$
[A\ ]
$$

$$
[A\ ]
$$

$$
= \begin{bmatrix} & & & \\ & \ddots & & \\ & & & \\ & & & \end{bmatrix}
$$

$$
[A\ \ ]
$$

$$
[A\ ]
$$

where [ ] and [A] are general tridiagonal square blocks containing the coefficients of the inner pressures along pipe from difference equations (2.17). The blocks, [ ] and [A], are sandwiched between single rows corresponding to the 1 connectivity equations (2.23) and downstream flow boundary equation (2.19) for pipe , and single columns containing the coefficients of the pressures at the pipe junctions and the downstream end. These rows and columns maintain the tridiagonal structure of and ; the non-zero

and in the matrix has the form

The row corresponding to the flow boundary equation (2.19) at the downstream end, in the matrix has the form

and in the matrix has the form

In this section, we firstly prove that the matrix of an 0 model is full rank if 0. We next prove that the 0 system eigenvalues are real if 0. Lastly, we prove that the 0 system eigenvalues are within the unit circle for 1 2 1.

All theorems rely on the following inequalities. Γ 0, Γ 0, 0, 0, 0, 0, Ω 0, 0 and Φ 0 for all pipes, nodes and junctions.

We firstly define three new matrices.

We define the diagonal matrix, , where the diagonal element of is equal to the value of Γ at the node along the linear gas network (starting at node 1 of the

Next, for $\theta \neq 0$, let the matrix $M = -(1/\theta)(I - E)$. Then it can be easily verified that

$$E = I + \theta M \tag{2.26}$$

and

$$A = I - (1 - \theta)M . \tag{2.27}$$

By inspection, M is real and tridiagonal, with all off-diagonal elements, m with $|i - j| = 1$, non-zero and negative. Hence, from Theorem 12.3 in the appendix, all the eigenvalues of M are real.

Lastly, let $G = M$. By inspection, G has the following properties:

- tridiagonal
- diagonally dominant with strict inequality at $i = 1$
- $g > 0$, $g < 0$ for all i and j with $|i - j| = 1$.

From Theorem 12.1 in the appendix, we have that G is full rank.

$\theta > 0$ E $\mathcal{M}0$

Let = . Assuming 0, we can derive = + , which, due to the properties of and , must be strictly diagonally dominant. Hence, from Theorem 12.2 in the appendix, is full rank, and hence = must be full rank also.

0 $\mathcal{M}0$

Since, if 0, the matrix is invertible, from equations (2.26), (2.27), we have

$$(-) = 0 \iff ((+) (- (1 -)) -) = 0$$

Thus, for $\in$ ( ) and $\in$ ( ), for = 1 ,

$$= \frac{1 - (1 -)}{1 + }$$

where $\lambda(A_0, E_0)$ denotes the spectrum of the matrix $E_0{}^1A_0$ and $\lambda(M_0)$ denotes the spectrum of the matrix M_0. Hence, since the eigenvalues, τ_i, of M_0 are real then so are the eigenvalues, μ_i, of $(E_0{}^1A_0)$ real.

$\mathcal{M}0$

$(1/2)\leq\theta\leq 1$

From equations (2.26), (2.27), we have

$$det(A_0 - \mu E_0) = det((1-\mu)I + ((1-\mu)\theta - 1)M_0). \tag{2.28}$$

Since the determinant of the product of two matrices is equal to the product of the determinants of the individual matrices, from equation (2.28) we can derive

$$det(A_0 - \mu E_0) = det((1-\mu) \quad {}_0{}^1 + ((1-\mu)\theta - 1)G_0)det(\quad {}_0).$$

We show $det(A_0 - \mu E_0)\neq 0$ for $|\mu|\geq 1$ and $(1/2)\leq\theta\leq 1$.

The matrix $\quad {}_0$ is full rank, and hence $det(\quad {}_0)\neq 0$.

By inspection, if $\mu\geq 1$, then $(1-\mu)\leq 0$ and $((1-\mu)\theta - 1)\leq -1$. Also, if $\mu\leq -1$, then $(1-\mu)\geq 2$ and $((1-\mu)\theta - 1)\geq 0$.

So, for $|\mu|\geq 1$, we have the following two cases.

If $((1-\mu)\theta - 1) = 0$ then $(1-\mu)\geq 2$ and $((1-\mu) \quad {}_0{}^1 + ((1-\mu)\theta - 1)G\ ) = (1-\mu)$ which is full rank. Then $det((1-\mu) \quad + ((1-\mu)\theta - 1)G\ )\neq 0$.

If $((1-\mu)\theta - 1)\neq 0$ then, due to the properties of and G, the matrix $((1-\mu) \quad + ((1-\mu)\theta - 1)G\ )$ has the following properties

- tridiagonal
- diagonally dominant with strict inequality for $i = 1$
- off-diagonal elements with $|i-j| = 1$ are non-zero and of opposite sign to diagonal elements.

and, from Theorem 12.1 in the appendix, is full rank.

Then $det((1-\mu)\ \ _0^{-1} + ((1-\mu)\theta - 1)G_0) \neq 0$.

Hence, for $|\mu| \geq 1$, $det(A_0 - \mu E_0) = det((1-\mu)\ \ _0^{-1} + ((1-\mu)\theta - 1)G_0)det(\ \ _0) \neq 0$.

Thus, if $(1/2) \leq \theta \leq 1$, the eigenvalues of the $\mathcal{M}0$ system matrices have modulus less than 1, and the $\mathcal{M}0$ model is asymptotically stable. □

The *Lax stability* [37] of the $\mathcal{M}0$ model is defined in terms of the boundedness of the solution to the finite difference equations at a fixed timestep, T, as δt and δx tend to zero with $r = \delta t/(\delta x)^2$ kept fixed. It is related via Lax's quivalence Theorem [37] to the convergence of the solution of the $\mathcal{M}0$ system to the solution of the governing differential equations (2.16), as the computational mesh is refined. However, unlike the asymptotic, or Liapunov, stability already investigated above, Lax stability is not directly dependent on the eigenvalues of the system. Some attempt was made to provide proofs of both the Lax stability of the $\mathcal{M}0$ system and the convergence of the solution of the $\mathcal{M}0$ system to the solution of the governing differential equations (2.16), as the computational mesh was refined. Unfortunately, this was not achieved, the difficulty being the space-varying nature of the system coefficients. Two good references that deal with this specific problem are [36] and [16]. Providing such stability and convergence proofs for $\mathcal{M}0$ systems and all other systemsorednsouldeorthwhile of future research.

Hoever,erimentally, the solution of the 0 m$\mathcal{M}$del was found to be convergent, for both $\theta = 1/$and $\#\ 1$, as the computational mesh was refined with $\neq 0\ 6666$ for all pipes.

This base $\mathcal{M}0$ model has also been tested thoroughly in [34] with real gas network data, and was found to model the behaviour of real gas networks quite accurately.

Chapter 3

Formulation of a New $\mathcal{M}1$ Variant Model

The gas networks we wish to estimate are linear with pressure measurement only; and these measurements are only available at the upstream source and at sites of flow demand. We now show how a new model variation, denoted by $\mathcal{M}1$, which is capable of estimating flow demands, may be constructed from a base $\mathcal{M}0$ model. The $\mathcal{M}1$ model is simply a pressure driven model, and is derived from an $\mathcal{M}0$ model by first removing the $g-1$ connectivity equations and the downstream flow boundary equation from the system, and then removing the g flow demand variables. The $\mathcal{M}1$ model is still in the form of a discrete descriptor system, but where the state vector now contains the nodal pressures *except* those pressures at sites of gas outflow. The $\mathcal{M}1$ model is essentially a disconnected set of equations for each pipe.

The base $\mathcal{M}0$ model can be rearranged and partitioned as

$$\begin{bmatrix} \mathcal{E}_{1,1} & \mathcal{E}_{1,2} \\ \mathcal{E}_{2,1} & \mathcal{E}_{2,2} \end{bmatrix} \begin{bmatrix} \underline{p}_1(k+1) \\ \underline{p}_2(k+1) \end{bmatrix} = \begin{bmatrix} \mathcal{A}_{1,1} & \mathcal{A}_{1,2} \\ \mathcal{A}_{2,1} & \mathcal{A}_{2,2} \end{bmatrix} \begin{bmatrix} \underline{p}_1(k) \\ \underline{p}_2(k) \end{bmatrix} + \begin{bmatrix} \mathcal{B}^1_{1,1} & 0 \\ 0 & \mathcal{B}^1_{2,2} \end{bmatrix} \begin{bmatrix} \underline{p}_3(k+1) \\ \underline{d}(k+1) \end{bmatrix} + \begin{bmatrix} \mathcal{B}^2_{1,1} & 0 \\ 0 & \mathcal{B}^2_{2,2} \end{bmatrix} \begin{bmatrix} \underline{p}_3(k) \\ \underline{d}(k) \end{bmatrix}, \tag{3.1}$$

where $\underline{p}_2(k)$ is a g dimensional vector containing measured pressure perturbation state variables at the sites of flow demand, $\underline{p}_1(k)$ is a $n-g$ dimensional vector containing the remaining pressure perturbation state variables along the pipes, $\underline{p}_3(k)$ is the upstream

pressure input (assumed known), and $\underline{d}(k)$ is a g dimensional vector containing the flow demand perturbation input variables that we wish to estimate. The top $n-g$ rows correspond to general difference equations (2.17), and the lower g rows correspond to the $g-1$ connectivity equations and the single downstream flow boundary equation.

The new $\mathcal{M}1$ system has the form

$$\mathcal{E}_{1,1}\underline{p}_1(k+1) = \mathcal{A}_{1,1}\underline{p}_1(k) - \mathcal{E}_{1,2}\underline{p}_2(k+1) + \mathcal{B}^1_{1,1}\underline{p}_3(k+1) + \mathcal{A}_{1,2}\underline{p}_2(k) + \mathcal{B}^2_{1,1}\underline{p}_3(k) \quad (3.2)$$

which can be expressed in the general descriptor system form

$$E_1\underline{x}_1(k+1) = A_1\underline{x}_1(k) + B^1_1\underline{u}_1(k+1) + B^2_1\underline{u}_1(k) \quad (3.3)$$

where

$$\underline{u}_1(k) = [\underline{p}_3(k)^T, \underline{p}_2(k)^T]^T.$$

If we arrange the pressure variables in the state vector in their order along the pipe network, i.e. in the following way

$$\underline{x}_1(k) = [p^1_{1,k}, p^1_{2,k}, ..., p^1_{s^1-1,k}, p^2_{1,k}, p^2_{2,k}, ..., p^2_{s^2-1,k}, ..., p^g_{1,k}, p^g_{2,k}...., p^g_{s^g-1,k}]^T,$$

where each pipe has $s^{pipe}+1$ nodes, then the $\mathcal{M}1$ system matrices, E_1 and A_1, are tridiagonal. E_1 and A_1 take the form

$$E_1 = \begin{bmatrix} [\mathrm{E}^1] & & & & \\ & [\mathrm{E}^2] & & & \\ & & \ddots & & \\ & & & [\mathrm{E}^{g-1}] & \\ & & & & [\mathrm{E}^g] \end{bmatrix}$$

$$A_1 = \begin{bmatrix} [\mathrm{A}^1] & & & & \\ & [\mathrm{A}^2] & & & \\ & & \ddots & & \\ & & & [\mathrm{A}^{g-1}] & \\ & & & & [\mathrm{A}^g] \end{bmatrix}$$

where $[E^z]$ and $[A^z]$ are general tridiagonal square blocks containing the coefficients of the inner pressures along pipe z from difference equations (2.17). The general square blocks $[E^z]$ and $[A^z]$ are as previously described for the $\mathcal{M}0$ model.

As an $\mathcal{M}$

pipes, nodes and junctions.

We firstly define three new types of matrix.

We define the general diagonal matrix, D^z, corresponding to pipe z for $z = 1$

For a general pipe section z, let $\mathrm{F}^z = \mathrm{E}^z\mathrm{D}^{z^{-1}}$. Assuming $\theta > 0$, we can derive $\mathrm{F}^z = \mathrm{D}^{z^{-1}} + \theta\mathrm{G}^z$, which, due to the properties of D^z and G^z, must be strictly diagonally dominant. Hence, from Theorem 12.2 in the appendix, F^z is full rank, and hence $\mathrm{E}^z = \mathrm{F}^z\mathrm{D}^z$ must be full rank also. □

Theorem 3.2 *If $\theta > 0$, the eigenvalues of an $\mathcal{M}1$ model are real.*

Proof

To show the eigenvalues of an $\mathcal{M}1$ model are real, we show the eigenvalues of the blocks $\mathrm{E}^{z^{-1}}\mathrm{A}^z$ are real.

For a general pipe section z, since the matrix E^z is invertible if $\theta > 0$, from equations (3.7), (3.8), we have

$$det(\mathrm{A}^z - \mu\mathrm{E}^z) = 0 \Longleftrightarrow det((I + \theta\mathrm{M}^z)^{-1}(I - (1-\theta)\mathrm{M}^z) - \mu I) = 0.$$

Thus, for $\mu_i \in \lambda(\mathrm{A}^z, \mathrm{E}^z)$ and $\tau_i \in \lambda(\mathrm{M}^z)$, for $i = 1, ..., s^z - 1$,

$$\mu_i = \frac{1 - (1-\theta)\tau_i}{1 + \theta\tau_i}.$$

Hence, since the eigenvalues, τ_i, of M^z are real then so are the eigenvalues, μ_i, of $(\mathrm{E}^{z^{-1}}\mathrm{A}^z)$ real. □

Theorem 3.3 *An $\mathcal{M}1$ model has system eigenvalues within the unit circle, and hence is asymptotically stable, if $(1/2) \leq \theta \leq 1$.*

Proof

To show the eigenvalues of an $\mathcal{M}1$ model are within the unit circle, we show the eigenvalues of the blocks $\mathrm{E}^{z^{-1}}\mathrm{A}^z$ are within the unit circle.

For a general pipe section z, from equations (3.7), (3.8), we have

$$det(\mathrm{A}^z - \mu\mathrm{E}^z) = det((1-\mu)I + ((1-\mu)\theta - 1)\mathrm{M}^z). \tag{3.9}$$

Since the determinant of the product of two matrices is equal to the product of the determinants of the individual matrices, from equation (3.9) we can derive

$$det(\mathrm{A}^z - \mu \mathrm{E}^z) = det((1-\mu)\mathrm{D}^{z^{-1}} + ((1-\mu)\theta - 1)\mathrm{G}^z) det(\mathrm{D}^z).$$

We show $det(\mathrm{A}^z - \mu \mathrm{E}^z) \neq 0$ for $|\mu| \geq 1$ and $(1/2) \leq \theta \leq 1$.

The matrix D^z is full rank, and hence $det(\mathrm{D}^z) \neq 0$.

By inspection, if $\mu \geq 1$, then $(1-\mu) \leq 0$ and $((1-\mu)\theta - 1) \leq -1$. Also, if $\mu \leq$ Tmc(-;Tj1;TD(denTjTD

3.2 Experiments

For all experiments in this thesis, a standard $\mathcal{M}0$ model of the linear three pipe network from chapter 1, was run to simulate a real gas network with the upstream pressure, junction demand flows, and downstream flow demand specified as boundary inputs to the system. The parameters for this base $\mathcal{M}0$ model, and all other models investigated in this thesis, are given in the appendix. Except for a few experiments in chapter 10, the flows at demand sites A/B, B/C and C were in the ratio 2:5:13.

When the $\mathcal{M}0$ model had been running for a while, the pressures at the upstream end and the sites of flow demand were recorded at each timestep and fed into an $\mathcal{M}1$ model. The flow demands predicted by the $\mathcal{M}1$ model were then compared with the true flows used as inputs to the $\mathcal{M}0$ model. For experiments 3.1 to 3.3, the $\mathcal{M}0$ model simulating a gas network was identical to the $\mathcal{M}0$ model upon which the $\mathcal{M}1$ model was constructed. For experiments 3.4 and 3.5, the $\mathcal{M}0$ model simulating a gas network had a much finer discretisation (in both space and time) than the $\mathcal{M}1$ model to give some idea of the effects of the modelling error due to the finite difference approximation of the original differential equations.

For each experiment, the true flow demand profiles for the demands, $D_k^{A/B}$, $D_k^{B/C}$ and D_k^C are shown as thick lines in Figs. A, B and C respectively, and the state estimates for $D_k^{A/B}$, $D_k^{B/C}$ and D_k^C are shown as thin lines. The percentage errors between the state estimates of $D_k^{A/B}$, $D_k^{B/C}$ and D_k^C and their true values are shown in Figs. D, E and F respectively.

Experiment 3.3) $\mathcal{M}1$ Model with $\theta = 0.5$

Data taken from $\mathcal{M}0$ model with much finer mesh - $\mathcal{M}1$ model has 5 spatial nodes along each pipe.

Experiment 3.4) $\mathcal{M}1$ Model with $\theta = 1$

Data taken from $\mathcal{M}0$ model with much finer mesh - $\mathcal{M}1$ model has 10 spatial nodes along each pipe.

Experiment 3.5) $\mathcal{M}1$ Model with $\theta = 1$

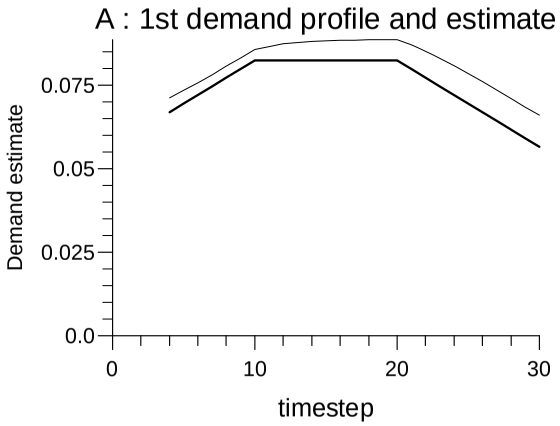
A : 1st demand profile and estimate
Demand estimate
0.075
0.05
0.025
0.0
0
10
20
30
timestep

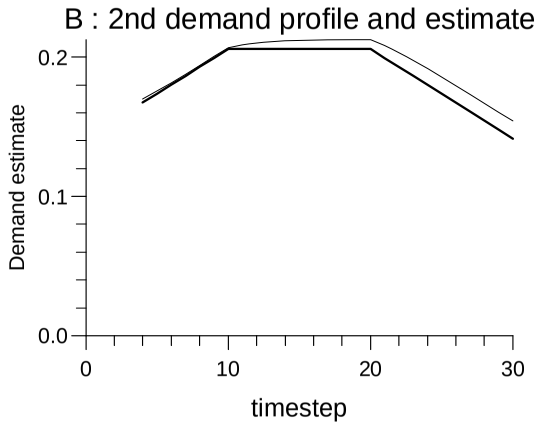
B : 2nd demand profile and estimate
Demand estimate
0.2
0.1
0.0
0
10
20
30
timestep

Experiment 3.2

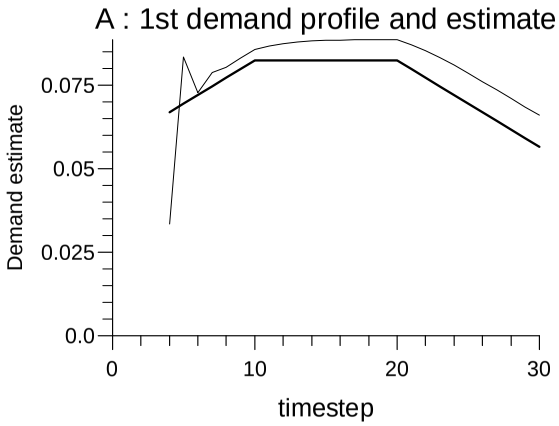

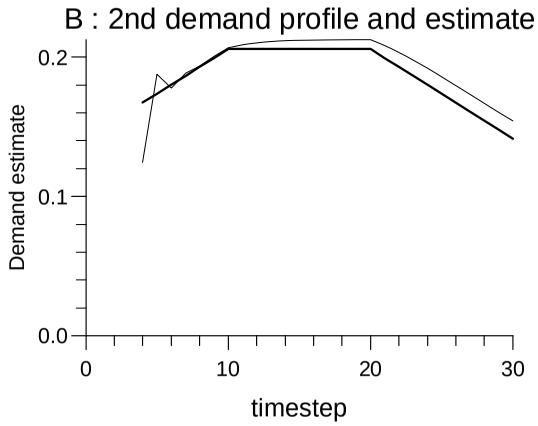

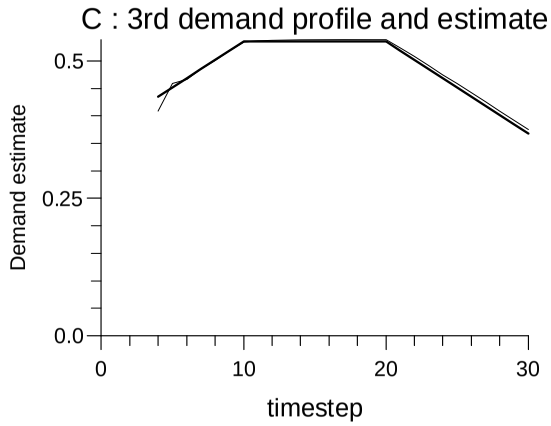

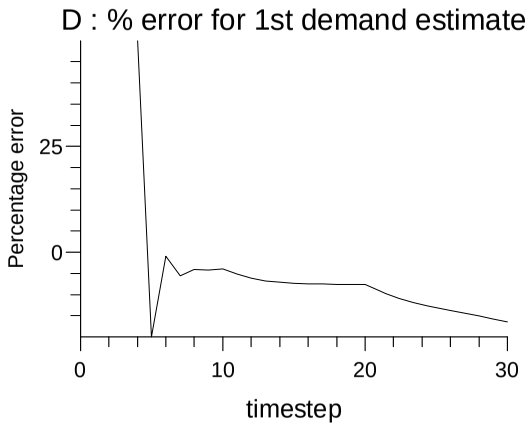

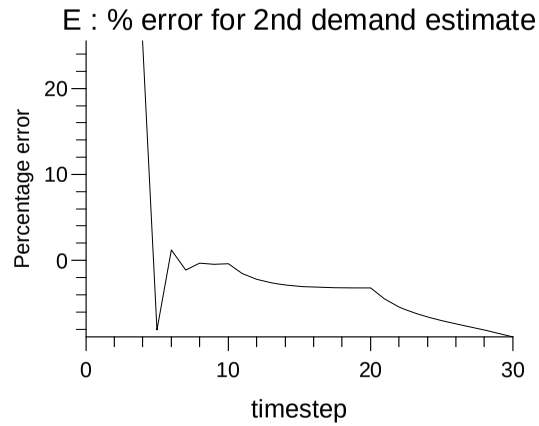

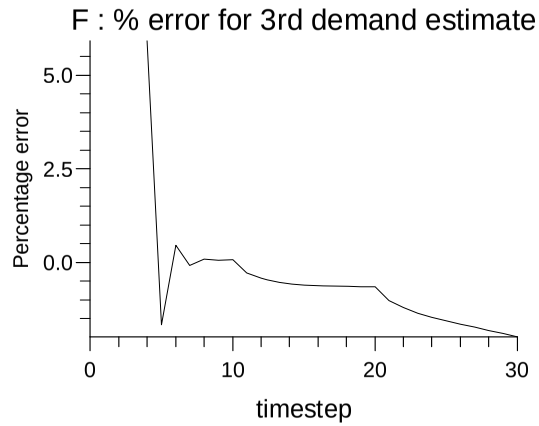

Experiment 3.3

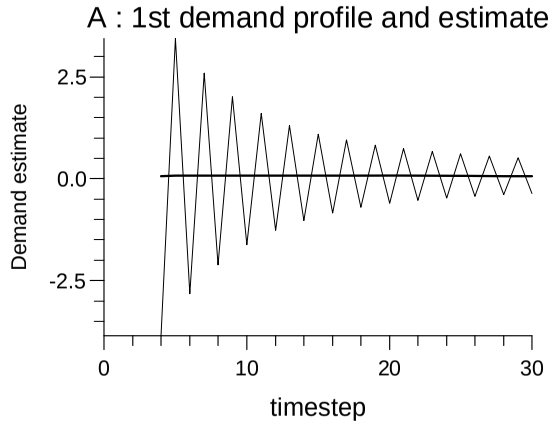

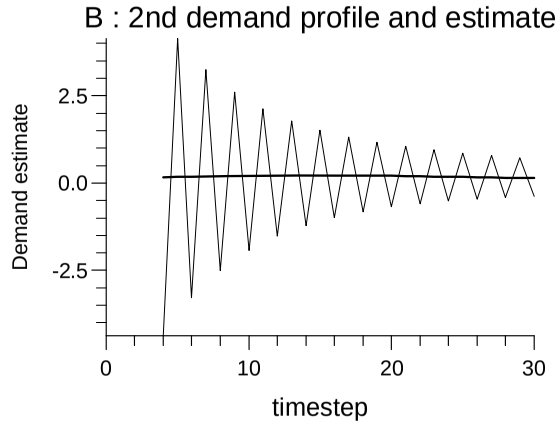

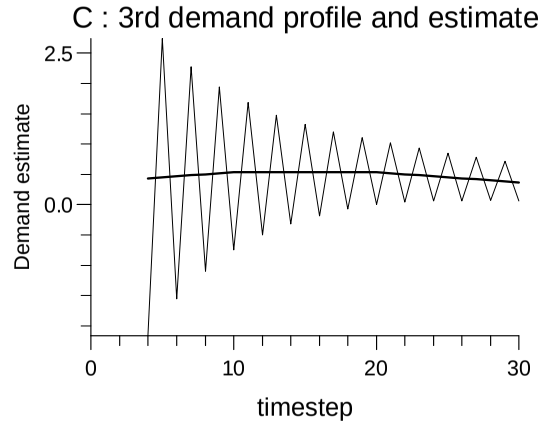

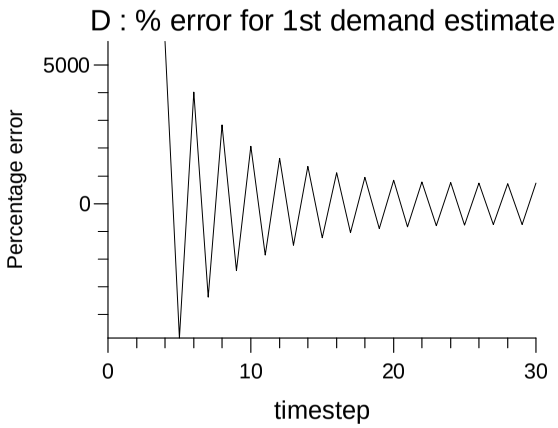

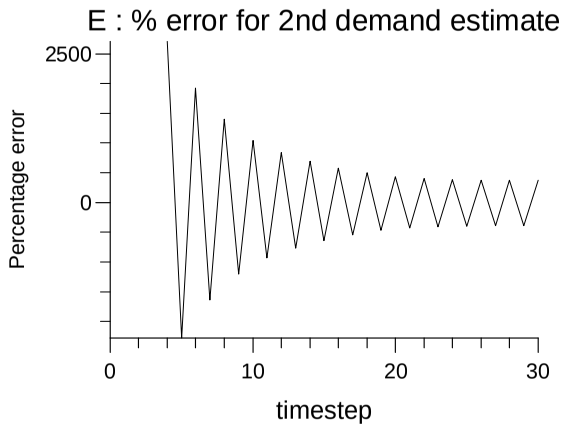

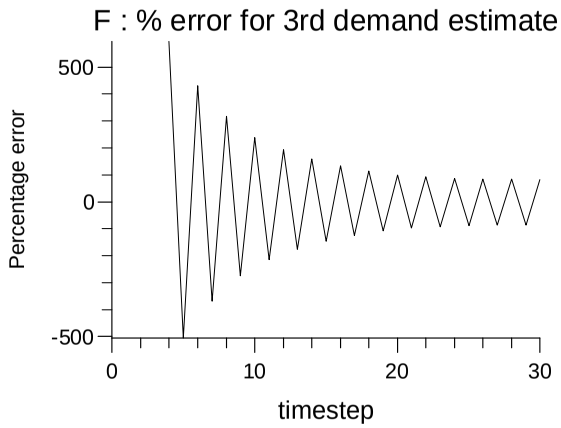

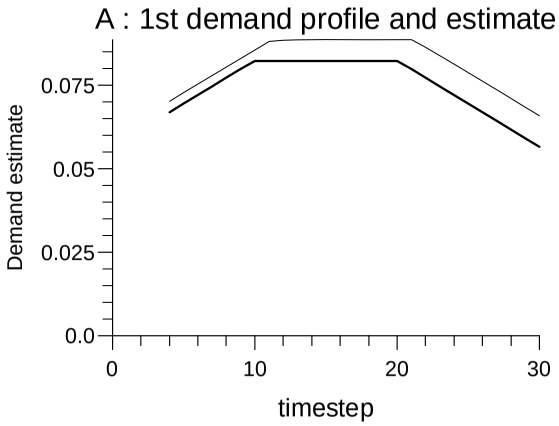
A : 1st demand profile and estimate
Demand estimate
0.075
0.05
0.025
0.0
0
10
20
30
timestep

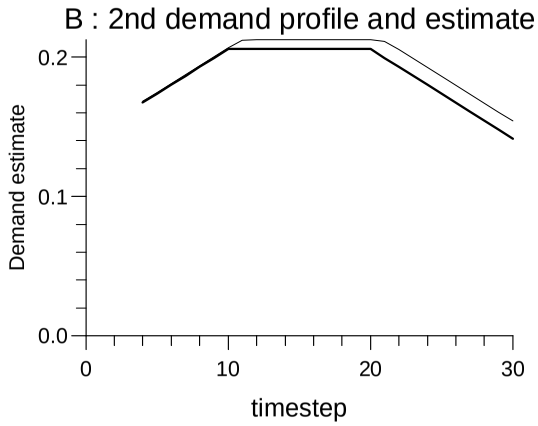
B : 2nd demand profile and estimate
Demand estimate
0.2
0.1
0.0
0
10
20
30
timestep

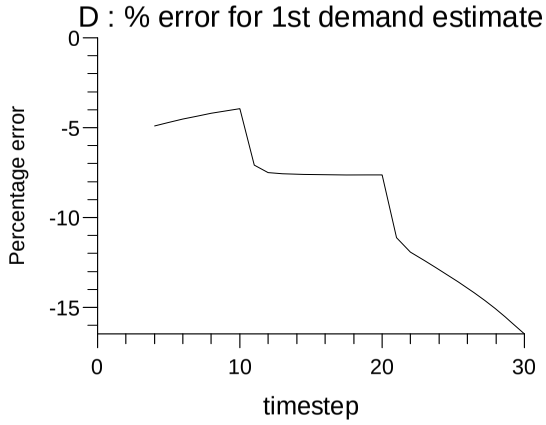
D : % error for 1st demand estimate
Percentage error
0
-5
-10
-15
0
10
20
30
timestep

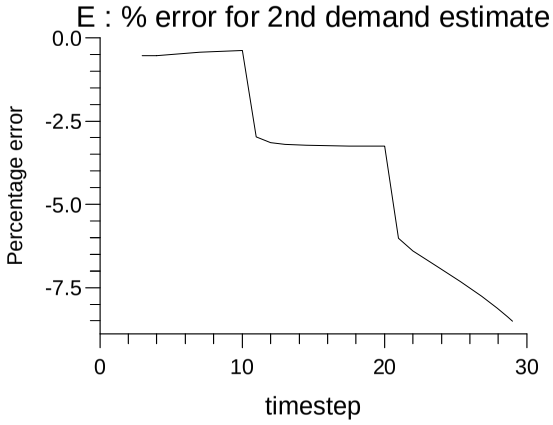
E : % error for 2nd demand estimate
Percentage error
0.0
-2.5
-5.0
-7.5
0
10
20
30
timestep

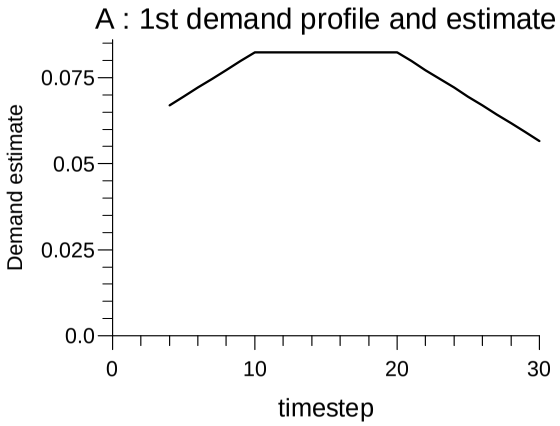
A : 1st demand profile and estimate
Demand estimate
0.075
0.05
0.025
0.0
0
10
20
30
timestep

3.3 Discussion

In all experiments, there was some error due to the crude forwards and backwards difference appro

equation (2.13). In the next chapter we investigate a new model, which we term an $\mathcal{M}2$ model, which uses a central difference approximation of equation (2.13). It is shown that the flow estimates of such a model contain significantly less error.

Chapter 4

Formulation of a New $\mathcal{M}2$ Variant Model

We now show how a new pressure driven model variation, denoted by $\mathcal{M}2$, which is capable of estimating flow demands from the available pressure telemetry, may be constructed from a base $\mathcal{M}0$ model using the same central difference discretisation of equation (2.13) that the base $\mathcal{M}0$ model uses. The $\mathcal{M}2$ model is derived from an $\mathcal{M}0$ model by swapping over the flow variables from the input vector with the loclomelbT1

The new $\mathcal{M}2$ system has the form

$$\begin{bmatrix} E' & -B^{1''} \end{bmatrix} \begin{bmatrix} \underline{p}_1(k+1) \\ \underline{d}(k+1) \end{bmatrix} = \begin{bmatrix} A' & B^{2''} \end{bmatrix} \begin{bmatrix} \underline{p}_1(k) \\ \underline{d}(k) \end{bmatrix} + \begin{bmatrix} B^{1'} & -E'' \end{bmatrix} \begin{bmatrix} \underline{p}_3(k+1) \\ \underline{p}_2(k+1) \end{bmatrix}$$

$$+ \begin{bmatrix} B^{2'} & A'' \end{bmatrix} \begin{bmatrix} \underline{p}_3(k) \\ \underline{p}_2(k) \end{bmatrix} \tag{4.2}$$

which can be expressed in the general descriptor system form

$$E_2 \underline{x}_2(k+1) = A_2 \underline{x}_2(k) + B_2^1 \underline{u}_2(k+1) + B_2^2 \underline{u}_2(k). \tag{4.3}$$

4.1 Theorems

We are able to derive similar theoretical results as for $\mathcal{M}0$ and $\mathcal{M}1$ models; however, sufficient conditions for asymptotic stability are slightly more restrictive. Firstly, we prove that the matrix E_2 of an $\mathcal{M}2$ model is full rank if $\theta > 0$. It is then proved that the $\mathcal{M}2$ system eigenvalues are real if $\theta > 0$. Next, it is proved that the $\mathcal{M}2$ system eigenvalues are within the unit circle for $1/2 < \theta \leq 1$, and are within or on the unit circle for $\theta = 1/2$. Lastly, we prove the following. When pressure data is fed from a base $\mathcal{M}0$ model into its corresponding $\mathcal{M}2$ model, then, if the $\mathcal{M}2$ model is asymptotically stable, the system state of the $\mathcal{M}2$ model tends with time to the state of the base $\mathcal{M}0$ model and its flow inputs.

As with $\mathcal{M}0$ models, all theorems rely on the following inequalities. $\Gamma_{node}^{pipe} > 0$, $\Gamma^{junction} > 0$, $\delta x^{pipe} > 0$, $r^{pipe} > 0$, $\theta > 0$, $\Omega_{node}^{pipe} > 0$, $\epsilon_3^{pipe} > 0$ and $\Phi^{junction} > 0$ for all pipes, nodes and junctions.

If the base $\mathcal{M}0$ model is rearranged and partitioned as equation (3.1), then the corresponding $\mathcal{M}2$ model has the form

$$\begin{bmatrix} \mathcal{E}_{1,1} & 0 \\ \mathcal{E}_{2,1} & -\mathcal{B}_{2,2}^1 \end{bmatrix} \begin{bmatrix} \underline{p}_1(k+1) \\ \underline{d}(k+1) \end{bmatrix} = \begin{bmatrix} \mathcal{A}_{1,1} & 0 \\ \mathcal{A}_{2,1} & \mathcal{B}_{2,2}^2 \end{bmatrix} \begin{bmatrix} \underline{p}_1(k) \\ \underline{d}(k) \end{bmatrix} + \begin{bmatrix} \mathcal{B}_{1,1}^1 & -\mathcal{E}_{1,2} \\ 0 & -\mathcal{E}_{2,2} \end{bmatrix} \begin{bmatrix} \underline{p}_3(k+1) \\ \underline{p}_2(k+1) \end{bmatrix}$$

$$+ \begin{bmatrix} \mathcal{B}_{1,1}^2 & \mathcal{A}_{1,2} \\ 0 & \mathcal{A}_{2,2} \end{bmatrix} \begin{bmatrix} \underline{p}_3(k) \\ \underline{p}_2(k) \end{bmatrix}. \tag{4.4}$$

W

Proof

Above it was shown that the eigenvalues, μ_i, of an $\mathcal{M}2$ system are given by the eigenvalues of the matrix blocks $\mathcal{E}_{1,1}^{-1}\mathcal{A}_{1,1}$ and $(-\mathcal{B}_{2,2}^{1})^{-1}\mathcal{B}_{2,2}^{2}$. By Theorem 3.3, the eigenvalues of $\mathcal{E}_{1,1}^{-1}\mathcal{A}_{1,1}$ are within the unit circle for $1/2 \leq \theta \leq 1/2$. The eigenvalues of $(-\mathcal{B}_{2,2}^{1})^{-1}\mathcal{B}_{2,2}^{2}$ are its diagonal elements $-(1-\theta)/\theta$. For $\theta = 1/2$ these diagonal elements are equal to -1, and hence the $\mathcal{M}2$ system will have g eigenvalues equal to -1. For $(1/2) < \theta \leq 1$, we have $|(1-\theta)| < 1/2$, and hence we have $|(1-\theta)|/|\theta| < 1$. Thus, for $(1/2) < \theta \leq 1$, we have $|-(1-\theta)/\theta| < 1$ and the g eigenvalues of $(-\mathcal{B}_{2,2}^{1})^{-1}\mathcal{B}_{2,2}^{2}$ are within the unit circle. □

The advantage of an $\mathcal{M}2$ model over an $\mathcal{M}1$ model is that an $\mathcal{M}2$ model uses the original $g-1$ 'connectivity equations' (2.23) and the single downstream flow boundary equation (2.19) in the estimation of the flow demands. These flow equations are based on *central* difference approximations of equation (2.13); whereas to estimate the flow demands with an $\mathcal{M}1$ model requires the use of less accurate forward or backward differences of equation (2.13). For $\mathcal{M}2$ models we have the following theorem.

Theorem 4.4 *When pressure data is fed from a base $\mathcal{M}0$ model into its corresponding $\mathcal{M}2$ model, then for $1/2 < \theta \leq 1$, the system state of the $\mathcal{M}2$ model tends with time to the state of the base $\mathcal{M}0$ model and its flow inputs.*

Proof

We can rewrite the $\mathcal{M}0$ model as

$$E'\underline{p}_1(k+1) + E''\underline{p}_2(k+1) - B^{1'}\underline{p}_3(k+1) - B^{1''}\underline{d}(k+1) =$$

$$A'\underline{p}_1(k) + A''\underline{p}_2(k) + B^{2'}\underline{p}_3(k) + B^{2''}\underline{d}(k) \qquad (4.5)$$

and we can rewrite the $\mathcal{M}$

where the $\mathcal{M}2$ state vector is

$$\underline{x}_2(k) = [\tilde{\underline{p}}_1^T(k)\ ,\ \tilde{\underline{d}}^T(k)]^T.$$

Subtracting equation (4.6) from equation (4.5) gives

$$E'(\underline{p}_1(k+1) - \tilde{\underline{p}}_1(k+1)) - B^{1''}(\underline{d}(k+1) - \tilde{\underline{d}}(k+1)) = A'(\underline{p}_1(k) - \tilde{\underline{p}}_1(k)) + B^{2''}(\underline{d}(k) - \tilde{\underline{d}}(k)). \tag{4.7}$$

If we define the errors

$$\underline{e}_1(k) = \underline{p}_1(k) - \tilde{\underline{p}}_1(k)$$

$$\underline{e}_2(k) = \underline{d}(k) - \tilde{\underline{d}}(k)$$

then equation (4.7) becomes

$$E'\underline{e}_1(k+1) - B^{1''}\underline{e}_2(k+1) = A'\underline{e}_1(k) + B^{2''}\underline{e}_2(k). \tag{4.8}$$

Equation (4.8) can be arranged as the system

$$E_2\underline{e}(k+1) = A_2\underline{e}(k)$$

where $\underline{e}(k)$ is n dimensional and has the form

$$\underline{e}(k) = \begin{bmatrix} \underline{e}_1(k) \\ \underline{e}_2(k) \end{bmatrix}$$

and E_2 and A_2 are identical to the system matrices of the $\mathcal{M}2$ model.

From Theorem 4.3, if $1/2 < \theta \leq 1$ then $\mathcal{M}2$ system is asymptotically stable, and we can see that the error, $\underline{e}(k)$, decays away. Then the system state of the $\mathcal{M}2$ model tends with time to the state of the base $\mathcal{M}0$ model and its flow inputs. □

If a real gas network, from which pressure data was taken to drive the $\mathcal{M}2$ model, was accurately modelled by the base $\mathcal{M}0$ model, then for $\theta \in (1/2, 1]$ the $\mathcal{M}2$ model state should tend to the true state of the gas network.

4.2 Experiments

When the $\mathcal{M}0$ model had been running for a while, the pressures at the upstream end and the sites of flow demand were recorded at each timestep and fed into an $\mathcal{M}2$ model. The

flow demands predicted by the $\mathcal{M}2$ model were then compared with the true flows used as inputs to the $\mathcal{M}0$ model. For experiments 4.1 to 4.3, the $\mathcal{M}0$ model simulating a gas network was identical to the $\mathcal{M}0$ model upon which the $\mathcal{M}2$ model was constructed. For experiment 4.4, the $\mathcal{M}0$ model simulating a gas network had a much finer discretisation (in both space and timeisation

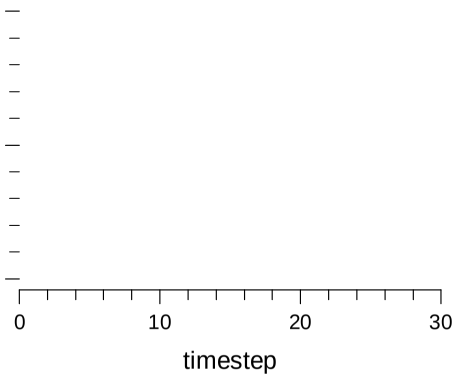
0
10
20
30
timestep

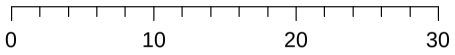
0
10
20
30

4.3 Discussion

It is immediately apparant that the central difference approximation of equation (2.13) has very greatly reduced the error in the estimates of the flow demands. Indeed, it can be seen that, for $1/2 < \theta \leq 1$, with identical meshes the state of the $\mathcal{M}2$ model tends with time to the *exact* state of the base $\mathcal{M}0$ model and its flow inputs. However, like the $\mathcal{M}1$ models, we have not presented a theoretical guarantee of the convergence of the solution to the $\mathcal{M}2$ model to the solution of the governing differential equations (2.16), (2.13), as the computational mesh is refined. The possibility of such a proof w

Ch pter 5

Observers

For a dynamical system, only a few measurements may be available; and the challenge of state estimation is to determine the state of the whole system from these measurements over time. If a dynamical system has measurements available corresponding to linear combinations of state variables of its system model, then the system may be *completely observable*, and an observer employed for state estimation [29], [2].
We consider the time-invariant linear descriptor system

$$E\underline{x}(k+1) = A\underline{x}(k) + B^1\underline{u}(k+1) + B^2\underline{u}(k) \tag{5.1}$$

where $E, A \in \mathbf{R}^{n\times n}$, $B^1, B^2 \in \mathbf{R}^{n\times m}$, with discrete measurements of the real system given by

$$\underline{y}(k) = C\underline{x}(k) \quad for\ k = 0, 1, 2, ..., \tag{5.2}$$

where $C \in \mathbf{R}^{g\times n}$. We assume E is full rank, and C is full row rank.

We firstly define *complete observability* and then discuss techniques, known collectively as *observers*, capable of estimating the entire system state of discrete dynamical systems (5.1), (5.2) that have the property of *complete observability*.

5.1 Observability

The system (5.1), (5.2) is *completely observable* if and only if knowledge of the inputs and measurements over some timesteps is enough to determine uniquely an initial state

$x(0)$.

The following theorem gives a necessary and sufficient condition for complete observability, known as the *Hautus condition* [42], [13], [25].

Theorem 5.1 *A system of the form (5.1), where the matrix E is non-singular, with measurements available of the form (5.2), is completely obseurtetele if rtetnd only if we have the following condition.*

For all $\mu \in \mathbf{C}$

$$(A - \mu E)\underline{v} = \underline{0} \quad , \quad C\underline{v} = \underline{0} \iff \underline{v} = \underline{0} \tag{5.3}$$

where $\underline{v} \in \mathbf{R}^n$.

5.2 Design A : The *Direct* Observer

Assume the behaviour of a system is described by (5.1), (5.2). The method solves the matrix equation

$$\Theta \underline{\mathcal{X}} = \underline{\Delta}, \tag{5.4}$$

where Θ is the matrix

$$\begin{bmatrix} A & -E & & & . & . & . & . & . \\ & A & -E & & & . & . & . & . \\ & & A & -E & & & . & . & . \\ & & & & & & & & \\ & & & & & & & & \\ C & & & & . & . & . & . & . \\ & C & & & . & . & . & . & . \\ & & C & & . & . & . & . & . \\ & & & C & . & . & . & . & . \\ & & & & & & & & \\ & & & & & & & & \end{bmatrix},$$

and

$$\underline{\mathcal{X}}^T = [\underline{\hat{x}}(k)^T, \underline{\hat{x}}(k+1)^T, \underline{\hat{x}}(k+2)^T, ...\underline{\hat{x}}(k+n-1)^T]$$

where $\underline{\hat{x}}(k)$ is the observer estimate for $\underline{x}(k)$, and

$$\underline{\Delta}^T = [-(B^1\underline{u}(k+1) + B^2\underline{u}(k))^T, -(B^1\underline{u}(k+2) + B^2\underline{u}(k+1))^T, ...$$

(_(+ 1) + _(+ 2)) _ ( ) _ (+ 1) _ (+ 1)]

—

_ _ _ _ _

_ _ _

_ _ _ _ _ _

_ _

_ _ _

_ _ _

or

$$\_(\quad +1) = (\qquad\qquad)\_(\quad) \tag{5 8}$$

We require $\_(\quad) \quad \underline{0}$ as $\qquad$; and for this we require the eigenvalues of the matrix

$$\begin{matrix} - & - \\ - & - \end{matrix}$$

and is , upper triangular and non-singular. If equation (5.10) is rearranged and factorisation (5.11) substituted in, then

$$= \quad (\qquad\qquad)$$

from which

$$= \quad \tilde{} \; (\qquad\qquad) \tag{5 12}$$

and

$$0 = \quad (\qquad\qquad) \tag{5 13}$$

quation (5.13) implies

$$(\qquad\qquad)\_ \qquad (\quad) \qquad = 1 \tag{5 14}$$

or

$$\_ \qquad (\qquad\qquad)$$

where represents the right null space. If the dimension, , of the measurement vector is greater than one, then there is a certain amount of freedom in the choice of the _ . This freedom may be utilised in selecting a set of _ such that the observer eigenvalues are as insensitive as possible to perturbations in the matrices and .

A generalised eigenvalue of the matrix pencil ( ) can be described by the

x 0x pair (6=()Hffixkgfi(ΘOkH(ffiandfidef40n ΘkaΔfnsiftvΘkHffixHofi6ΔΘΘffiLkpfiΘDuffix,Hofi6ΘktofiΔ (where x is the cartesian product of the spaces of complex and

real numbers respectively) where the associated eigenvalue is = , for = 1 .

Then from equations (5.9) and (5.10), we assume that for lef6ΔHOffiΘkfromFΔ-fi67x8xthan one,is

_

_ _

_ _

_ _

_ _

and $\underline{x}_i$ and $\underline{y}_i$ are assumed to be normalised such that

$$\underline{y}_i^T E \underline{x}_i = \delta_i, \tag{5.18}$$

$$\underline{y}_i^T (A - GC)\underline{x}_i = \mu_i, \tag{5.19}$$

[39].

Now, since we are assuming E is full rank, we may assume we have a set of eigenvector/eigenvalue pairs, $(\underline{x}_i, \underline{y}_i), (\mu_i, \delta_i)$, for $i = 1, ..., n$, where the eigenvectors are scaled such that $\|\underline{y}_i\|_2 = 1$ and $\delta_i = 1$ for $i = 1, ..., n$. Then to minimise the condition numbers (5.17), we need to minimise the $\|\underline{x}_i\|_2$. From equation (5.18) with all $\delta_i = 1$, we have

$$Y^T E X = I, \tag{5.20}$$

from which we have

$$X = (Y^T E)^{-1}. \tag{5.21}$$

So to minimise the $\|\underline{x}_i\|_2$, we can select the $\underline{y}_i$ such that

$$\|(Y^T E)^{-1}\|_F = \|X\|_F = (\Sigma_i \|\underline{x}_i\|_2^2)^{1/2}$$

is minimised.

To select a set of left eigenvectors, $\underline{y}_i$, such that $\|(Y^T E)^{-1}\|_F$ is minimised, we use a simple method that, although it cannot be guaranteed to converge to the minimum value of $\|(Y^T E)^{-1}\|_F$ attainable, has been found to significantly reduce the value of $\|(Y^T E)^{-1}\|_F$ over a number of iterations.

The method begins by selecting a set of vectors which satisfy equation (5.13). For each eigenvalue in the set Λ, we calculate the QR decomposition

$$Q_1^T (A - \lambda_i E) Q_c = R_1 \tag{5.22}$$

where

$$Q_1^T = \begin{matrix} \tilde{S}_i^T \\ S_i^T \end{matrix}$$

eneral Eigenvalue Assignment Algorithm

1) Compute the QR decomposition of C

$$C \quad = QR,$$

where

$$Q \quad = \begin{matrix} \tilde{Q} \\ Q \end{matrix} \quad ,$$

and

$$R = \begin{matrix} C \\ 0 \end{matrix} \quad .$$

2) For each eigenvalue λ for $i = 1, ..., n$ in the set Λ, calculate the QR decomposition

$$Q \ (A \quad \lambda E)Q \ = R \ ,$$

where

$$Q \quad = \begin{matrix} \tilde{S} \\ S \end{matrix}$$

and

$$R \quad = \begin{matrix} \tilde{R} \\ 0 \end{matrix}$$

and S is $n \quad p$.

3) For each $\quad = 1 \qquad$, choose any vector, $\_$ from span $\qquad$ as one of the columns of the matrix $\quad$.

4) For $\quad = 1 \qquad$, let

$$= [\_ \qquad \_ \quad \_ \qquad \_]$$

and calculate the QR decomposition

$$=$$

where

$$= \tilde{\quad} \quad -$$

and

$$= \tilde{\quad} \quad 0$$

Let

$$= \quad - \quad -$$

5) Calculate ( ) .

6) Repeat steps (4) and (5) until ( ) reaches a local minimum.

7) Let

$$= \tilde{\quad} (\quad)$$

$$- \quad - \quad - \quad - \quad - \quad -$$

$$- \quad - \quad -$$

then subtracting equation (5.25) from equation (5.1) gives

$$(\qquad)\_(\quad+1) = (\qquad)\_(\quad) \tag{5.27}$$

If can be chosen such that ( ) is nonsingular, then its inverse can be calculated to give an explicit expression for _(+1) from equation (5.27). We notice that ( ) would multiply all the terms on the right hand side of equation (5.27). Therefore, if ( ) could be made small for a suitable norm, then the effects of certain forms of modelling error, that will be described later, should be reduced. It would also be advisable to ensure the condition number of ( ) is not too large since this matrix has to be inverted implicitly in equation (5.25) to calculate _(+1).

We know that if

$$= \quad \Sigma \tag{5.28}$$

is the singular value decomposition of ( ), where $\Sigma =$ [ ] and the are arranged in nonincreasing order, then

$$=$$

– – –

We use a method from [34], [4] for determining the matrix with of the singular values of ( ) assigned arbitrarily.

Let the QR-decomposition of matrix be

$$= \tag{5 29}$$

where

$$= \tilde{}$$

and

$$= \quad 0$$

If equation (5.28) is transposed and the factorisation (5.29) applied to then we have

$$= \quad (\quad \Sigma \quad) \tag{5 30}$$

– – – – –

– – –

– –

– –

and since rank( ) = and rank( ) = we have

$$\Sigma =$$

Refering now to the matrices and in equations (5.28) and (5.30), let

$$= [\tilde{} \quad \tilde{}] \tag{5 33}$$

where $\tilde{}$ and $\tilde{}$ are from equation (5.32) and let

$$= [\quad \tilde{} \quad \tilde{}] \tag{5 34}$$

where $\tilde{}$ is also from equation (5.32), and $\tilde{}$ and are from equation (5.29). It can be verified that the _ _ and satisfy the condition (5.31) for = 1 , where

and

$$(\qquad) = \quad (\qquad)$$

For a more robust observer design, we ideally want

$$(\ \ ) \qquad (\Sigma\ ) \quad (\Sigma\ ) \quad (\ \ )$$

1) Compute the decomposition of

$$=$$

where

$$\tilde{} \\ =$$

and

$$= \\ 0$$

2) Form and calculate the SVD

$$[\tilde{} \quad \tilde{}\ ] = \tilde{}\ [\Sigma \quad 0]$$

where

$$\Sigma \ =$$

is a diagonal matrix with the singular values which cannot be modified.

Chapter 6

Formulation of a New $\mathcal{M}3$ Variant Model for Use in Direct and Dynamic Observers

We now show how a new model variation, denoted by $\mathcal{M}3$, which is capable of estimating flow demands, may be constructed from a base $\mathcal{M}0$ model using information about the flow demands, such that these new $\mathcal{M}3$ models are observable.

Since, in practice the flow demands change very slowly with time, the $\mathcal{M}3$ models assume

$$flow\ demand_{k+1}^{demand\ site} = flow\ demand_{k}^{demand\ site},$$

i.e.

$$d_{k+1}^{demand\ site} = d_{k}^{demand\ site} \quad for\ all\ k. \tag{6.1}$$

The key feature of $\mathcal{M}3$ models is that they contain difference equations of the form (6.1).

Then to form an $\mathcal{M}3$ model, we start from a base $\mathcal{M}0$ model and move the g dimensional vector, $\underline{d}(k)$, from the input vector to the state vector. We then introduce g new trivial difference equations of the form

$$\underline{d}(k+1) = \underline{d}(k) \tag{6.2}$$

into the new system. Assuming the base $\mathcal{M}0$ model is arranged and partitioned as in

equation (4.1), then the new $n+g$ dimensional $\mathcal{M}3$ system has the form

$$\begin{bmatrix} E_0 & -B^{1''} \\ 0 & I \end{bmatrix} \begin{bmatrix} \underline{x}_0(k+1) \\ \underline{d}(k+1) \end{bmatrix} = \begin{bmatrix} A_0 & B^{2''} \\ 0 & I \end{bmatrix} \begin{bmatrix} \underline{x}_0(k) \\ \underline{d}(k) \end{bmatrix} + \begin{bmatrix} B^{1'} \\ 0 \end{bmatrix} \underline{p}_3(k+1) + \begin{bmatrix} B^{2'} \\ 0 \end{bmatrix} \underline{p}_3(k) \tag{6.3}$$

which can be expressed in the general descriptor system form

$$E_3 \underline{x}_3(k+1) = A_3 \underline{x}_3(k) + B_3^1 \underline{u}_3(k+1) + B_3^2 \underline{u}_3(k). \tag{6.4}$$

For such an $\mathcal{M}3$ model, the only input required is the upstream pressure (assumed known). The g pressure measurements of the real gas network at the sites of flow demand are not needed as inputs to the $\mathcal{M}3$ model, and are in fact measurements of its state variables

$$\underline{y}_3(k) = C_3 \underline{x}_3(k) \tag{6.5}$$

available for use in a direct or dynamic observer.

6.1 Theorems

In this section, we firstly prove that the matrix E_3 of an $\mathcal{M}3$ model is full rank if $\theta > 0$. We next prove that if $\theta > 0$, then an $\mathcal{M}0$ model with pressure measurements available at the sites of flow demand is completely observable. This result is then used to prove that for $1/2 \leq \theta \leq 1$, $\mathcal{M}3$ models are completely observable if there are pressure measurements available at all the sites of flow demand. Lastly, it is proved that $\mathcal{M}3$ models are not completely observable if there are fewer measured pressures than flow demands.

Theorem 6.1 *If $\theta > 0$, the matrix E_3 of an $\mathcal{M}3$ model is full rank.*

Proof

E_3 is $(n+g)\times(n+g)$ and takes the form

$$E_3 = \begin{bmatrix} E_0 & -B^{1''} \\ 0 & I \end{bmatrix}$$

where I is $g \times g$.

By construction, since we have already shown E_0 is invertible for $\theta > 0$, E_3^{-1} is $(n+g)\times(n+g)$ and takes the form

$$E_3^{-1} = \begin{bmatrix} E_0^{-1} & E_0^{-1}B^{1''} \\ 0 & I \end{bmatrix}$$

where I is $g\times g$.

Hence, the matrix E_3 of an $\mathcal{M}3$ model is full rank. □

Theorem 6.2 *If $\theta > 0$, an $\mathcal{M}0$ model with pressure measurements available at the sites of flow demand is completely observable.*

Proof

The $\mathcal{M}0$ system (2.24) has g pressure measurements available at the sites of flow demand, corresponding to the following g dimensional vector of state variables

$$\underline{y}_0(k) = C_0\underline{x}_0(k) \tag{6.6}$$

where C_0 is $g\times n$ and is the measurement matrix.

Since we have shown that the eigenvalues of an $\mathcal{M}0$ system are real for $\theta > 0$, the $\mathcal{M}0$ system with measurements (6.6), is observable if and only if for $\mu\in\mathbf{R}$

$$(A_0 - \mu E_0)\underline{v} = \underline{0} \tag{6.7}$$

$$C_0\underline{v} = \underline{0} \tag{6.8}$$

$$\Longleftrightarrow$$

$$\underline{v} = \underline{0} \tag{6.9}$$

where $\underline{v}\in\mathbf{R}^n$.

Equation (6.9) $\Longrightarrow$ equations (6.7), (6.8) trivially.

We assume the pressure variables are arranged in the state v

where each pipe has $s^{pipe} + 1$ nodes. E

The $\mathcal{M}3$ system is observable if and only if for all μ

Hence, we have $\underline{v}_n = \underline{0}$, $\underline{v}_g = \underline{0}$; and so equations (6.10), (6.11) $\Longrightarrow$ (6.12).

We secondly consider the case $\mu = 1$.

Let the base $\mathcal{M}0$ system be partitioned according to equation (4.1). Then equation (6.13) can be written as the following system of n equations for the $n+g$ dimensional vector $\underline{v}$

$$[(A' - \mu E') \quad (A'' - \mu E'') \quad (B^{2''} - \mu(-B^{1''}))] \begin{bmatrix} \underline{v}'_n \\ \underline{v}''_n \\ \underline{v}_g \end{bmatrix} = \underline{0} \tag{6.19}$$

where

$$\underline{v}_n = \begin{bmatrix} \underline{v}'_n \\ \underline{v}''_n \end{bmatrix}$$

and $\underline{v}'_n \in \mathbf{R}^{n-g}$ and $\underline{v}''_n \in \mathbf{R}^g$.

Equation (6.15) zeros the elements of $\underline{v}''_n$. Removing $\underline{v}''_n$ from system (6.19) gives the system

$$[(A' - \mu E') \quad (B^{2''} - \mu(-B^{1''}))] \begin{bmatrix} \underline{v}'_n \\ vBvDcjfDmfDD\theta jD{>}jDv{>}fDc\lambda/cmImD \end{bmatrix}$$

Theorem 6.4 *An $\mathcal{M}3$ model will* not *be completely observable if there are fewer measured pressures than flow demand state variables.*

Proof

We assume we have g flow demand state variables, and less than g pressure measurements.

Necessary and sufficient conditions for the complete observability of an $\mathcal{M}3$ system are given by equations (6.10), (6.11) and (6.12).

If $\mu = 1$, then, since there are g flow demand state variables, the bottom g rows of the matrix $(A_3 - \mu E_3)$ are zero vectors. Hence the maximum rank of $(A_3 - \mu E_3)$ is n. Also, since there are less than g pressure measurements, the maximum rank of C_3 is less than g.

Hence, for $\mu = 1$, if we combine systems (6.10) and (6.11) into a single system to solve for $\underline{v}$, such a system would have rank less than $n + g$. Hence, equations (6.10) and (6.11) would have non-zero solutions for $\underline{v}$.

Thus, equations (6.10) and (6.11) do not imply equation (6.12), and hence the $\mathcal{M}3$ system is not observable. □

For $\mathcal{M}3$ models constructed with trivial difference equations of the form (6.1), it was found direct observers did not work well. Thus to estimate the flow demands in the gas network, a *dynamic* observer constructed upon an $\mathcal{M}3$ model is run assuming all the pressure and flow perturbations are initially zero. The pressure perturbation measurements are fed in at each time level, and the observer state tends to the state of the gas network with time. Perfect asymptotic convergence is not obtained unless the flow demands do not vary with time, since equations (6.2) contain modelling error. If the flow demands are changing, although not too rapidly, the observer still tracks the state of the gas network fairly well. Indeed, typically, the flow demands in gas networks change only slowly throughout the day.

6.2 Weighted $\mathcal{M}3$ odels

In fact, the profiles of the flow demands are fairly well known from other measured demands that change thoughout the day with similar patterns of gas consumption. More accurate $\mathcal{M}3$ models may be constructed using such information available about the *shapes* of the flow demand profiles with time. This corresponds to knowing the constants $f_k^{demand\ site}$ in

$$flow\ demand_{k+1}^{demand\ site} = flow\ demand_k^{demand\ site} + f_k^{demand\ site}$$

where the $f_k^{demand\ site}$ may be estimated from the telemetry from other *measured* demand flows. After normalisation, we would have

$$normalised\ flow\ demand_{k+1}^{demand\ site} = normalised\ flow\ demand_k^{demand\ site} + \tilde{f}_k^{demand\ site}$$

where $\tilde{f}_k^{demand\ site} = f_k^{demand\ site}/Nq$, i.e., we would have

convergence because we have lost the modelling error in the extra trivial difference equations (6.22) for the flow demand perturbations. However, now *direct* observers work well enough to be used as well. Obviously, in practice, the estimates of the $\tilde{f}_k^{demand\ site}$ would not be exact, and there would still be some error in the observer estimate.

6.3 Experiments

When the $\mathcal{M}0$ model had been running for a while, the pressures at the upstream end and the sites of flow demand were recorded at each timestep and fed into the various $\mathcal{M}3$ model-based observers. The flow demands predicted by these techniques were compared

6.3.1 Experiments with *no* weightings, $\tilde{f}_k^{demand\ site}$

Experiment 6.16) Observer Design C (small eigenvalues) with $\theta = 1$

Data taken from $\mathcal{M}0$ model with much finer mesh - $\mathcal{M}3$ model has 5 spatial nodes along each pipe.

Experiment 6.17) Observer Design A with $\theta = 1$

Experiment 6.18) Observer Design A with $\theta = 0.5$

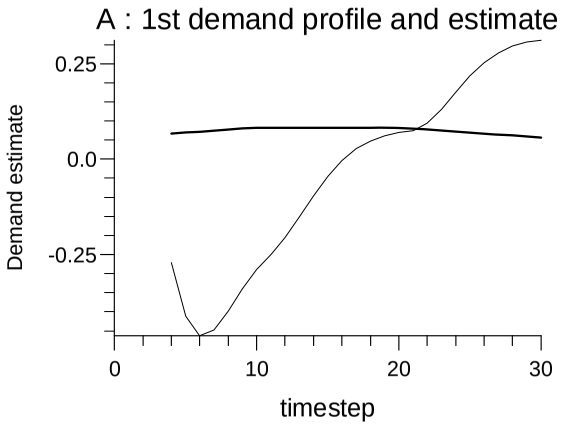
A : 1st demand profile and estimate
Demand estimate
0.25
0.0
-0.25
0
10
20
30
timestep

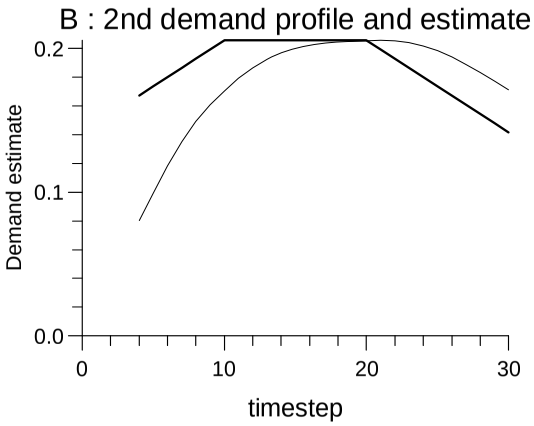
B : 2nd demand profile and estimate
Demand estimate
0.2
0.1
0.0
0
10
20
30
timestep

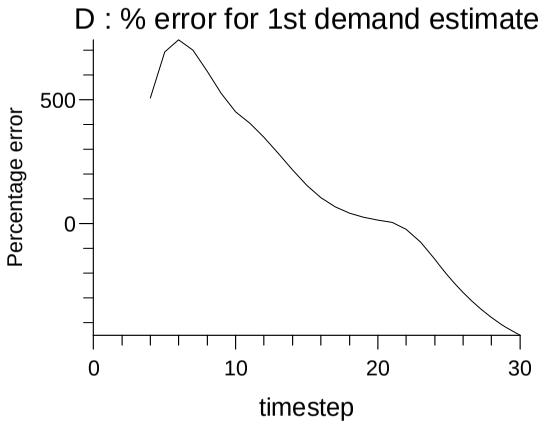
D : % error for 1st demand estimate
Percentage error
500
0
0
10
20
30
timestep

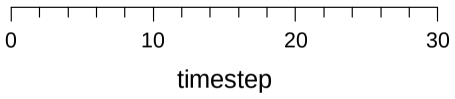
0
10
20
30
timestep

Experiment 6.2

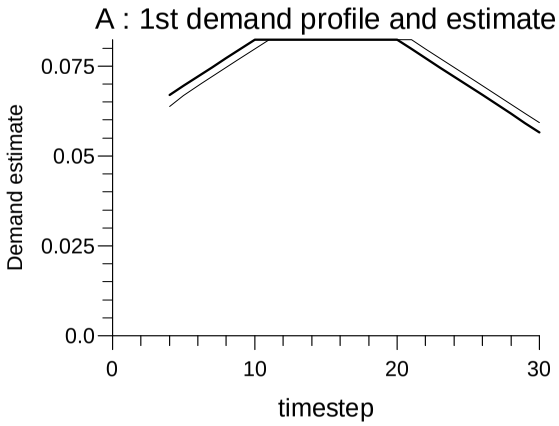

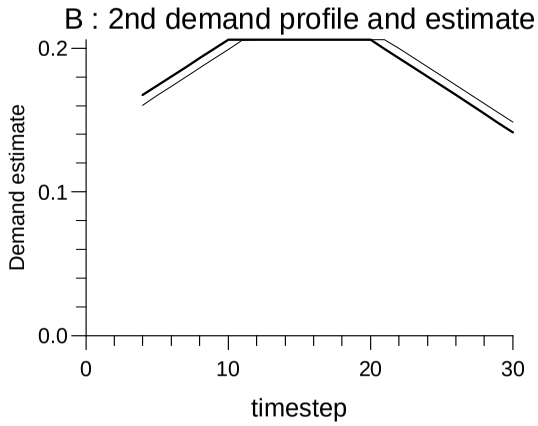

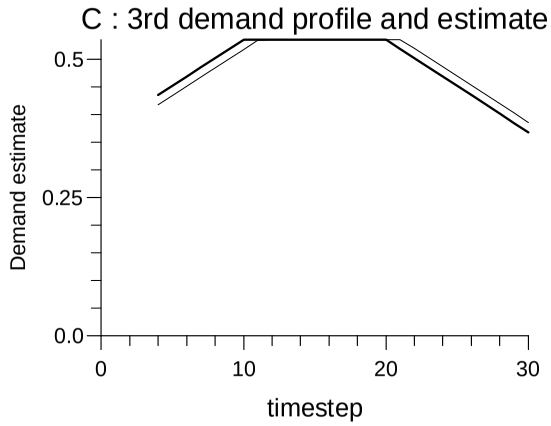

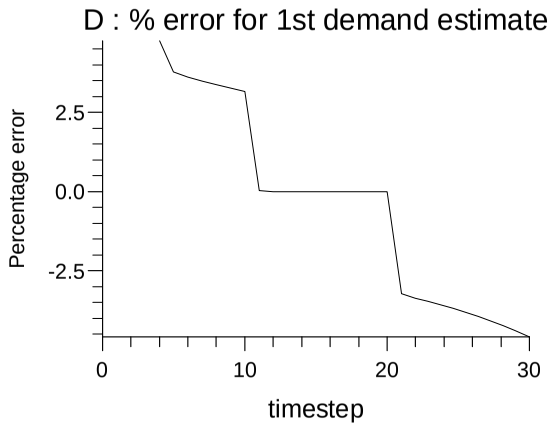

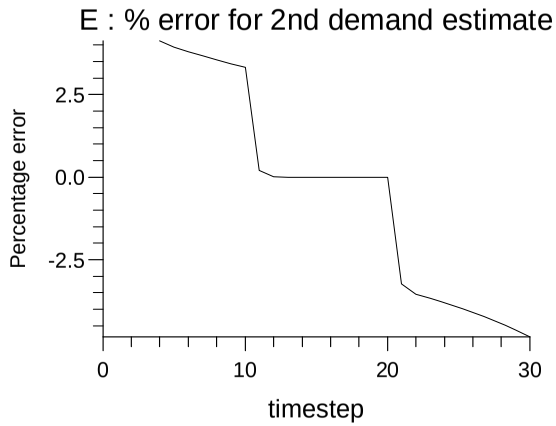

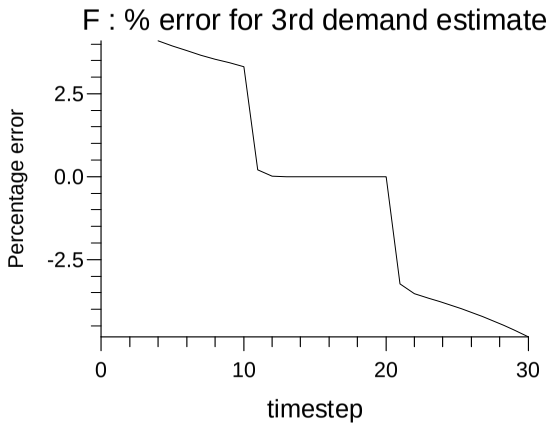

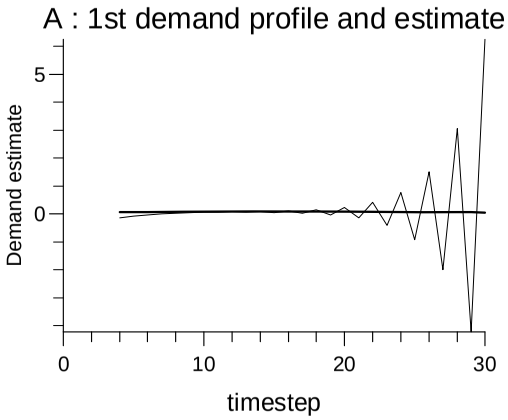
A : 1st demand profile and estimate
Demand estimate
5
0
0
10
20
30
timestep

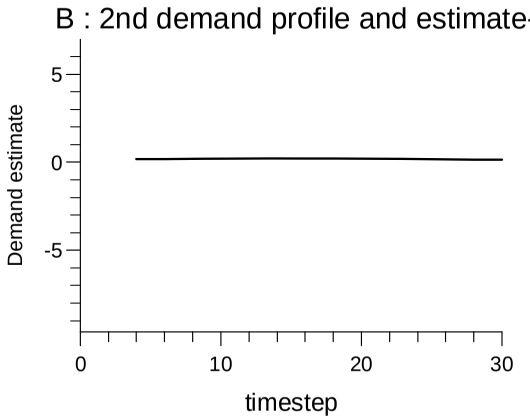
B : 2nd demand profile and estimate-5
Demand estimate
5
0
-5
0
10
20
30
timestep

Experiment 6.4

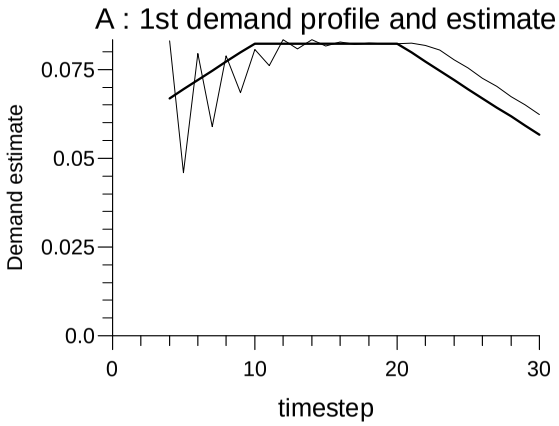

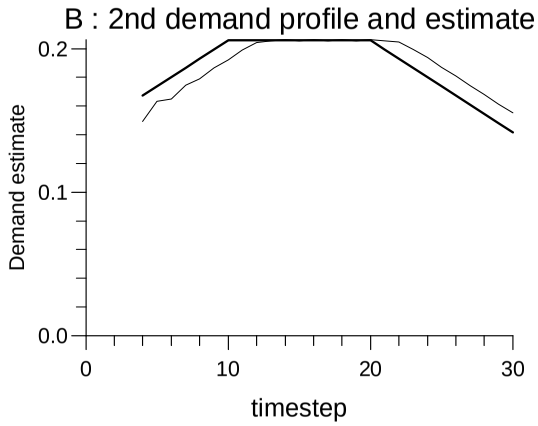

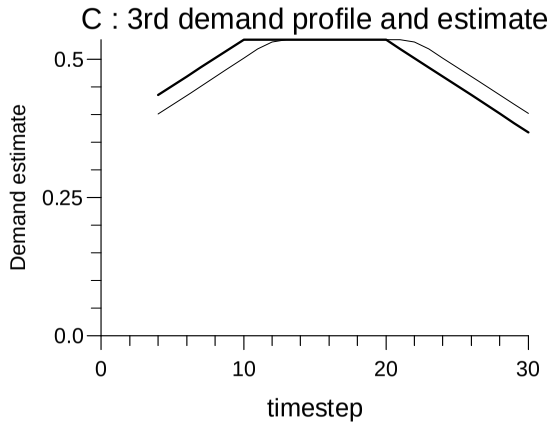

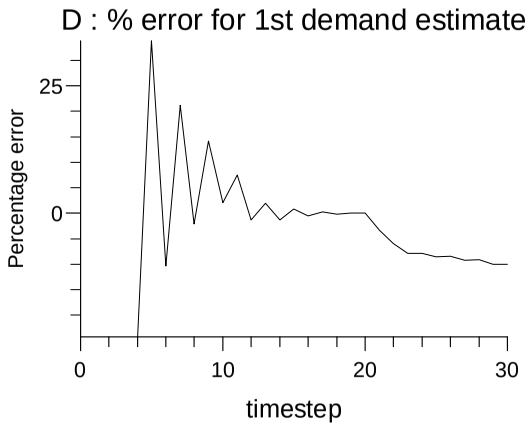

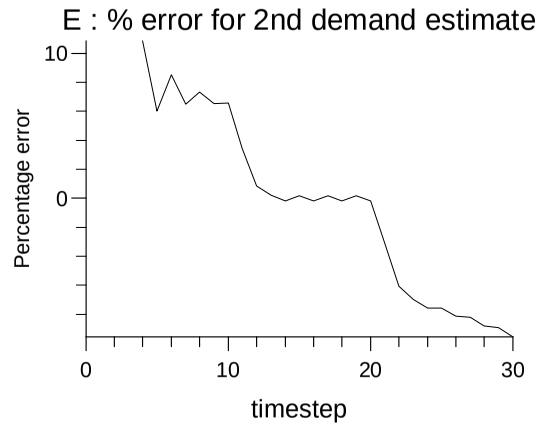

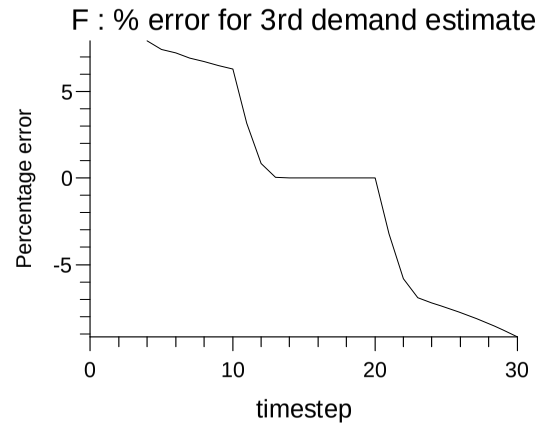

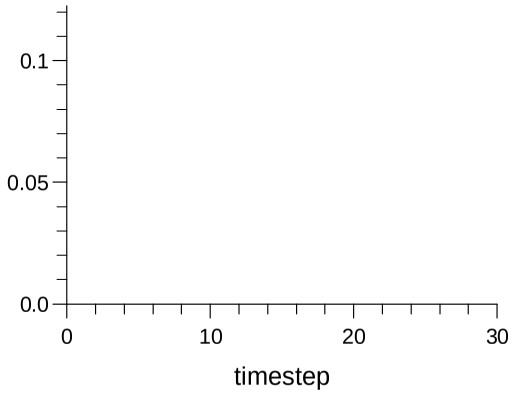
0.1
0.05
0.0
0
10
20
30
timestep

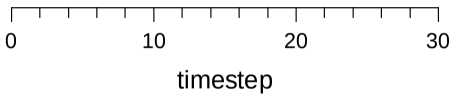
0
10
20
30
timestep

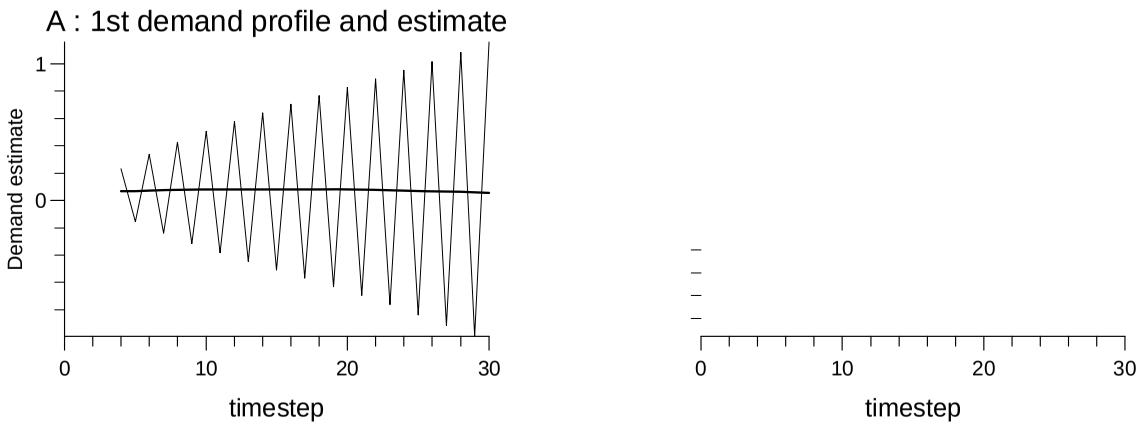
A : 1st demand profile and estimate
Demand estimate
1
0
0
10
20
30
timestep
0
10
20
30
timestep

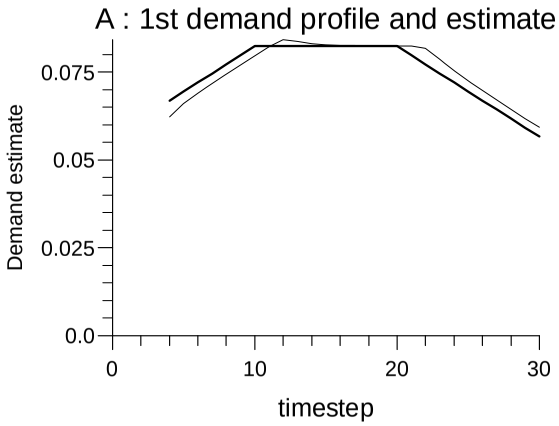
A : 1st demand profile and estimate
Demand estimate
0.075
0.05
0.025
0.0
0
10
20
30
timestep

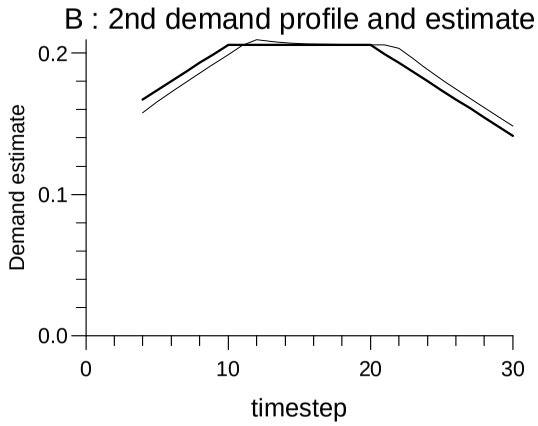
B : 2nd demand profile and estimate
Demand estimate
0.2
0.1
0.0
0
10
20
30
timestep

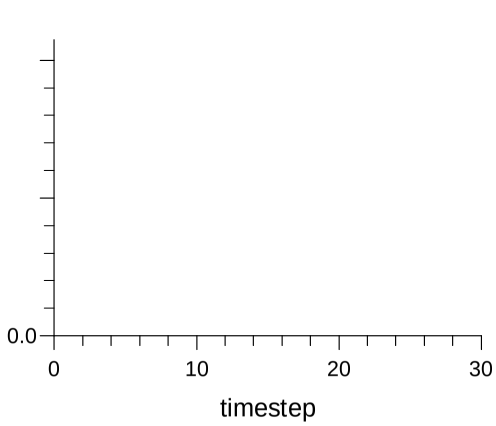
0.0
0
10
20
30
timestep

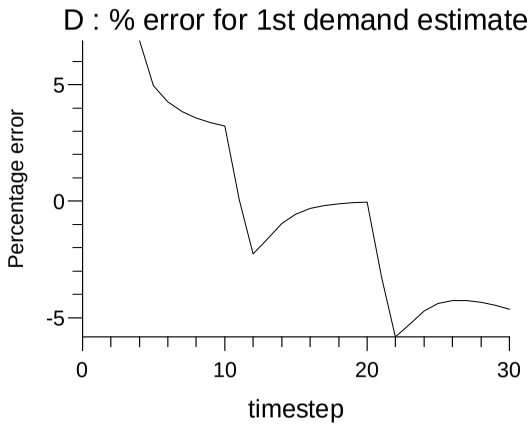
D : % error for 1st demand estimate
Percentage error
5
0
-5
0
10
20
30
timestep

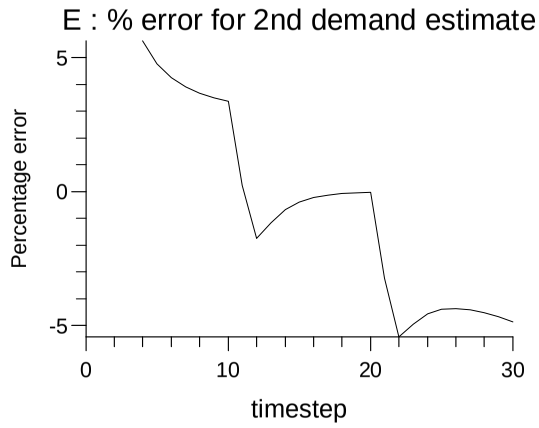
E : % error for 2nd demand estimate
Percentage error
5
0
-5
0
10
20
30
timestep

Experiment 6.9

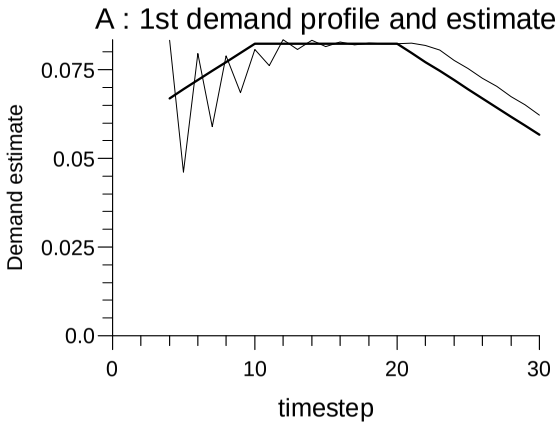

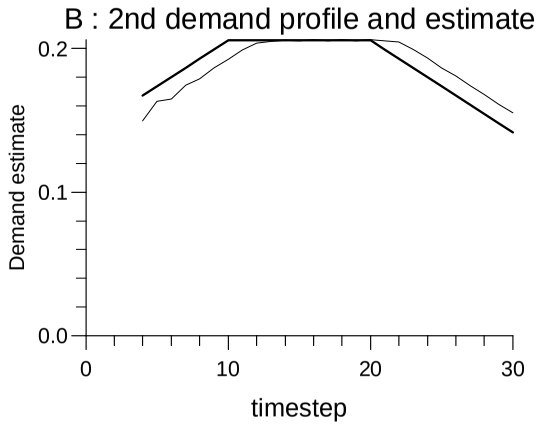

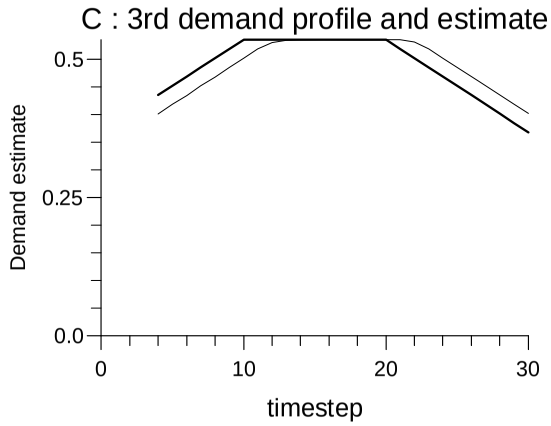

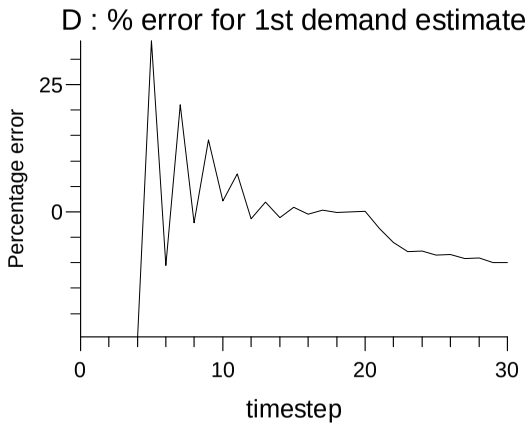

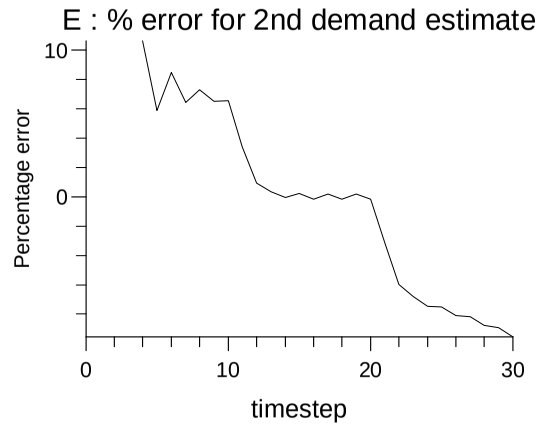

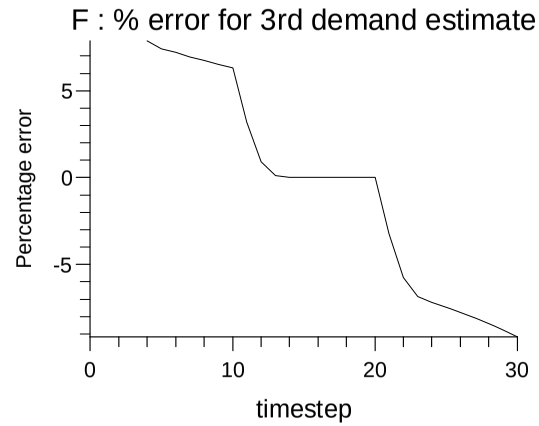

Experiment 6.10

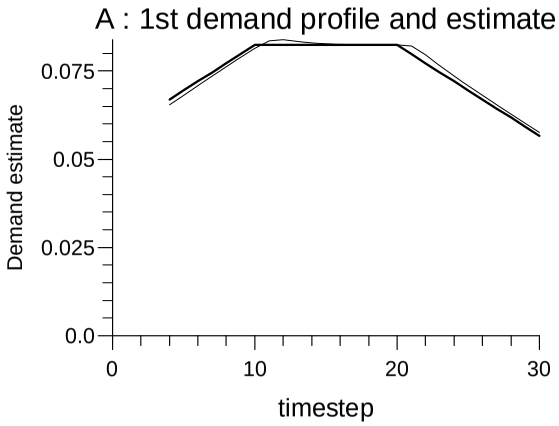

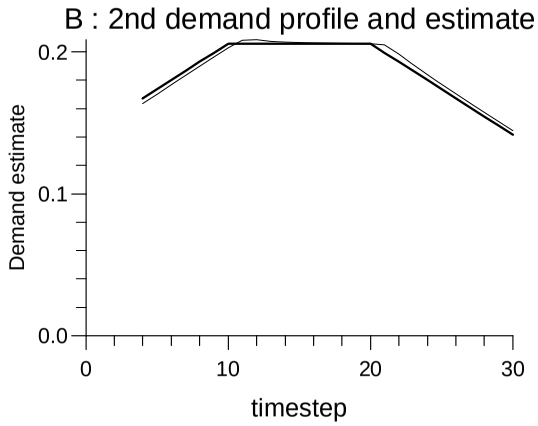

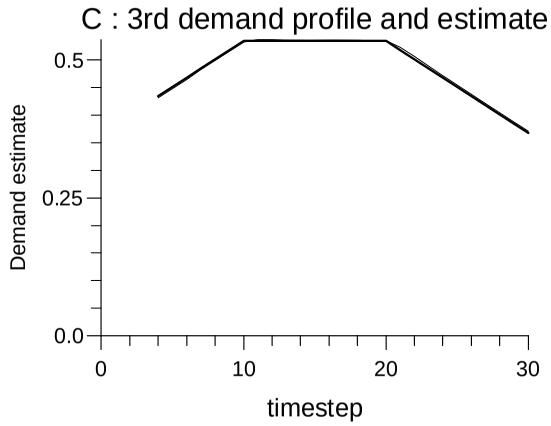

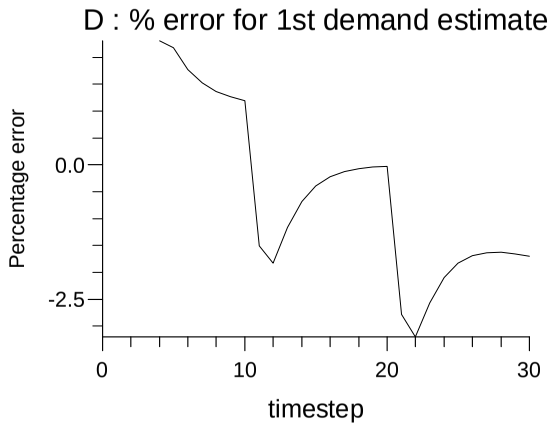

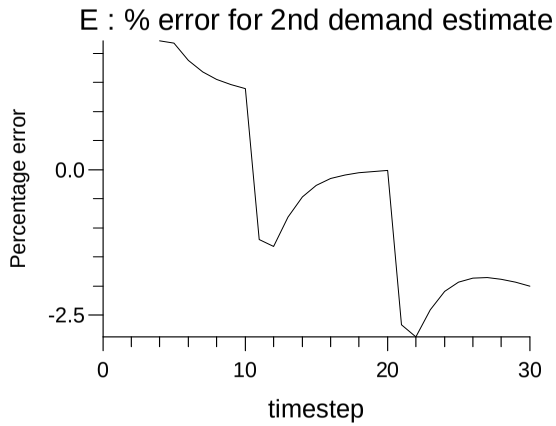

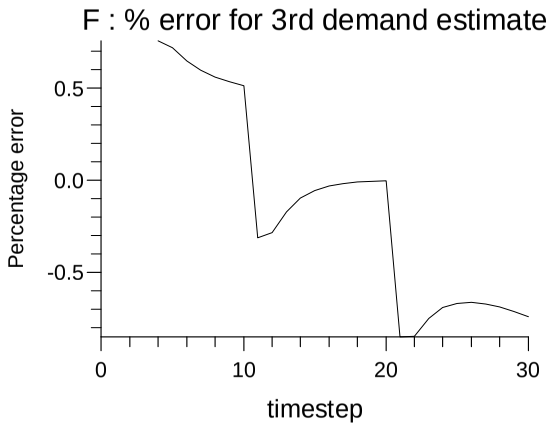

Experiment 6.12

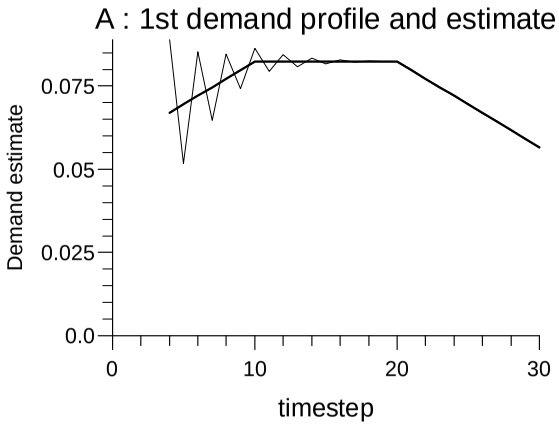

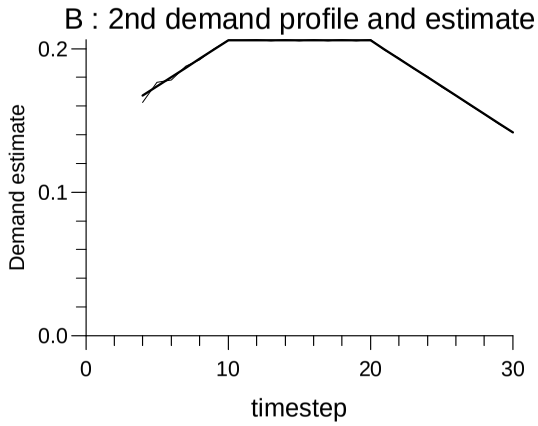

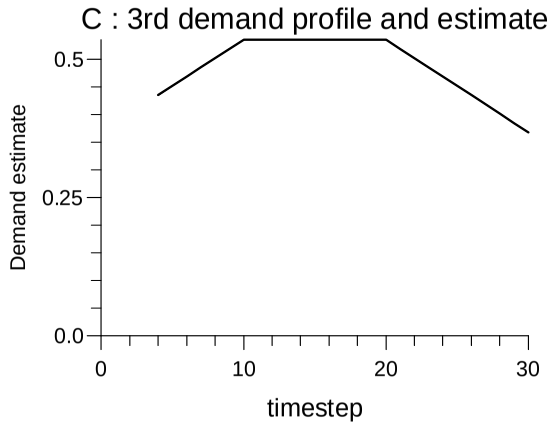

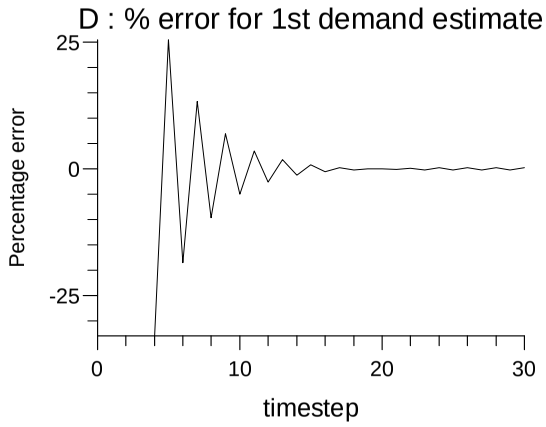

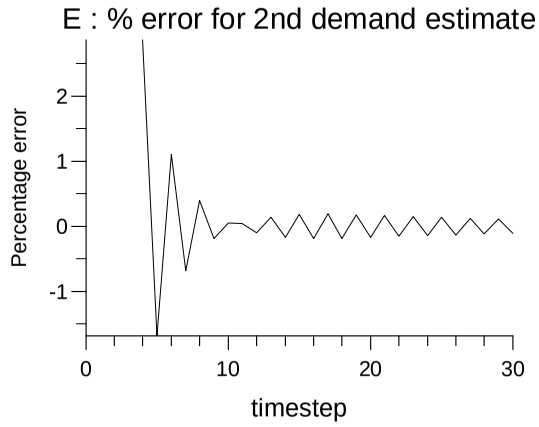

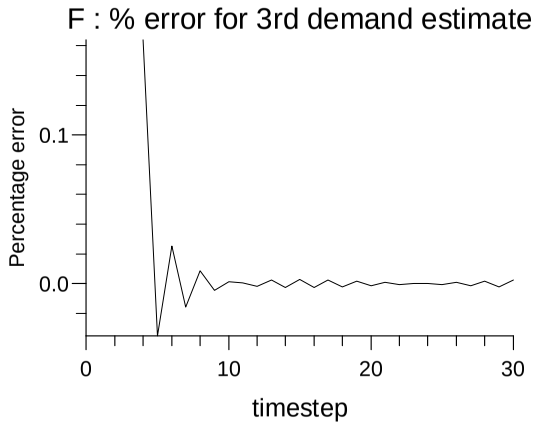

Experiment 6.13

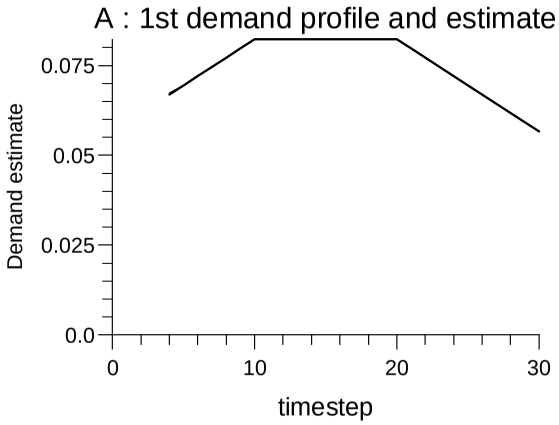

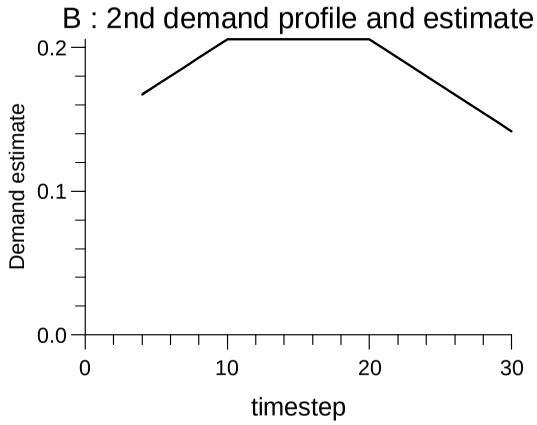

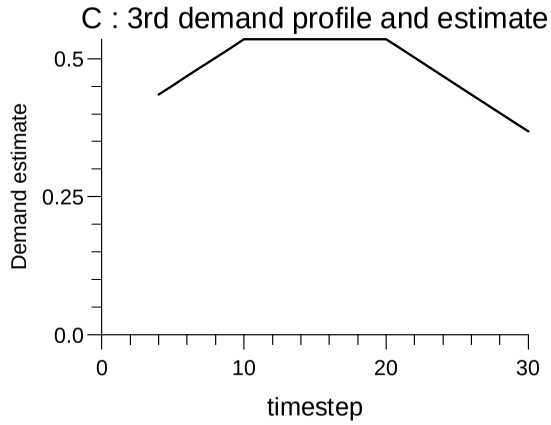

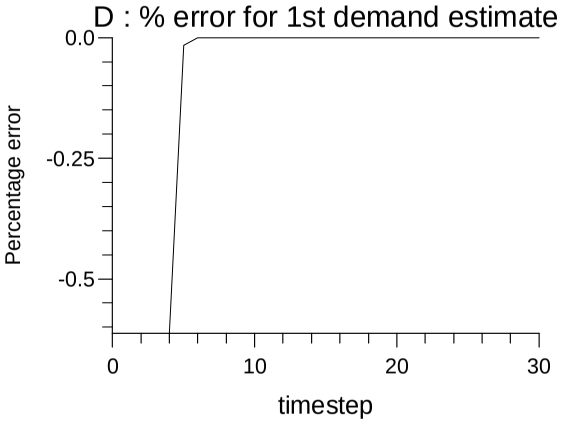

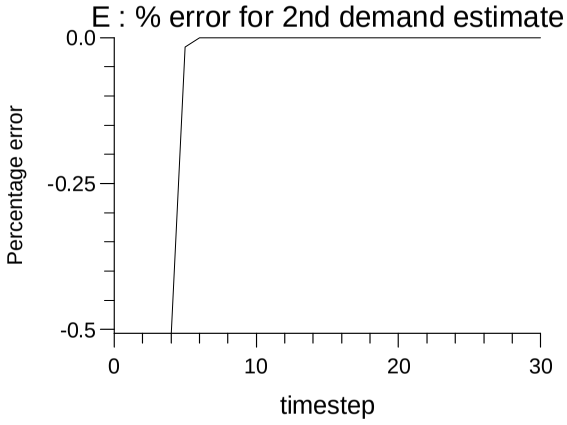

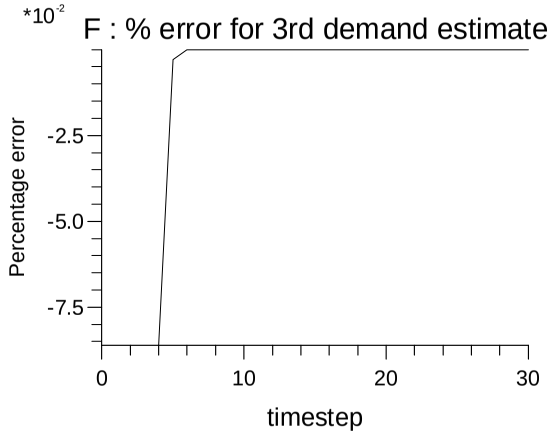

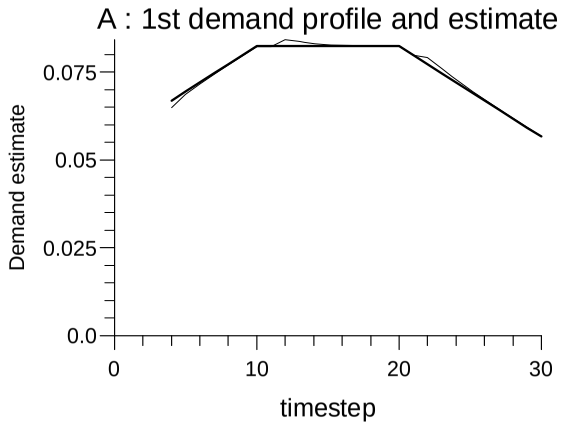
A : 1st demand profile and estimate
Demand estimate
0.075
0.05
0.025
0.0
0
10
20
30
timestep

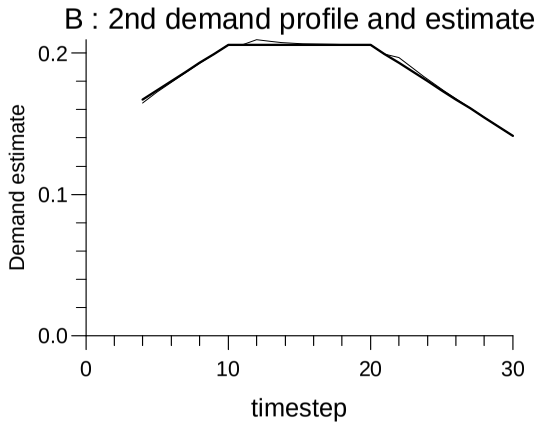
B : 2nd demand profile and estimate
Demand estimate
0.2
0.1
0.0
0
10
20
30
timestep

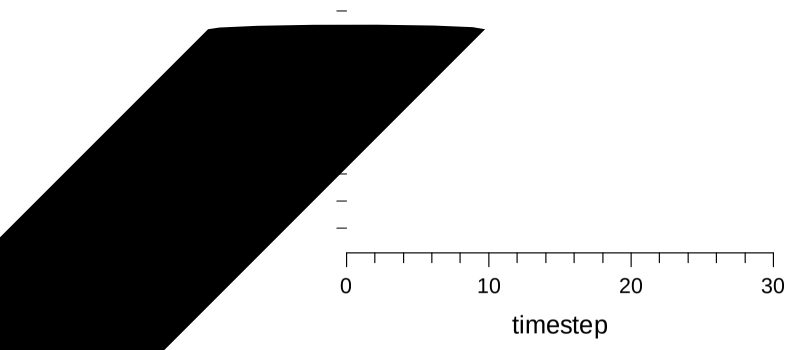
0
10
20
30
timestep

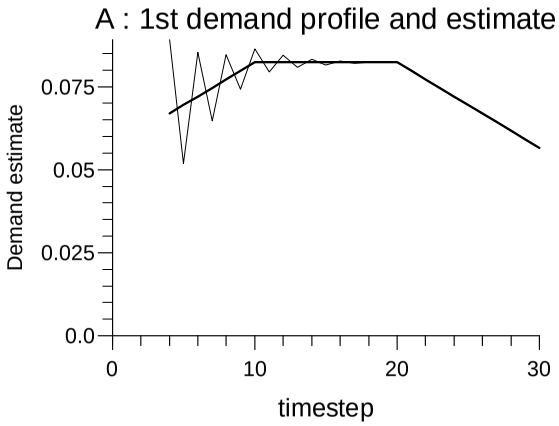
A : 1st demand profile and estimate
Demand estimate
0.075
0.05
0.025
0.0
0
10
20
30
timestep

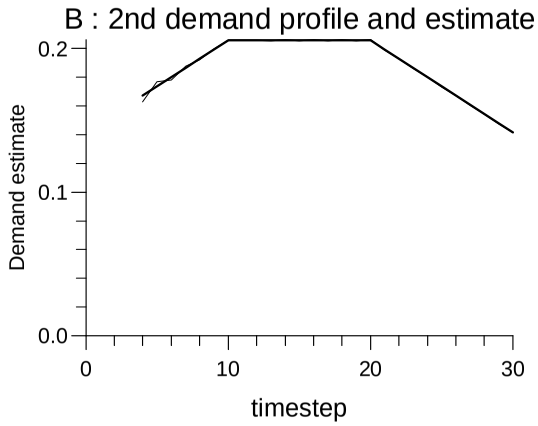
B : 2nd demand profile and estimate
Demand estimate
0.2
0.1
0.0
0
10
20
30
timestep

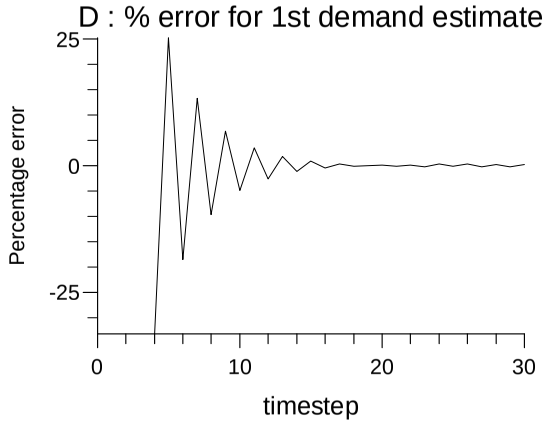
D : % error for 1st demand estimate
Percentage error
25
0
-25
0
10
20
30
timestep

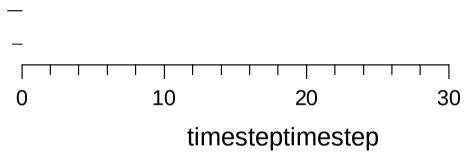
0
10
20
30
timesteptimestep

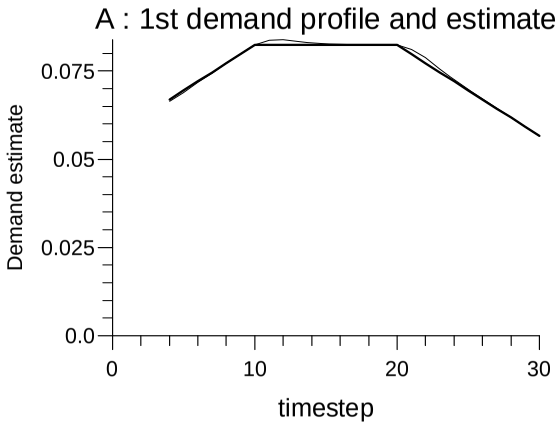
A : 1st demand profile and estimate
Demand estimate
0.075
0.05
0.025
0.0
0
10
20
30
timestep

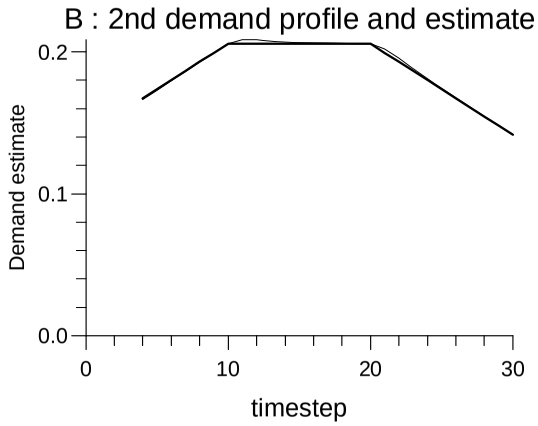
B : 2nd demand profile and estimate
Demand estimate
0.2
0.1
0.0
0
10
20
30
timestep

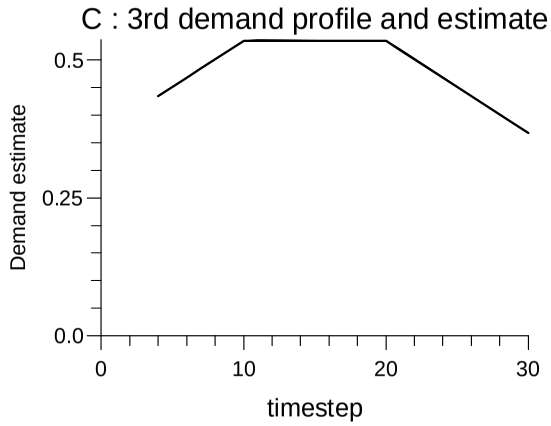
C : 3rd demand profile and estimate
Demand estimate
0.5
0.25
0.0
0
10
20
30
timestep

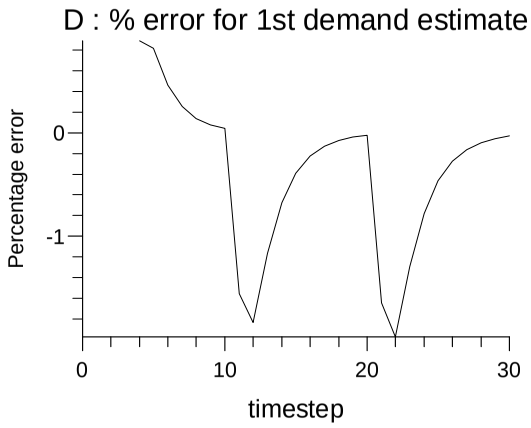
D : % error for 1st demand estimate
Percentage error
0
-1
0
10
20
30
timestep

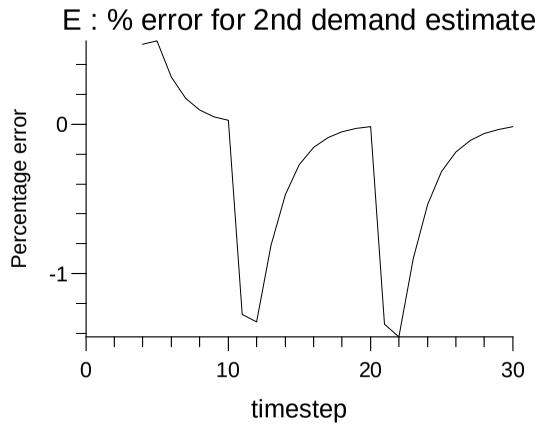
E : % error for 2nd demand estimate
Percentage error
0
-1
0
10
20
30
timestep

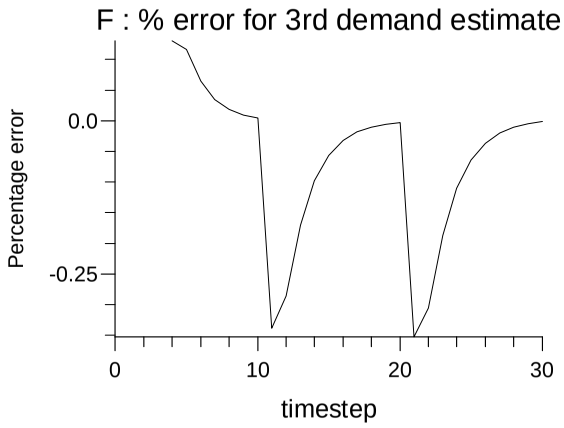
F : % error for 3rd demand estimate
Percentage error
0.0
-0.25
0
10
20
30
timestep

Experiment 6.17

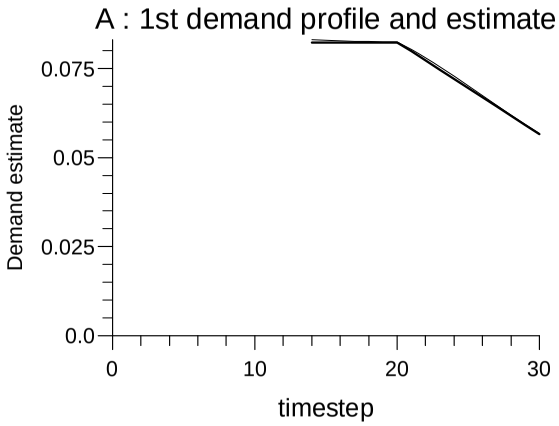

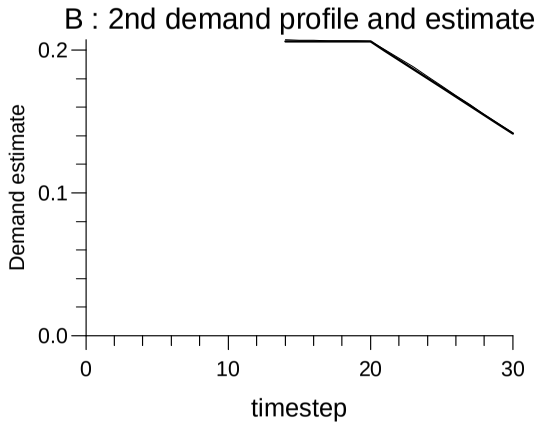

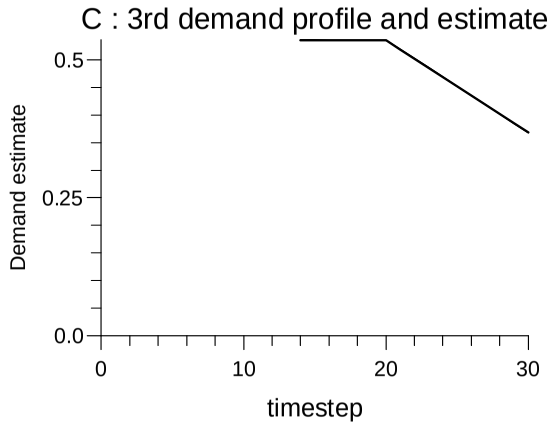

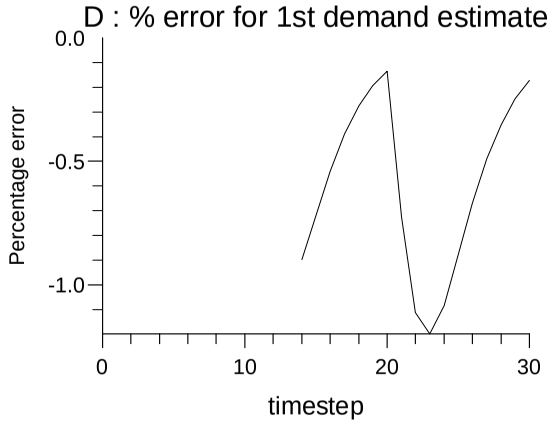

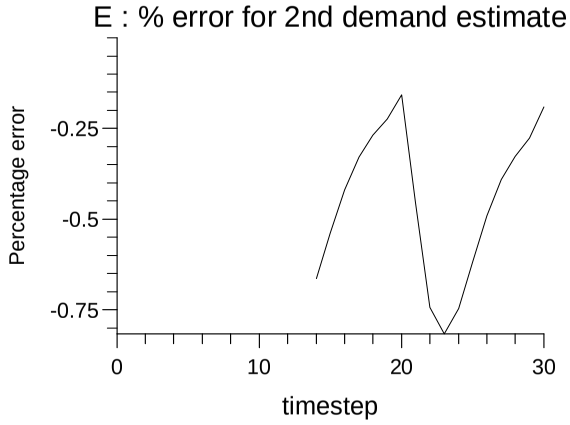

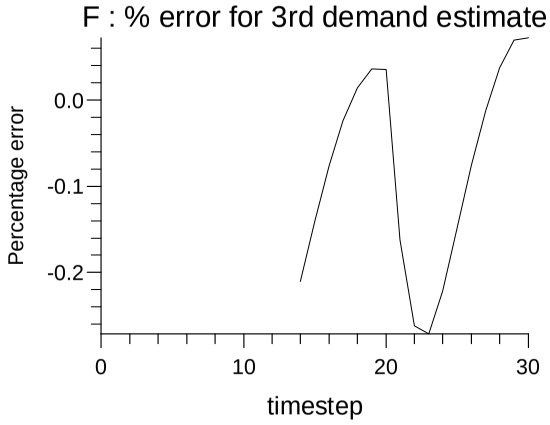

Experiment 6.18

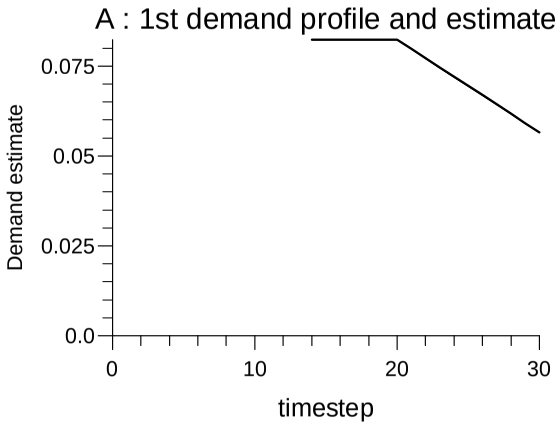

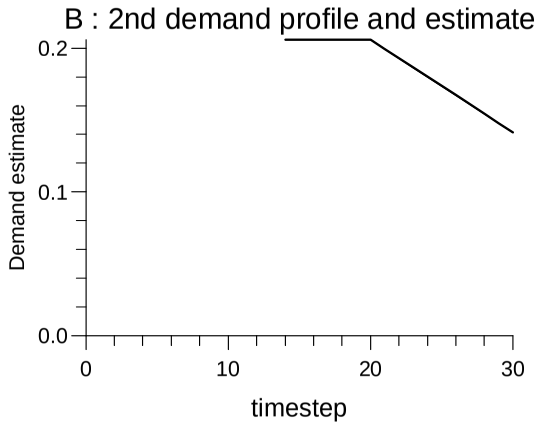

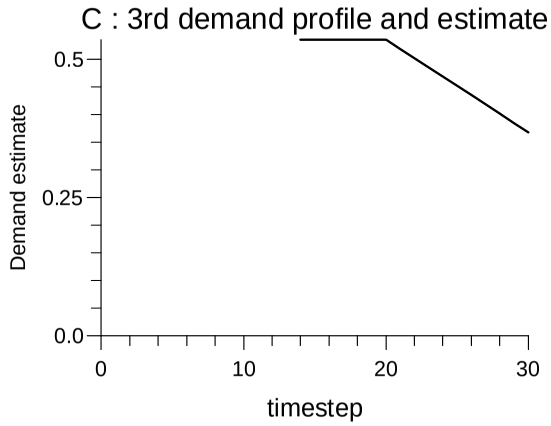

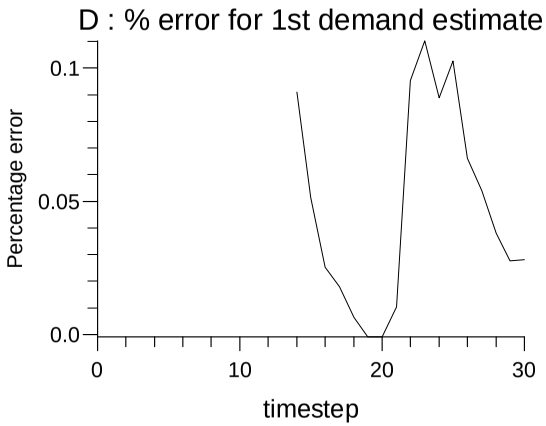

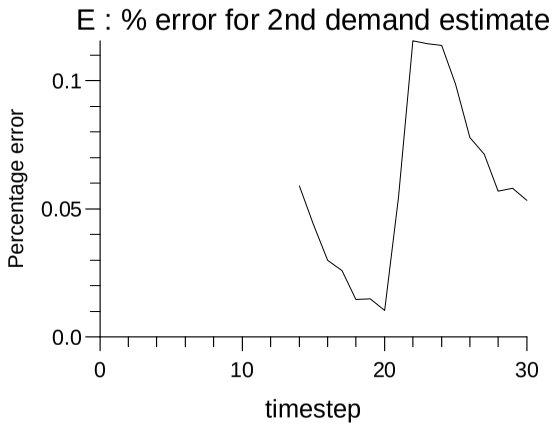

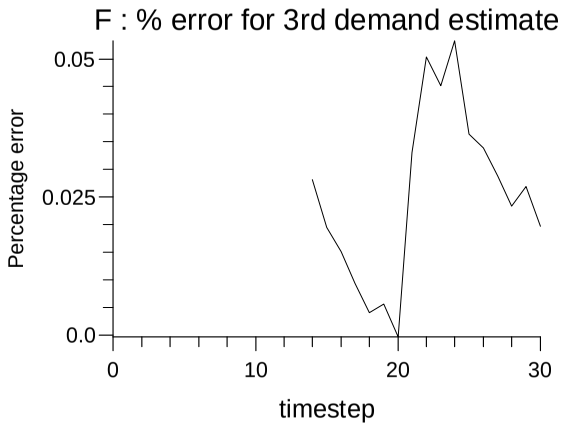

6.4 Discussion

6.4.1 Observer Design A : The Direct Observer

When the weightings, $\tilde{f}_k^{demand\ site}$, were not included in the $\mathcal{M}3$ model, the direct observer gave poor results. However, when the $\tilde{f}_k^{demand\ site}$ were included, for all values of $\theta \in [1/2, 1]$, the state estimate of the direct observer contained no error when data was taken from an $\mathcal{M}0$ model with an identical mesh, and contained only a small amount of error when data was taken from an $\mathcal{M}0$ model with a much finer mesh. Curiously, in contrast to dynamic observer designs, the direct observer gave the most accurate state estimates with $\theta = 1/2$ rather than with $\theta = 1$. The graphs presented begin at timestep 14 due to the need to build up enough timesteps to be able to solve equation (5.4) directly for the state estimate.

The main disadvantage with the direct observer was the large amount of computational work involved.

6.4.2 Observer Design B : The Dynamic Observer Without Feedback at the Current Time-Level

When the weightings, $\tilde{f}_k^{demand\ site}$, were not included in the $\mathcal{M}3$ model, after an initial large error over the first few timesteps characteristic of observer designs, design B observers gave fair estimates of the demand flows when small eigenvalues were assigned. However, these dynamic observers gav

However, if the demand flo

We show that an upper bound on the norm of the error in the state estimate of an $\mathcal{M}3$ model based dynamic observer, caused by modelling error presen

observer system helped to reduce the error in the state estimate.

When the weightings, $\tilde{f}_k^{demand\ site}$, were included in the $\mathcal{M}3$ model, the design B dynamic observer state estimates converged perfectly for $\theta = 1$, with both small and large system eigenvalues. Assigning small system eigenvalues to the design B dynamic observers gave faster convergence. However, as θ moved to 1/2, a very small amount of error began to persist in the state estimate.

Lastly, when pressure data was taken from an $\mathcal{M}0$ model constructed upon a much finer mesh, only a small amount of e f rerytedelato sma a

As with design B observers, $\underline{l}_3(k)$ acts as a forcing term on the errors. However, the matrix H was chosen to minimise the 2-norm of $(E_3 - HC_3)^{-1}$, and this matrix is implicitly multiplied into the forcing term, $\underline{l}_3(k)$, thus reducing its effects. With $\theta = 1$, in the experiments with dynamic observers the 2-norm of the matrix E_3^{-1} was 1.50, while the 2-norm of $(E_3 - HC_3)^{-1}$ was 0.56; this is believed to explain the improvement in the accuracy of the state estimate when feedback is included at the current time-level.

In an equivalent manner to design B observers, it may be shown that the robust eigenstructure assignment technique might help to reduce the error introduced into the state estimate by the form of the modelling error presen

$_3)$

When the weightings, $\tilde{f}_k^{demand\ site}$, were included in the $\mathcal{M}3$ model, the design C dynamic observer state estimates converged perfectly for $\theta = 1$.

Lastly, as with design A and B observers, taking pressure data from an $\mathcal{M}0$ model constructed upon

where I is $g \times g$, and where the H matrix is zero for a design B dynamic observer. This gives a new state estimate for $k = 0, 1, ...$

ith Cycle

This process can be repeated for a number of cycles, each time making use of the discrete jumps in the demands estimated by the previous cycle. The *ith* cycle estimate, $\underline{\hat{x}}_3^i(k)$ for $k = 0, 1, ...,$ is calculated from

$$(E_3 - HC_3)\underline{\hat{x}}_3^i(k+1) = (A_3 - GC_3)\underline{\hat{x}}_3^i(k) + B_3^1\underline{u}_3(k+1) + B_3^2\underline{u}_3(k) - H\underline{y}_3(k+1) + G\underline{y}_3(k)$$
$$+ \begin{bmatrix} 0 & 0 \\ 0 & I \end{bmatrix} (\underline{\hat{x}}_3^{i-1}(k+1) - \underline{\hat{x}}_3^{i-1}(k)) \qquad (7.2)$$

where I is $g \times g$, and where the H matrix is zero for a design B dynamic observer. This gives a new state estimate for $k = 0, 1, ...$

Each further cycle is simply another dynamic observer travelling along the time axis, incorporating information from the state estimate of the previous cycle (dynamic observer). It is not immediately obvious how many cycles should be used; it may be that only a second cycle is needed for a significant improvement in the state estimate. A natural question to ask is what happens to the state estimate, $\underline{\hat{x}}_3^i(k)$ for any timestep k, as $i \longrightarrow \infty$. We have the following convergence theorem for cycling based upon a design C observer only.

Theorem 7.1 *When cycling is performed upon a design C observer, for each timestep, k, $\underline{\hat{x}}_3^i(k)$ tends to a limit as more cycles are performed, i.e.*

$$\underline{\hat{x}}_3^i(k) \longrightarrow \underline{\hat{x}}_3(k) \quad as \quad i \longrightarrow \infty,$$

if and only if all the eigenvalues of $(E_3 - HC_3)^{-1}\Upsilon$ are within the unit circle.

Proof

Consider a timestep T. We wish to investigate the convergence of $\underline{\widehat{x}}_3^i(k)$ for $k = 1, ..., T$, as the number of cycles increases. Define

$$\underline{z}^i = \begin{bmatrix} \underline{\widehat{x}}_3^i(T) \\ \underline{\widehat{x}}_3^i(T-1) \\ \\ \vdots \\ \\ \underline{\widehat{x}}_3^i(2) \\ \underline{\widehat{x}}_3^i(1) \end{bmatrix}.$$

Then from the general cycle equation (7.2), it can be seen $\underline{z}$

$$\underline{v} = \begin{bmatrix} B_3^1 \underline{u}_3(T) + B_3^2 \underline{u}_3(T-1) - H \underline{y}_3(T) + G \underline{y}_3(T-1) \\ B_3^1 \underline{u}_3(T-1) + B_3^2 \underline{u}_3(T-2) - H \underline{y}_3(T-1) + G \underline{y}_3(T-2) \\ \\ \vdots \\ \\ B_3^1 \underline{u}_3(2) + B_3^2 \underline{u}_3(1) - H \underline{y}_3(2) + G \underline{y}_3(1) \\ B_3^1 \underline{u}_3(1) + B_3^2 \underline{u}_3(0) - H \underline{y}_3(1) + G \underline{y}_3(0) + (\end{bmatrix}$$

where $\underline{l}_3(k)$ is a vector containing the $\tilde{f}_k^{demand\ site}$ terms.

The general ith cycle (for $i > 1$) is given by equation (7.2). If we define the error between the ith cycle observer estimate and the model (7.4) to be

$$\underline{e}^i(k) = \underline{x}_3(k) - \underline{\hat{x}}_3^i(k) \tag{7.5}$$

then subtracting equation (7.2) from equation (7.4) gives

$$(E_3 - HC_3)\underline{e}^i(k+1) = (A_3 - GC_3)\underline{e}^i(k) + \underline{l}_3(k) - \Upsilon\underline{\hat{x}}_3^{i-1}(k+1) + \Upsilon\underline{\hat{x}}_3^{i-1}(k)$$

which, using equation (7.5), can be rewritten as

$$(E_3-HC_3)\underline{e}^i(k+1) = (A_3-GC_3)\underline{e}^i(k)+\underline{l}_3(k)-\Upsilon[\underline{x}_3(k+1)-\underline{e}^{i-1}(k+1)]+\Upsilon[\underline{x}_3(k)-\underline{e}^{i-1}(k)]. \tag{7.6}$$

Inspection of the structure of the $\mathcal{M}3$ model (7.4) shows

$$\underline{l}_3(k) = \Upsilon\underline{x}_3(k+1) - \Upsilon\underline{x}_3(k). \tag{7.7}$$

Adding equation (7.7) to equation (7.6) gives

$$(E_3 - HC_3)\underline{e}^i(k + \mathrm{q\ u\ \ w} \qquad \mathrm{T\ f)} \qquad \mathrm{T\ m)\ ,\ T\ j)\ T} \qquad \mathrm{T\ D)\ \ A\ d\ d\ i\ n}$$

where the matrices R and S are as previously defined,

$$\underline{w} = \begin{bmatrix} 0 \\ 0 \\ \\ \vdots \\ \\ 0 \\ f(\underline{e}(0)) \end{bmatrix},$$

$\underline{e}(0) = \underline{e}^i(0)$ for all i, is the error in the observer initial conditions for all cycles, and $f(\underline{e}(0)) = [(A_3 - GC_3) - \Upsilon]\underline{e}(0)$. If system (7.9) has its system eigenvalues within the unit circle and is convergent to a limit, $\underline{\varepsilon}$, then this limit satisfies

$$R\underline{\varepsilon} = S\underline{\varepsilon} + \underline{w},$$

i.e.

$$(R - S)\underline{\varepsilon} = \underline{w}. \tag{7.10}$$

Then we can see that

$$\underline{\varepsilon}^i \longrightarrow (R - S)^{-1}\underline{w} \quad as \quad i \longrightarrow \infty,$$

where the matrix $(R-S)$ is invertible since system (7.9) does not have an eigenvalue equal to 1. From the previous analysis, a sufficient condition for this is $\|(E_3 - HC_3)^{-1}\|_2 < 1$. We can see that if the observers are given (7.10 corrected isTuTD)tcorrectD)tcorrectD)t')tTD)'TjTcorre

as

$$\begin{bmatrix} [(E_3 - HC_3) - \Upsilon] & [-(A_3 - GC_3) + \Upsilon] & & & \\ & \ddots & \ddots & & \\ & & & [(E_3 - HC_3) - \Upsilon] & [-(A_3 - GC_3) + \Upsilon] \\ & & & & [(E_3 - HC_3) - \Upsilon] \end{bmatrix} \begin{bmatrix} \underline{e}(T) \\ \underline{e}(T-1) \\ \vdots \\ \underline{e}(2) \\ \underline{e}(1) \end{bmatrix} = \begin{bmatrix} 0 \\ 0 \\ \vdots \\ 0 \\ f(\underline{e}(0)) \end{bmatrix}$$

where

$$\underline{\varepsilon} = [\underline{e}(T)^T, \underline{e}(T-1)^T, ..., \underline{e}(1)^T]^T.$$

By inspection of the above, we find

$$[(E_{3.(3$$

$$,G,$$

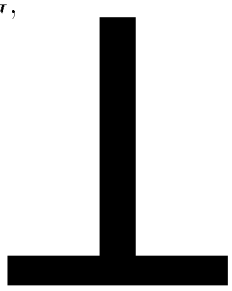

stepping through time. By inspection of the above system, it is immediately apparant that the trivial difference equations for the flows, and thus the modelling error they contain, have been removed. However, it can be shown that it is not now possible to find feedback matrices G and H to assign arbitrary eigenvalues to this new system. This is further explored in the discussion of the experimental results.

7.1 Experiments

When the $\mathcal{M}0$ model had been running for a while, the pressures at the upstream end and the sites of flow demand were recorded at each timestep and fed into the $\mathcal{M}3$ model-based cycling observers. The flow demands predicted by these techniques were then compared with the true flows used as inputs to the $\mathcal{M}0$ model.

For each experiment, the true flow demand profiles for the demands, $D_k^{A/B}$, $D_k^{B/C}$ and D_k^C are shown as thick lines in Figs. A, B and C respectively and the state estimates for $D_k^{A/B}$, $D_k^{B/C}$ and D_k^C are shown as thin lines. The percentage errors between the state estimates of $D_k^{A/B}$, $D_k^{B/C}$ and D_k^C and their true values are shown in Figs. D, E and F respectively.

In all experiments, data was taken from an $\mathcal{M}0$ model with an identical mesh - both $\mathcal{M}0$ and $\mathcal{M}3$ models have 10 Tf)ish en ha

hDTj)Tn hpi

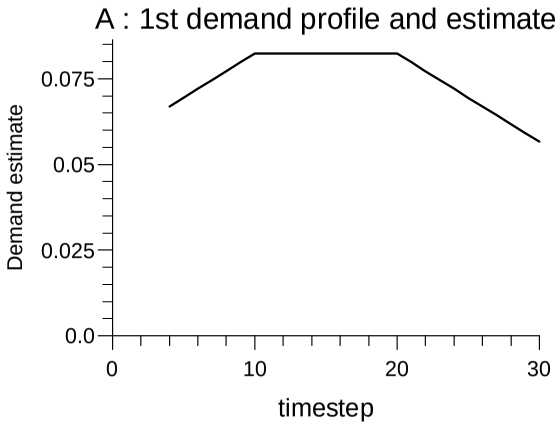
A : 1st demand profile and estimate
Demand estimate
0.075
0.05
0.025
0.0
0
10
20
30
timestep

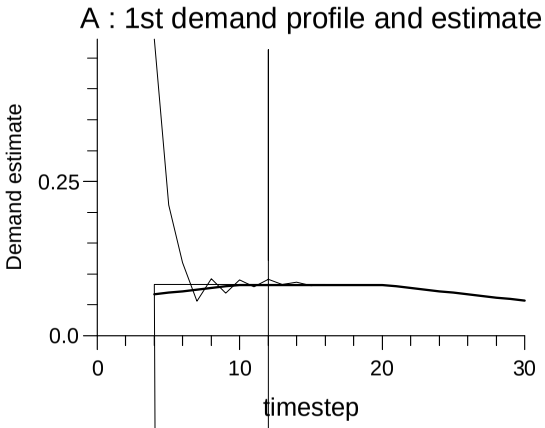
A : 1st demand profile and estimate
Demand estimate
0.25
0.0
0
10
20
30
timestep

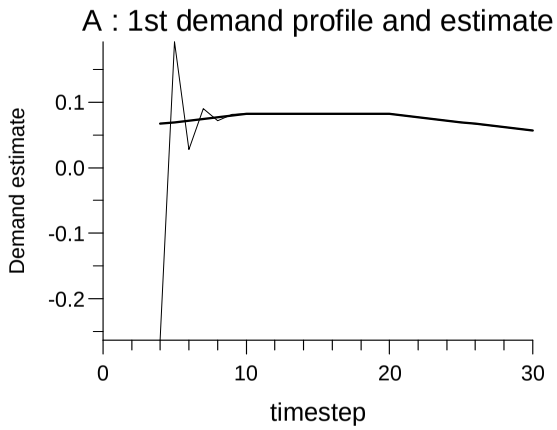
A : 1st demand profile and estimate
Demand estimate
0.1
0.0
-0.1
-0.2
0
10
20
30
timestep

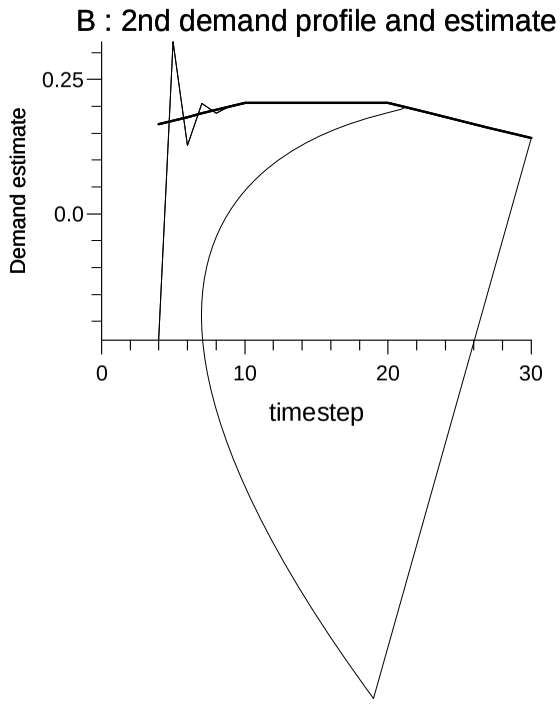
B : 2nd demand profile and estimate
Demand estimate
0.25
0.0
0
10
20
30
timestep

7.2 Discussion

The graphical results of these experiments should be compared to the graphical results of the previous chapter.

Regarding the '2 cycle' experiments, 7.1 to 7.3, only with the design C observer, was the state estimate much improved over the entire flow profile. However, with the design B observer, there was significant improvement in the state estimate of certain parts of the flow profiles from the second cycle. The second cycles seemed to perform badly where the gradient of the flow profile changed sharply, but significantly improved those parts of the flow profiles for which the demand jumps, $\tilde{f}_k^{demand\ site}$, were constant. This is not yet understood, but it may be that it would be possible to determine periods in the day where those parts of the flow profiles would respond well to a second cycle.

Regarding the 'many-cycle' experiment, 7.4, the cycling technique was found to be convergent only when a design C observer was being used. This behaviour can be explained by noting that with the design C observer, with $\theta = 1$, we had $\|(E_3 - HC_3)^{-1}\|_2 = 0.56 < 1$, and hence, as the previous analysis showed, the cycling technique was convergent. Without feedback at the current time-level being incorporated into the basic dynamic observer design, this convergence was lost.

The error in the design C observer state estimates, was seen to be very significantly reduced by cycling to convergence for $\theta = 1$. Indeed, the error was seen to decay completely away with time. This behaviour can be explained by the following.

When a cycling technique, based upon a design C observer with $\|(E_3 - HC_3)^{-1}\|_2 < 1$, converged, we showed that the error in the state estimate obeyed equation (7.11)

$$[(E_3 - HC_3) - \Upsilon]\underline{e}(k+1) = [(A_3 - GC_3) - \Upsilon]\underline{e}(k).$$

If we assume the $\mathcal{M}3$ model is arranged according to equation (6.3), and that the base $\mathcal{M}0$ model is arranged according to equation (4.1), then the $\mathcal{M}3$ model may be written

need to be within the unit circle.

How best to use the cycling technique is still not understood. When the cycling technique is not convergent, we can still get some improvement in the state estimate of certain parts of the flow profiles from a second cycle. The second cycle seemed to improve significantly those parts of the flow profiles for which the demand jumps, $\tilde{f}_k^{demand\ site}$, were constant. This might be particularly useful for a design B observer with $\theta = 1/2$, since for $\theta = 1/2$, the corresponding $\mathcal{M}2$ model has multiple eigenvalues equal to -1, and is not asymptotically stable.

The most significant improvement in the state estimate came when the cycling tec

Chapter

The Effects of Pressure Measurement Bias on 1 and 2 Models, and 3 Model Based Observers

It may be the case that the pressure measurements at the sites of flow demand are subject to a constant bias, i.e. instead of using a true value for $\underline{p}_2(k)$, we drive the models and observers with

$$\underline{p}_{2_{measured}}(k) = \underline{p}_2(k) + \underline{b} \tag{8.1}$$

where $\underline{b}$ represents a vector of biases, constant with time. These constant biases will introduce error into the state estimates of the different estimation techniques. This is a serious problem for flow demand estimation due to the sensitivity of the flow demand variables to perturbations in the pressures.

We denote the corrupted model and observer state estimates by $\underline{x}_{est}(k)$ where

$$\underline{x}_{est}(k) = \underline{x}(k) + \underline{x}_{err}(k)$$

and $\underline{x}_{err}(k)$ is the error introduced into the state estimate due to the measurement bias. Similarly we specifically denote the corrupted state estimates of $\underline{p}_1(k)$, $\underline{p}_2(k)$ and $\underline{d}(k)$ by

$$\underline{p}_{1_{est}}(k) = \underline{p}_1(k) + \underline{p}_{1_{err}}(k),$$

$$\underline{p}_{2_{est}}(k) = \underline{p}_2(k) + \underline{p}_{2_{err}}(k),$$

dTjTd,tTjTerrTjkTmTTtkt/t

If we arrange the pressure variables in the state vector in their order along the pipe network, i.e. in the following way

$$\underline{x}_1(k) = [p^1_{1,k}, p^1_{2,k}, ..., p^1_{s^1-1,k}, p^2_{1,k}, p^2_{2,k}, ..., p^2_{s^2-1,k}, ...$$

From equation (8.8) we have

$$2\Gamma_j^z p_{j_{err}}^z = \Gamma_{j-1}^z p_{j-1_{err}}^z + \Gamma_{j+1}^z p_{j+1_{err}}^z. \tag{8.10}$$

Equation (8.10) combined with inequality (8.9) implies

$$\Gamma_{j-1}^z p_{j-1_{err}}^z = \Gamma_j^z p_{j_{err}}^z$$

$$\Gamma_{j+1}^z p_{j+1_{err}}^z = \Gamma_j^z p_{j_{err}}^z.$$

We can continue in this way to show that all the $\Gamma_i^z p_{i_{err}}^z$ are equal for $i = 0, ..., s^z$. So if we had a maximum value for $\Gamma_i^z p_{i_{err}}^z$ occur internally along the pipe, i.e. for $i = 1, ..., s^z - 1$, then for that particular *internal* node, say node j, we would have

$$\Gamma_j^z p_{j_{err}}^z = \Gamma_0^z p_{0_{err}}^z = \Gamma_{s^z}^z p_{s_{err}^z}^z. \tag{8.11}$$

Hence

$$\Gamma_i^z p_{i_{err}}^z \leq MAX(\Gamma_0^z p_{0_{err}}^z, \Gamma_{s^z}^z p_{s_{err}^z}^z) \quad for\ i = 1, ..., s^z - 1. \tag{8.12}$$

By considering a minimum value for $\Gamma_i^z p_{i_{err}}^z$ occurring along the pipe, we can similarly derive

$$\Gamma_i^z p_{i_{err}}^z \geq MIN(\Gamma_0^z p_{0_{err}}^z, \Gamma_{s^z}^z p_{s_{err}^z}^z) \quad for\ i = 1, ..., s^z - 1. \tag{8.13}$$

From bounds (8.12) and (8.13) we have for a general pipe z

$$MIN[\frac{\Gamma^{z-1/z} b^{z-1/z}}{\Gamma_i^z}, \frac{\Gamma^{z/z+1} b^{z/z+1}}{\Gamma_i^z}] \leq p_{i_{err}}^z \leq MAX[\frac{\Gamma^{z-1/z} b^{z-1/z}}{\Gamma_i^z}, \frac{\Gamma^{z/z+1} b^{z/z+1}}{\Gamma_i^z}] \ for\ any\ node\ i. \tag{8.14}$$

where we have denoted the upstream and downstream normalised measurement biases, $p_{0_{err}}^z$ and $p_{s_{err}^z}^z$, by $b^{z-1/z}$ and $b^{z/z+1}$ respectively. Equation (8.14) represents bounds on the constant errors in the normalised state estimate of the pressures along a general pipe z, due to measurement bias. It can be seen that the estimate errors depend only on the measurement biases at the two ends of the particular pipe z.

If we assume the measurement biases are not greater than 1 bar or less than −1 bar, then we have

$$-1 \leq b^{z-1/z} N_p \leq 1 \quad and \quad -1 \leq b^{z/z+1} N_p \leq 1. \tag{8.15}$$

However, for a typical gas network we would have

$$35\ bar \leq True\ pressure \leq 70\ bar. \tag{8.16}$$

Multiplying inequality (8.14) by N_p, and combining with inequalities (8.15) and (8.16), gives

$$\left|\frac{Error\ in\ pressure\ estimate}{True\ pressure}\right| \leq 1/35 \times MAX[\frac{\Gamma^{z-1/z}}{\Gamma_i^z}, \frac{\Gamma^{z/z+1}}{\Gamma_i^z}] \quad for\ node\ i\ of\ pipe\ z. \tag{8.17}$$

If the Γ^s do not vary greatly along each pipe, then we can see that the pressure estimates [illegible] mped by the error introduced by measurement bias.

[illegible] ow examine the asymptotic steady error in the st[illegible] timate of the flow demands d[illegible] e measurement b[illegible] is an $\mathcal{M}1$ [illegible] lised in [illegible] w p[illegible] at the ends of e[illegible] pe secti[illegible] by app[illegible] or b[illegible] ds [illegible] ence discreti[illegible] of equ[illegible] (2.13) [illegible] for a gene[illegible] an u[illegible] pip[illegible], we woul[illegible] e

$$q [illegible] = -\epsilon_3^z(\Gamma_1^z p_{1,k_{est}} - \Gamma_0^z p_{0,k_{est}}) \tag{8.18}$$

[illegible] downst[illegible] pip[illegible], we would have

$$[illegible] = -\epsilon_3^z(\Gamma_{s^z}^z p_{s^z}^z [illegible]$$

$$q^z_{s^z_{err}} = -\epsilon^z_3(\Gamma^z_{s^z} p^z_{s^z_{err}} - \Gamma^z_{s^z-1} p^z_{s^z-1_{err}})/\delta x^z \tag{8.22}$$

and

$$d^{z/z+1}_{err} = q^z_{s^z_{err}} - q^{z+1}_{0_{err}} \tag{8.23}$$

respectively, where $q^z_{0_{err}}$, $q^z_{s^z_{err}}$ and $d^{z/z+1}_{err}$ are the steady errors due to measurement bias in the estimates of $q^z_{0,k}$, $q^z_{s^z,k}$ and $d^{z/z+1}_k$ respectively.

Next we examine the solution to the $s^z - 1$ scalar equations (8.8) in order to derive an explicit formula for $q^z_{0_{err}}$ and $q^z_{s^z_{err}}$ in terms of the measurement biases $b^{z-1/z}$ and $b^{z/z+1}$. For a general pipe z, let

$$\eta^z = \Gamma^z_1 p^z_{1_{err}} - \Gamma^z_0 p^z_{0_{err}}. \tag{8.24}$$

The first scalar equation from the system of scalar equations (8.8) is

$$-\Gamma^z_0 p^z_{0_{err}} + 2\Gamma^z_1 p^z_{1_{err}} - \Gamma^z_2 p^z_{2_{err}} = 0. \tag{8.25}$$

Combining equation (8.25) with equation (8.24) gives

$$\eta^z = \Gamma^z_2 p^z_{2_{err}} - \Gamma^z_1 p^z_{1_{err}}. \tag{8.26}$$

We can continue to show for pipe z

$$\Gamma^z_{i+1} p^z_{i+1_{err}} - \Gamma^z_i p^z_{i_{err}} = \eta^z \quad for\ i = 0, ..., s^z - 1. \tag{8.27}$$

Substituting equation (8.27) into equation (8.21) and equation (8.22) gives

$$q^z_{0_{err}} = q^z_{s^z_{err}} = -\epsilon^z_3 \eta^z/\delta x^z. \tag{8.28}$$

However, adding all s^z equations of the form (8.27) i.e for $i = 0, ..., s^z - 1$, gives

$$\Gamma^z_{s^z} p^z_{s^z_{err}} - \Gamma^z_0 p^z_{0_{err}} = s^z \eta^z. \tag{8.29}$$

Rearranging equation (8.29) gives

$$\eta^z = (\Gamma^z_{s^z} p^z_{s^z_{err}} - \Gamma^z_0 p^z_{0_{err}})/s^z. \tag{8.30}$$

Substituting equation (8.30) into equation (8.28) and using $s^z \delta x^z = 1$, gives

$$q^z_{0_{err}} = q^z_{s^z_{err}} = -\epsilon^z_3(\Gamma^{z/z+1} b^{z/z+1} - \Gamma^{z-1/z} b^{z-1/z}). \tag{8.31}$$

The estimates of the flow demands can be shown to be more sensitive than the estimates of the pressures to measurement bias. If we assume the real gas network is operating in a fairly steady state, then system (3.2) also reaches a steady state. Then in a similar way as for equation (8.31), we can derive

$$q_0^z = q_{s^z}^z = -\epsilon_3^z(\Gamma^{z/z+1}p^{z/z+1} - \Gamma^{z-1/z}p^{z-1/z}) \tag{8.32}$$

where q_0^z, $q_{s^z}^z$, $p^{z-1/z}$ and $p^{z/z+1}$ are the steady states of $q_{0,k}^z$, $q_{s^z,k}^z$, $p_{0,k}^z$ and $p_{s^z,k}^z$ respectively. We assume we have a small inline flow in pipe section z and that we have linearised about $\mathcal{Q}^z = 0$, then from equations (8.31), (8.32) we may derive

Error in normalised pipe end flowlisederoul10Tf/TDc<Tj<Tf<DceTD<.kTj<TTf<TD<zTj<T<qT

8.2 $\mathcal{M}2$ odels

Consider the $\mathcal{M}$

which is identical to equation (8.5) for the $\mathcal{M}1$ model. $\underline{d}_{err}$ is then given by the last g rows of system (8.38), which correspond to the $g-1$ connectivity equations, and the single downstream flow boundary equation.

We denote the corrupted state estimates of the downstream flow of the last pipe $q^g_{s^g,k}$, and the demand flow $d_k^{z/z+1}$ at the general pipe junction $z/z+1$, by

$$q^g_{s^g,k_{est}} = q^g_{s^g,k} + q^g_{s^g,k_{erestimates}} \quad te\ rruted\ state\ estimates \quad ts \quad tetis \quad te\ rruted\ tate$$

$$+(\Phi^{z/z+1}\epsilon_3^{z+1}\Gamma_1^{z+1}(1-\theta)/\delta x^{z+1})p_{1,k_{err}}^{z+1} - \Phi^{z/z+1}(1-\theta)d_{k_{err}}^{z/z+1}.$$

Thus, the last g rows of system (8.38) contain $g-1$ scalar equations of the following form for the variables, $d_{err}^{z/z+1}$

$$-(\Phi^{z/z+1}\epsilon_3^z\Gamma_{s^z-1}^z/\delta x^z)p_{s^z-1_{err}}^z + (\Phi^{z/z+1}\epsilon_3^z\Gamma^{z/z+1}/\delta x^z + \Phi^{z/z+1}\epsilon_3^{z+1}\Gamma^{z/z+1}/\delta x^{z+1})p_{err}^{z/z+1}$$

$$-(\Phi^{z/z+1}\epsilon_3^{z+1}\Gamma_1^{z+1}/\delta x^{z+1})p_{1_{err}}^{z+1} + \Phi^{z/z+1}d_{err}^{z/z+1} = 0$$

and dividing through by $\Phi^{z/z+1}$ and rearranging gives

$$d_{err}^{z/z+1} = \{-\epsilon_3^z(\Gamma^{z/z+1}p_{err}^{z/z+1} - \Gamma_{s^z-1}^z p_{s^z-1_{err}}^z)/\delta x^z\} - \{-\epsilon_3^{z+1}(\Gamma_1^{z+1}p_{1_{err}}^{z+1} - \Gamma^{z/z+1}p_{err}^{z/z+1})/\delta x^{z+1}\}. \quad (8.40)$$

Returning again to the equations governing the errors in the flow estimates of an $\mathcal{M}1$ model, if we substitute equations (8.21) and (8.22) into equation (8.23), then we derive an equation which gives the error in a junction flow estimate of an $\mathcal{M}1$ model, and which is identical to equation (8.40). Hence, we have shown the asymptotic errors in the junction flow estimates of an $\mathcal{M}2$ model are equal to the asymptotic errors in the junction flow estimates of an $\mathcal{M}1$ model.

8.3 Observers Constructed Upon $\mathcal{M}3$ odels

We show that the error due to measurement bias introduced into state estimate of the direct observer, and the asymptotic steady error introduced into a dynamic observer, constructed upon $\mathcal{M}3$ models, are both equal to the asymptotic error introduced into an $\mathcal{M}2$ model. We assume the observers are constructed upon un-weighted $\mathcal{M}3$ models (6.4); however, the same results may be obtained for weighted $\mathcal{M}3$ models (6.23) by incorporating the vector of weightings, $\underline{l}_3(k)$, into the analysis.

If the $\mathcal{M}2$ model is arranged and partitioned according to equation (4.2), then equation (8.35) may be written in the form

$$\begin{bmatrix} E' & -B^{1''} \end{bmatrix} \begin{bmatrix} \underline{p}_{1_{est}}(k+1) \\ \underline{d}_{est}(k+1) \end{bmatrix} = \begin{bmatrix} A' & B^{2''} \end{bmatrix} \begin{bmatrix} \underline{p}_{1_{est}}(k) \\ \underline{d}_{est}(k) \end{bmatrix} + \begin{bmatrix} B^{1'} & -E'' \end{bmatrix} \begin{bmatrix} \underline{p}_3(k+1) \\ \underline{p}_2(k+1) + \underline{b} \end{bmatrix}$$

$$+ \begin{bmatrix} B^{2'} & A'' \end{bmatrix} \begin{bmatrix} \underline{p}_3(k) \\ \underline{p}_2(k) + \underline{b} \end{bmatrix}. \quad (8.41)$$

If equation (4.2) is subtracted from equation (8.41), we derive

$$\begin{bmatrix} E' & -B^{1''} \end{bmatrix} \begin{bmatrix} \underline{p}_{1_{err}}(k+1) \\ \underline{d}_{err}(k+1) \end{bmatrix} = \begin{bmatrix} A' & B^{2''} \end{bmatrix} \begin{bmatrix} \underline{p}_{1_{err}}(k) \\ \underline{d}_{err}(k) \end{bmatrix} - E''\underline{b} + A''\underline{b}. \quad (8.42)$$

System (8.42) is equivalent to system (8.37) and describes how the state estimate error due to constant measurement bias behaves. As explained previously for system (8.37), system (8.42) reaches a steady state given by

$$\left[\begin{array}{cc} [E' - A'] & [-B^{1''} - B^{2''}] \end{array} \right] \left[\begin{array}{c} \underline{p}_{1_{err}} \\ \underline{d}_{err} \end{array} \right] = -E''\underline{b} + A''\underline{b}. \tag{8.43}$$

We show that the error due to measuremen

$$[\underline{y}_3(k) + \underline{b}]^T, [\underline{y}_3(k+1) + \underline{b}]^T, ..., [\underline{y}_3(k+n-1) + \underline{b}]^T\},$$

and n is the number of timesteps over which equation (8.44) is solved.

If equation (5.4) is subtracted from equation (8.44), we derive

$$\Theta \underline{\mathcal{X}}_{err} = \underline{\Delta}_{bias}. \tag{8.45}$$

where

$$\underline{\mathcal{X}}^T_{err} = \{\underline{\widehat{x}}_{3_{err}}(k)^T, \underline{\widehat{x}}_{3_{err}}(k+1)^T, \underline{\widehat{x}}_{3_{err}}(k+2)^T, ...\underline{\widehat{x}}_{3_{err}}(k+n-1)^T\},$$

$\underline{\widehat{x}}_{3_{err}}(k)$ is the error due to measurement bias in the observer estimate for $\underline{x}_3(k)$, and

$$\underline{\Delta}^T_{bias} = \{\underline{0}^T, \underline{0}^T, ..., \underline{0}^T, \underline{b}^T, \underline{b}^T, ...\underline{b}^T\}.$$

We observe that system (5.4) is the usual direct observer constructed upon an $\mathcal{M}3$ model.

As shown previously in chapter 5, if the underlying $\mathcal{M}3$ model accurately deeo˜˜cbele11BT1n]bserv

where the matrix H may be zero for design B dynamic observers.

If equation (5.25) is subtracted from equation (8.51), we derive

$$(E_3 - HC_3)\underline{\hat{x}}_{3_{err}}(k+1) = (A_3 - GC_3)\underline{\hat{x}}_{3_{err}}(k) - H\underline{b} + G\underline{b}. \tag{8.52}$$

We observe that system (5.25) is the usual dynamic observer constructed upon an $\mathcal{M}3$ model. As shown previously in chapter 5, if the underlying $\mathcal{M}3$ model accurately describes the behaviour of the gas network, system (5.25) will tend asymptotically to the true state of the gas network. Then system (8.52) describes how the state estimate error, $\underline{\hat{x}}_{3_{err}}(k)$, due to constant measurement bias behaves.

Since the original observer system is assigned eigenvalues within the unit circle, system (8.52) also has its eigenvalues within the unit circle and is asymptotically stable. Also, since the input to system (8.52), $-H\underline{b} + G\underline{b}$, is constant, the system tends with time to a steady state, $\underline{\hat{x}}_{3_{err}}$, given by

$$[(E_3 - HC_3) - (A_3 - GC_3)]\underline{\hat{x}}_{3_{err}} = -H\underline{b} + G\underline{b}. \tag{8.53}$$

Assuming the $\mathcal{M}3$ model is arranged and partitioned as in equation (6.3), and the base $\mathcal{M}0$ system is arranged and partitioned according to equation (4.1), then equation (8.53) can be written in the form

$$\begin{bmatrix} [E' - A' \\ \\ \end{bmatrix}$$

which is identical to equation (8.43).

Hence, the asymptotic error in the $\mathcal{M}3$ model-based dynamic observer due to the constant measurement bias of equation (8.1), is identical to both the error introduced into the state estimate of a direct observer and the asymptotic error introduced into the state estimate of $\mathcal{M}2$ models, which in turn is identical to the asymptotic error introduced into the state estimate of $\mathcal{M}1$ models.

8.4 Experiments

As the $\mathcal{M}0$ model was run, the pressures at the upstream end and the sites of flow demand were recorded at each timestep. The pressure measurements at the three flow demand sites, A/B, B/C and C, were then corrupted by constant biases of 1 bar, -1 bar and 1 bar respectively. These corrupted pressures were then fed into the $\mathcal{M}1$ and $\mathcal{M}2$ models, and $\mathcal{M}3$ model based observers. The flow demands predicted by these estimation techniques were then compared with the true flows used as inputs to the $\mathcal{M}0$ model.

For each experiment, the true flow demand profiles for the demands, $D_k^{A/B}$, $D_k^{B/C}$ and D_k^C are shown as thick lines in Figs. A, B and C respectively, and the state estimates for $D_k^{A/B}$, $D_k^{B/C}$ and D_k^C are shown as thin lines. The percentage errors between the state estimates of $D_k^{A/B}$, $D_k^{B/C}$ and D_k^C and their true values are shown in Figs. D, E and F respectively.

The $\mathcal{M}3$ model based observers include the exact values of the weightings, $\tilde{f}_k^{demand\ site}$, in the trivial flow demand difference equations so that the effects of the measurement biases may be observed without other forms of error present.

Data taken from $\mathcal{M}0$ model with identical mesh - $\mathcal{M}0$, $\mathcal{M}1$, $\mathcal{M}2$ and $\mathcal{M}3$ models have 10 spatial nodes along each pipe.

Experiment 8.1) $\mathcal{M}1$ Model with $\theta = 1$

Experiment 8.2) $\mathcal{M}2$ Model with $\theta = 1$

Experiment 8.3) Observer Design B (small eigenvalues) with $\theta = 0.5$

Experiment 8.4) Observer Design C (small eigenvalues) with $\theta = 1$

Data taken from $\mathcal{M}0$ model with identical mesh - $\mathcal{M}0$ and $\mathcal{M}3$ models have 5 spatial nodes along each pipe.

Experiment 8.5) Observer Design A with $\theta = 0.5$

Experiment 8.1

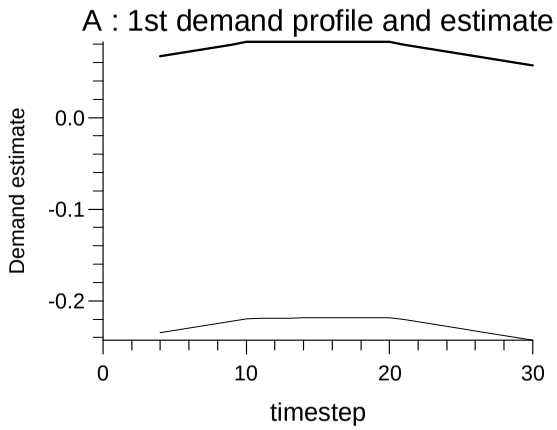

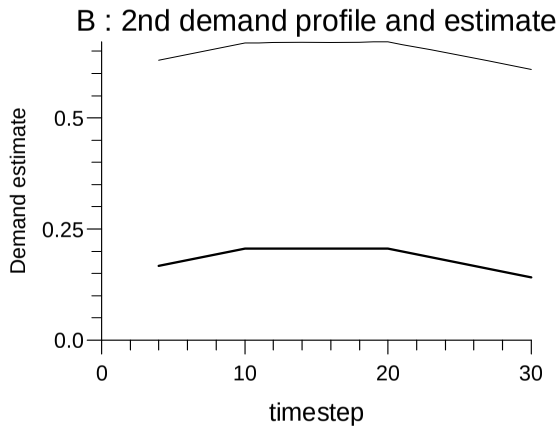

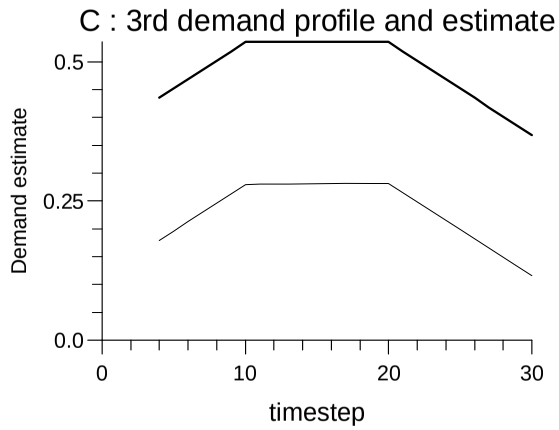

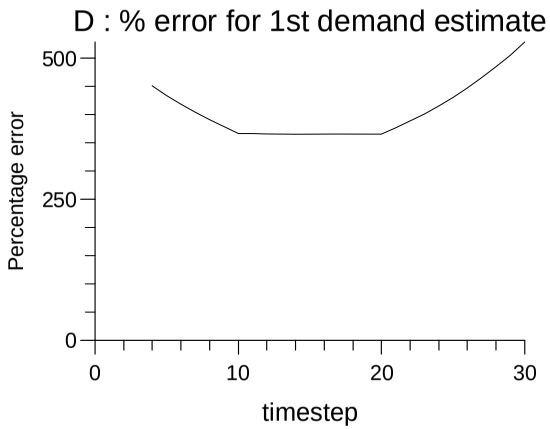

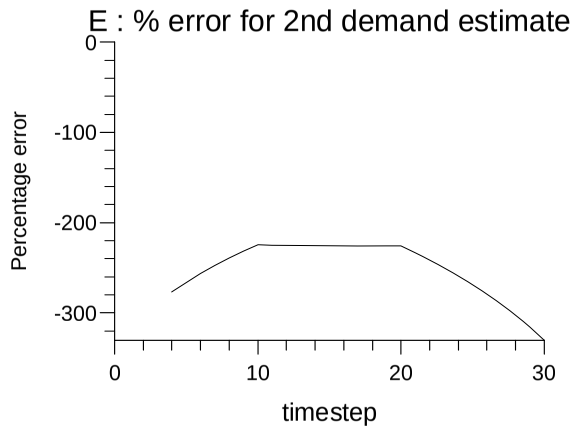

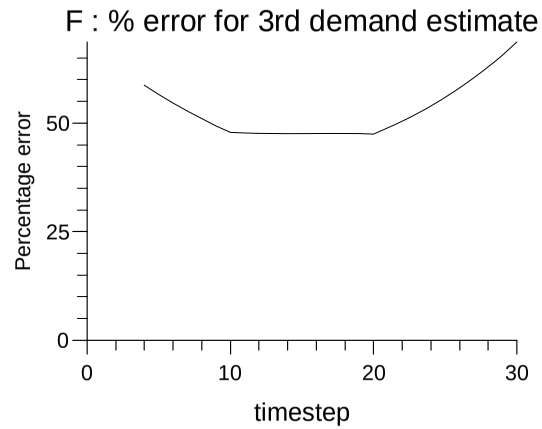

Experiment 8.3

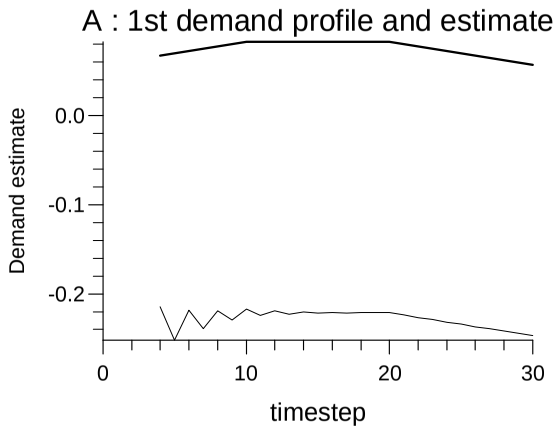

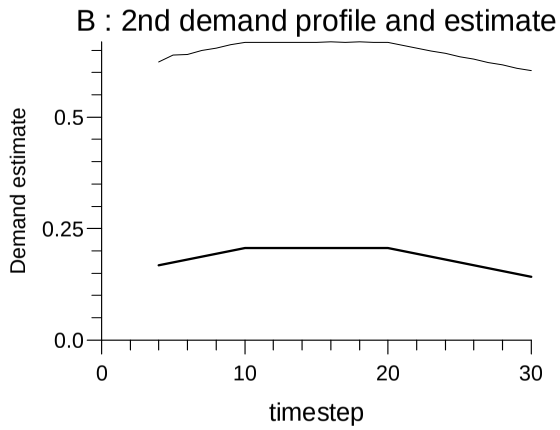

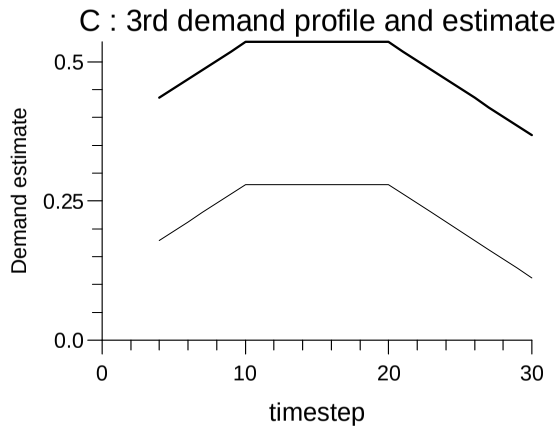

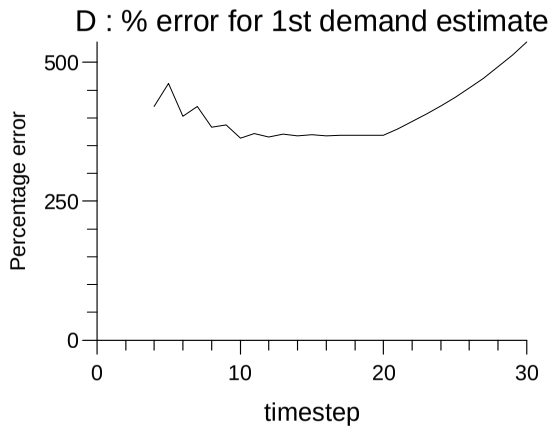

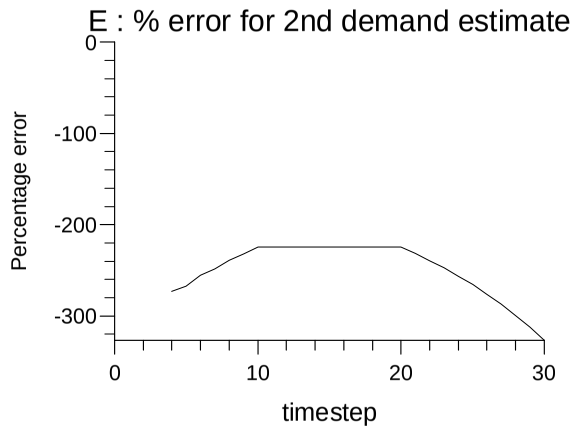

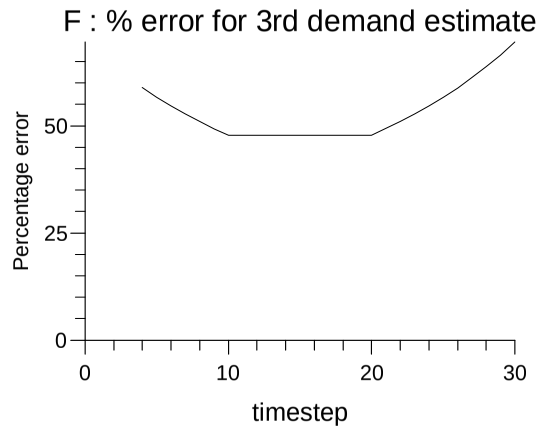

Experiment 8.5

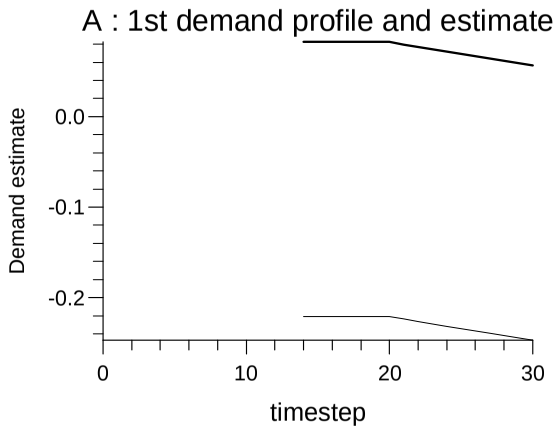

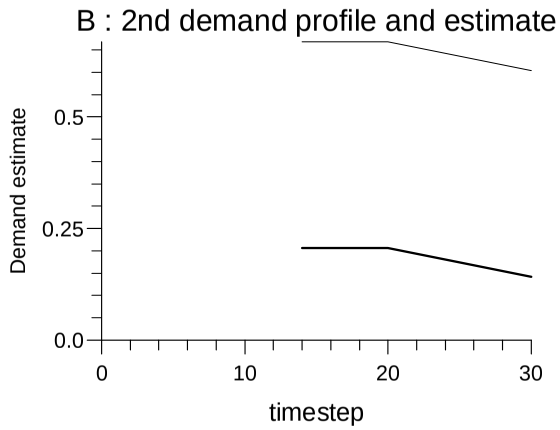

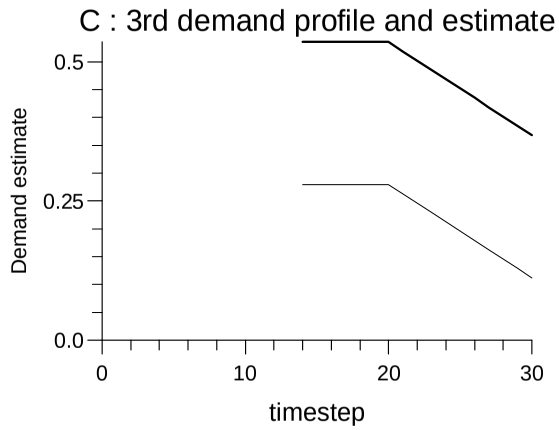

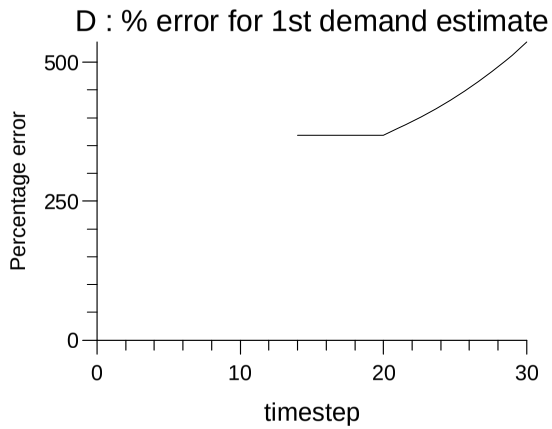

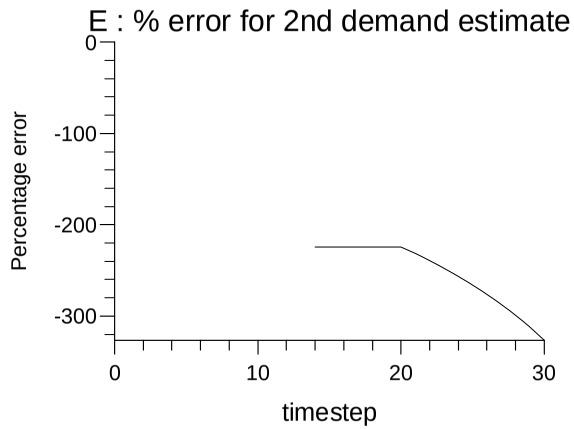

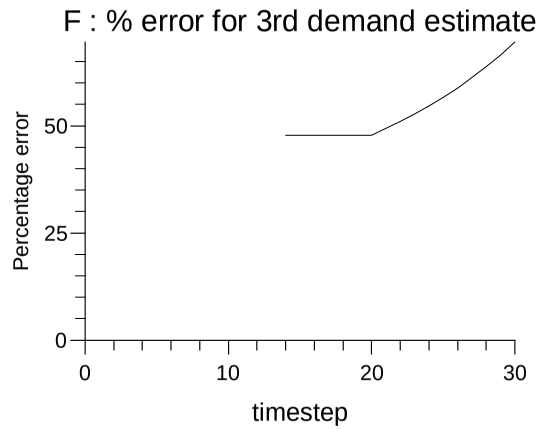

8.5 Discussion

The estimates of the flow demands, from all of the flow estimation techniques, were completely swamped by the error introduced by pressure measurement bias. Hence, a technique must be found to deal with such measurement biases. One approach would be to consider such biases as sensor faults and investigate fault diagnosis winiagnosistecfa[33].T1˜TD1

for some initial conditions. In the preceding analysis of this chapter, it was shown that the error in the direct observer estimate was given by a steady $\mathcal{M}3$ model sequence

$$E_3 \underline{\hat{x}}_{3_{err}}(k+1) = A_3 \underline{\hat{x}}_{3_{err}}(k) \tag{8.57}$$

consistent with constraints

$$C_3 \underline{\hat{x}}_{3_{err}}(k) = \underline{\hat{p}}$$

Chapter 9

Measurement Bias and 4 Models

It may be the case that the pressure measurements at the sites of flow demand are subject to a constant bias, i.e.

$$\underline{y}(k) = \underline{p}_2(k) + \underline{b}(k) \tag{9.1}$$

where $\underline{b}(k)$ is a g dimensional vector of constant measurement biases. This is a serious problem for flow demand estimation and these pressure measurement biases need also to be estimated.

The g measurement biases are assumed to obey

$$\underline{b}(k+1) = \underline{b}(k). \tag{9.2}$$

To try to estimate these biases, we construct a new model variation, which we denote by $\mathcal{M}4$. As with the construction of the earlier $\mathcal{M}3$ model, we start from a base $\mathcal{M}0$ model. As before we first incorporate the input variables, $\underline{d}(k)$, into the state vector, but this time the $\mathcal{M}4$ models assume trivial difference equations for the flow demands of the form

$$flow\ demand_{k+1}^{demand\ site} = w_k^{demand\ site} \times flow\ demand_k^{demand\ site}$$

where the $w_k^{demand\ site}$ are estimated from other measured flow demands. After normalisation, we would have

$$normalised\ flow\ demand_{k+1}^{demand\ site} = w_k^{demand\ site} \times normalised\ flow\ demand_k^{demand\ site},$$

that is, we would have

$$\mathcal{Q}^{demand\ site} + d_{k+1}^{demand\ site} = w_k^{demand\ site} \times (\mathcal{Q}^{demand\ site} + d_k^{demand\ site}). \tag{9.3}$$

Hence, the normalised and linearised gas network $\mathcal{M}4$ models now contain difference equations of the form

$$d_{k+1}^{demand\ site} \;=\; w_k^{demand\ site} \times d_k^{demand\ site} \;+\; (w_k^{demand\ site} - 1) \times \mathcal{Q}^{demand\ site}. \qquad (9.4)$$

These scalar equations may be written together as the following sub-system of the $\mathcal{M}4$ model

$$\underline{d}(k+1) \;=\; W(k$$

the sites of flow demand are not needed as inputs to the $\mathcal{M}4$ model, and are, in fact, measurements of its state variables

$$\underline{y}_4(k) = C_4\underline{x}_4(k), \tag{9.7}$$

available for use in a direct or dynamic observer.

9.1 Theorems

In this section, we firstly prove that the matrix E_4 of an $\mathcal{M}4$ model is full rank if $\theta > 0$. Secondly, we prove certain conditions to be sufficient to guarantee the assignability of eigenvalues to the observer at a particular timestep. In fact, we show that for $1/2 \leq \theta \leq 1$, if at a particular timestep, the diagonal elements of $W(k)$ are not equal to either 1 or to any of the eigenvalues of the corresponding $\mathcal{M}2$ model, then at that timestep the Hautus condition holds for the $\mathcal{M}4$ model (9.6). Finally, we show the necessity of the new $\mathcal{M}4$ model form of the profile difference equations for the flow demands. It is shown that if the profile difference equations of an $\mathcal{M}4$ model are replaced by the $\mathcal{M}3$ model profile difference equations, then the Hautus condition never holds at any timestep k.

Theorem 9.1 *If $\theta > 0$, the E_4 matrix of an $\mathcal{M}4$ model is full rank.*

Proof

E_4 is $(n+2g)\times(n+2g)$ and takes the form

$$E_4 = \begin{bmatrix} E_0 & -B^{1''} & 0 \\ 0 & I & 0 \\ 0 & 0 & I \end{bmatrix}$$

where I is $g\times g$.

By construction, since we have already shown E_0 is invertible if $\theta > 0$, E_4^{-1} is $(n+2g)\times(n+2g)$ and takes the form

$$E_4^{-1} = \begin{bmatrix} E_0^{-1} & E_0^{-1}B^{1''} & 0 \\ 0 & I & 0 \\ 0 & 0 & I \end{bmatrix}$$

where I is $g \times g$.

Hence, the E_4 matrix of an $\mathcal{M}4$ model is full rank. $\square$

Theorem 9.2 *For $1/2 \leq \theta \leq 1$, if at a particular timestep the diagonal elements of $W(k)$ are not equal either to 1 or to any of the eigenvalues of the corresponding $\mathcal{M}2$ model, then at that timestep the Hautus condition holds for the $\mathcal{M}4$ model (9.6).*

Proof

By inspection, at any particular timestep, k, the eigenvalues of an $\mathcal{M}4$ system consist of the n eigenvalues of the base $\mathcal{M}0$ system, g eigenvalues equal to the g variables $w_k^{demand\ site}$, and g eigenvalues equal to 1. Hence, the eigenvalues of the $\mathcal{M}4$ system are real.

The Hautus condition holds for the $\mathcal{M}4$ system if and only if for all $\mu \in \mathbf{R}$

$$(A_4(k) - \mu E_4)\underline{v} = \underline{0} \tag{9.8}$$

$$C_4\underline{v} = \underline{0} \tag{9.9}$$

$$\Longleftrightarrow$$

$$\underline{v} = \underline{0} \tag{9.10}$$

where $\underline{v} \in \mathbf{R}^{n+2g}$.

Equation (9.10) $\Longrightarrow$ equations (9.8), (9.9) triviallyection,onlexpressed(9.8),inconditeigenfolloD1ff

$$\Longleftrightarrow$$

$$\underline{v}_n = \underline{0} \ , \ \underline{v}_g = \underline{0} \ , \ \underline{\tilde{v}}_g = \underline{0} \tag{9.15}$$

where $\underline{v} = [\underline{v}_n^T, \underline{v}_g^T, \underline{\tilde{v}}_g^T]^T$, and $\underline{v}_n \in \mathbf{R}^n$, $\underline{v}_g \in \mathbf{R}^g$, $\underline{\tilde{v}}_g \in \mathbf{R}^g$.

We firstly consider the case where $\mu \neq 1$.

Equation (9.13) implies $\underline{\tilde{v}}_g = \underline{0}$.

Substituting $\underline{\tilde{v}}_g = \underline{0}$ into equation (9.14) gives

$$C_0 \underline{v}_n = \underline{0}. \tag{9.16}$$

If $\mu \neq w_k^{demand\ site}$ for all flow demands, equation (9.12) gives $\underline{v}_g = \underline{0}$.

Substituting $\underline{v}_g = \underline{0}$ into equation (9.11) gives

$$(A_0 - \mu E_0)\underline{v}_n = \underline{0}. \tag{9.}$$

and $\underline{v}_{n-g} \in \mathbf{R}^{n-g}$ and $\underline{\hat{v}}_g \in \mathbf{R}^g$.

Equation (9.16) zeros the elements of $\underline{v}_n$ corresponding to the measured pressures at the sites of flow demand; i.e. equation (9.16) zeros $\underline{\hat{v}}_g$. Removing $\underline{\hat{v}}_g$ from system (9.19) gives the system

$$[(A' - \mu E') \quad (B^{2''} - \mu(-B^{1''}))] \begin{bmatrix} \underline{v}_{n-g} \\ \underline{v}_g \end{bmatrix} = \underline{0}. \tag{9.20}$$

However, the system matrices of an $\mathcal{M}2$ model corresponding to the base $\mathcal{M}0$ model have the form

$$E_2 = [E' \quad -B^{1''}]$$

$$A_2 = [A' \quad B^{2''}].$$

If has w TD1(Tj foahessumeT Tf1 1gTj1T Tf1 TD1gTj1=T Tf1 T TD1flTj1wT Tf1

Hence we have $\underline{v} = \underline{0}$.

Hence, we have the result; equations (9.8), (9.9) $\Longrightarrow$ equation (9.10).

Hence, for $1/2 \leq \theta \leq 1$, if at a particular timestep the diagonal elements of $W(k)$ are not equal either to 1 or to any of the eigenvalues of the corresponding $\mathcal{M}2$ model, then at that timestep the Hautus condition will hold for the $\mathcal{M}4$ model (9.6). $\Box$

We construct dynamic observers for such an $\mathcal{M}4$ system by finding a new feedback matrix, $G(k)$, at each timestep to assign eigenvalues within the unit circle. Since, the matrix $A_4(k)$ is time-varying, assigning eigenvalues within the unit circle is not necessarily sufficient to cause the observer to converge asymptotically. However, if the dynamics of the real system are quite slow, from [15], it follows that assigning sufficiently small eigenvalues may well give convergence.

We can find the feedback matrix $G(k)$ to assign observer eigenvalues arbitrarily at each timestep k when the Hautus condition holds, and the above theorem implies the Hautus condition does not hold for only a few specific values of the coefficients w_k^{node}. At those particular timesteps we can run the simple $\mathcal{M}4$ model i.e. without the observer feedback term $G(y -$

Proof

If we had incorporated the previous $\mathcal{M}3$ model form of difference equation (6.22) into $\mathcal{M}4$ models, the $\mathcal{M}4$ system matrices would have been identical except that for the matrix block $W(k)$, we would have had $W(k) = I$ for all timesteps k. Thus, the matrices E_4 and A_4 would have had the form

$$E_4 = \begin{bmatrix} E_0 & -B^{1''} & 0 \\ 0 & I & 0 \\ 0 & 0 & I \end{bmatrix}$$

and

$$A_4 = \begin{bmatrix} A_0 & B^{2''} & 0 \\ 0 & I & 0 \\ 0 & 0 & I \end{bmatrix}.$$

The Hautus condition holds for this alternative $\mathcal{M}4$ system if and only if for all $\mu \in \mathbf{R}$

$$(A_4 - \mu E_3$$

9.2 Experiments

As the $\mathcal{M}0$ model was run, the pressures at the upstream end and the sites of flow demand were recorded at each timestep. The pressure measurements at the three flow demand sites, A/B, B/C and C, were then corrupted by constant biases of 1 bar, -1 bar and 1 bar respectively. These corrupted pressures were then fed into both design A and design B observers constructed upon an $\mathcal{M}4$ model. For the design B dynamic observer, the feedback matrix, G, was recalculated at each timestep, and the assigned eigenvalues were spread evenly in the interval $(0, 0.1)$. Experiments with design C observers are not presented since design C observers constructed upon $\mathcal{M}4$ models were found to behave similarly to design B observers. The flow demands predicted by the observers were then compared with the true flows used as inputs to the $\mathcal{M}0$ model. For experiments 9.1 to 9.3, the $\mathcal{M}0$ model simulating a gas network was identical to the $\mathcal{M}0$ model upon which the $\mathcal{M}4$ model was constructed. For experiments 9.4 to 9.8, the $\mathcal{M}0$ model simulating a gas network had a much finer discretisation (in both space and time) than the $\mathcal{M}4$ model.

In all experiments, the $\mathcal{M}4$ models were given the exact values of the profile coefficients, $w_k^{demand\ site}$, calculated from the flow demand inputs to the $\mathcal{M}0$ model.

For each experiment, the true flow demand profiles for the demands, $D_k^{A/B}$, $D_k^{B/C}$ and D_k^C are shown as thick lines in Figs. A, B and C respectively, and the state estimates for $D_k^{A/B}$, $D_k^{B/C}$ and D_k^C are shown as thin lines. The percentage errors between the state estimates of $D_k^{A/B}$, $D_k^{B/C}$ and D_k^C and their true values are shown in Figs. D, E and F respectively.

Data taken from $\mathcal{M}0$ model with identical mesh - both $\mathcal{M}0$ and $\mathcal{M}4$ models have 10 spatial nodes along each pipe.

Experiment 9.1) Observer Design B with $\theta = 1$

Experiment 9.2) Observer Design B with $\theta = 0.75$

Experiment 9.3) Observer Design B with $\theta = 0.5$

Data taken from $\mathcal{M}0$ model with much finer mesh - $\mathcal{M}4$ model has 5 spatial nodes along each pipe.

Experiment 9.4) Observer Design A with $\theta = 1$

Experiment 9.5) Observer Design A with $\theta = 0.75$

Experiment 9.6) Observer Design A with $\theta = 0.5$

Data taken from $\mathcal{M}0$ model with much finer mesh - $\mathcal{M}4$ model has 10 spatial nodes along each pipe.

Experiment 9.7) Observer Design B with $\theta = 1$

Experiment 9.8) Observer Design B with $\theta = 0.75$

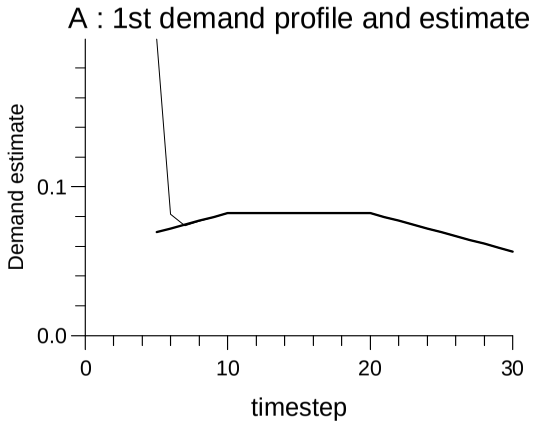
A : 1st demand profile and estimate
Demand estimate
0.0
0.1
0
10
20
30
timestep

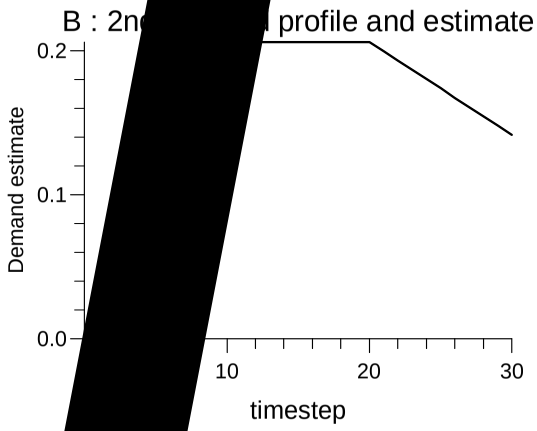
B : 2nd
profile and estimate
Demand estimate
0.0
0.1
0.2
0
10
20
30
timestep

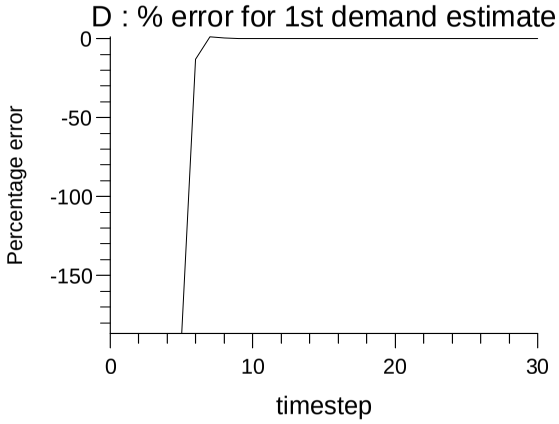
D : % error for 1st demand estimate
Percentage error
0
-50
-100
-150
0
10
20
30
timestep

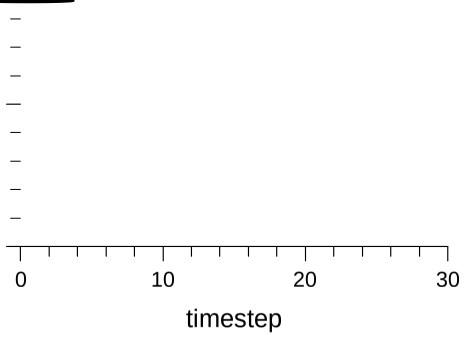
0
10
20
30
timestep

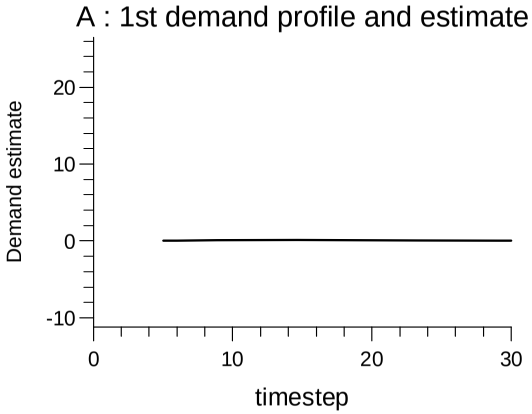
A : 1st demand profile and estimate
Demand estimate
20
10
0
-10
0
10
20
30
timestep

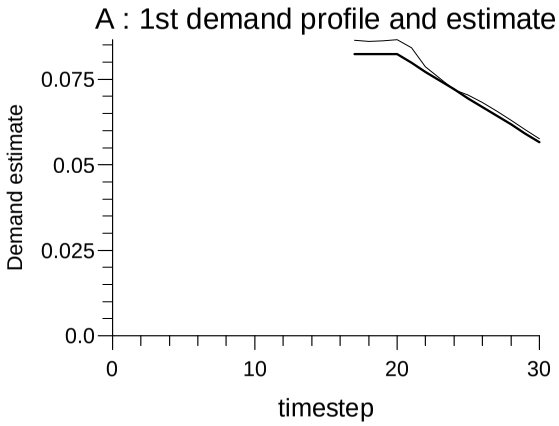
A : 1st demand profile and estimate
Demand estimate
0.075
0.05
0.025
0.0
0
10
20
30
timestep

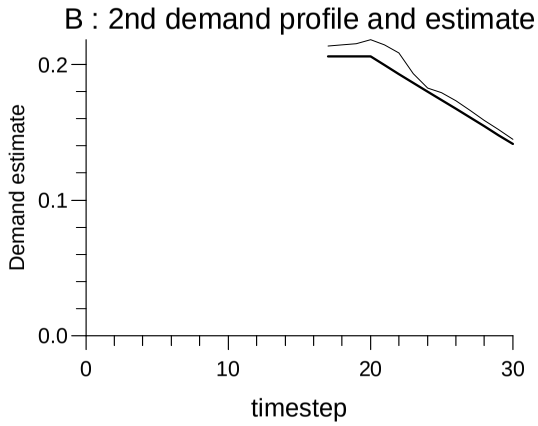
B : 2nd demand profile and estimate
Demand estimate
0.2
0.1
0.0
0
10
20
30
timestep

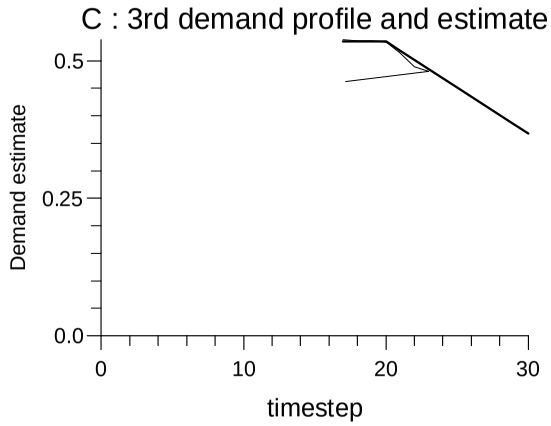
C : 3rd demand profile and estimate
Demand estimate
0.5
0.25
0.0
0
10
20
30
timestep

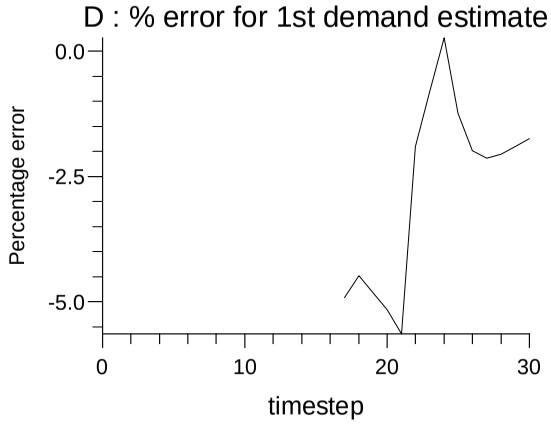
D : % error for 1st demand estimate
Percentage error
0.0
-2.5
-5.0
0
10
20
30
timestep

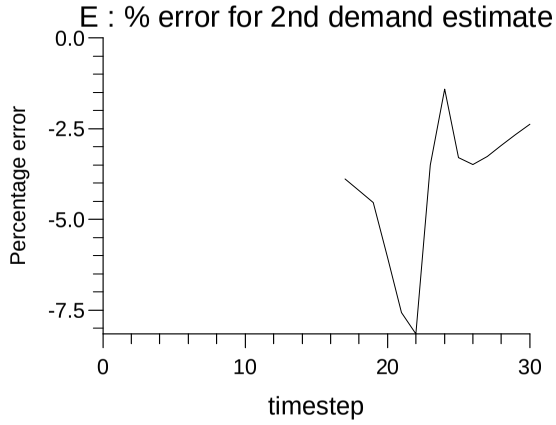
E : % error for 2nd demand estimate
Percentage error
0.0
-2.5
-5.0
-7.5
0
10
20
30
timestep

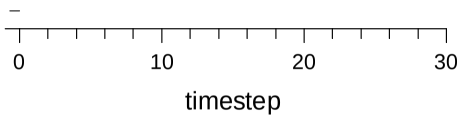
0
10
20
30
timestep

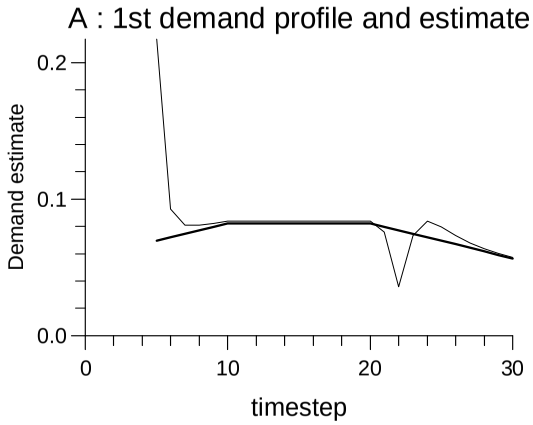
A : 1st demand profile and estimate
Demand estimate
0.2
0.1
0.0
0
10
20
30
timestep

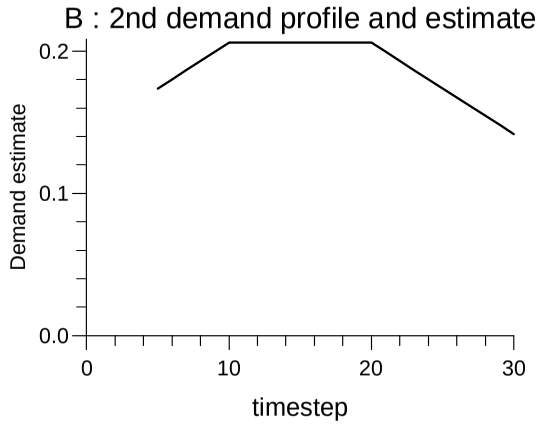
B : 2nd demand profile and estimate
Demand estimate
0.2
0.1
0.0
0
10
20
30
timestep

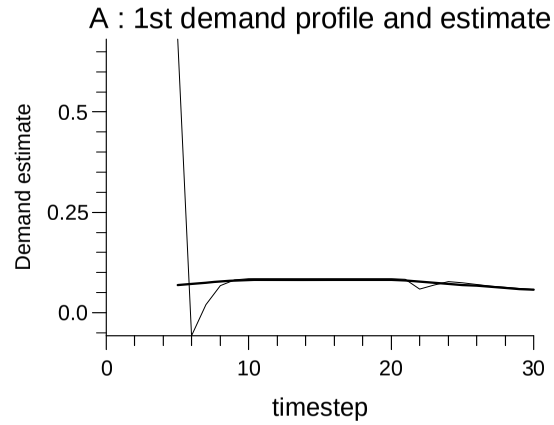
A : 1st demand profile and estimate
Demand estimate
0.5
0.25
0.0
0
10
20
30
timestep

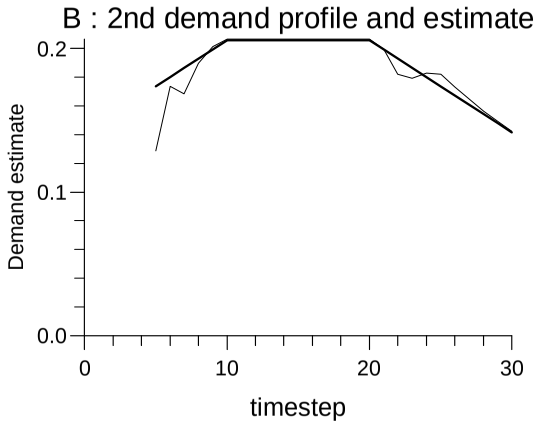
B : 2nd demand profile and estimate
Demand estimate
0.2
0.1
0.0
0
10
20
30
timestep

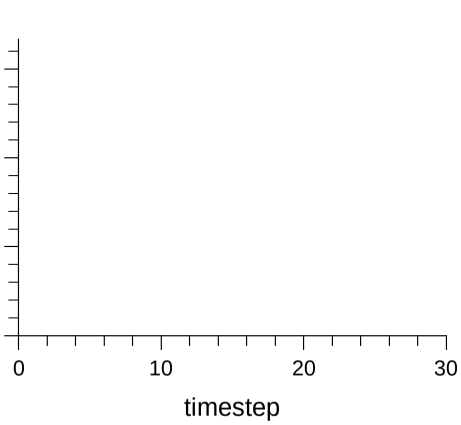
0
10
20
30
timestep

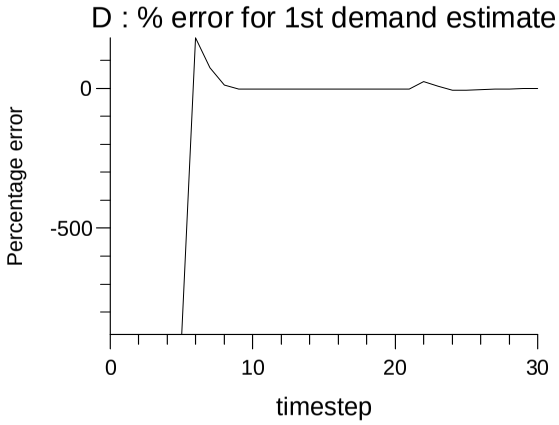
D : % error for 1st demand estimate
Percentage error
0
-500
0
10
20
30
timestep

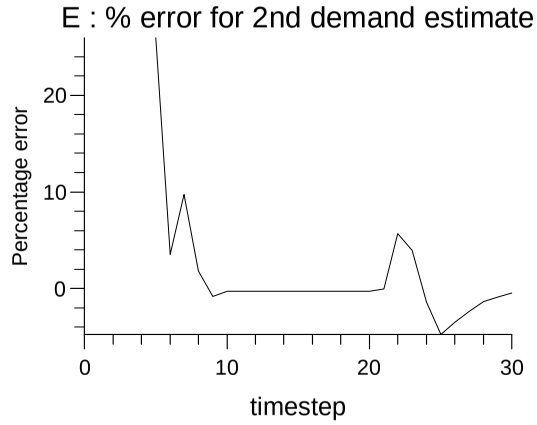
E : % error for 2nd demand estimate
Percentage error
20
10
0
0
10
20
30
timestep

9.3 Discussion

The chosen flow profile was a severe test for the observers due to the long central period for which the flow demands remained constant. For this period the feedback was omitted from the dynamic observer leaving the simple $\mathcal{M}4$ model.

When data was taken from an $\mathcal{M}0$ model with an identical mesh, the direct observer gave perfect state estimates for all timesteps (although these graphs are ommitted), for all values of $\theta \in [1/2, 1]$. However, if fewer spatial nodes were used, the direct observer could fail during the period for which the flows remained constant. Increasing the number of spatial nodes increased the dimension of the $\mathcal{M}4$ model, and hence, the number of timesteps over which equation (5.4) was solved.

rect and dynamic observers behaved poorly for $\theta = 1$. Direct and dynamic observers constructed upon $\mathcal{M}4$ models are in some sense more sensitive to modelling (and measurement) error than previous estimation techniques investigated in this thesis. From various experiments performed, it was seen that the error present in the state estimates generally seems to have the following form. The error seems to decrease over periods when the profile coefficients, $w_k^{demand\ site}$, are constant, but increase suddenly when there is a sudden change in the values of $w_k^{demand\ site}$. This is not understood, but it may be the case that an alternative observer design could help to reduce such error. Perhaps an observer that switched between the different models, $\mathcal{M}3$ and $\mathcal{M}4$, at certain times of day could be designed to estimate the biases, where the $\mathcal{M}4$ model based observer would run over certain 'favourable' timesteps only. Then these estimates of the biases may be kept while an $\mathcal{M}3$ model based observer is run over periods where an $\mathcal{M}4$ model based observer would fail.

However, as θ moved from 1 to 1/2, the error introduced by taking data from a finer mesh was reduced. For $\theta = 1/2$, the dynamic observer failed due to the sensitivity of the observer eigenvalues; however, the direct observer coped very well indeed.

In the next chapter, we look at the problem of pressure measurement noise. Experimental results show clearly the extra sensitivity of $\mathcal{M}4$ models, the flow state estimates of which are completely swamped by the error introduced by measurement noise. To deal with this problem, we examine two simple smoothing techniques, and derive two final model variations, $\mathcal{M}5$ and $\mathcal{M}6$, to deal with the problem of the sensitivity of the flow demand estimates. $\mathcal{M}5$ and $\mathcal{M}6$ models have only a single total flow demand perturbation state variable that is the sum of all the individual demand flow perturbation variables. Such models are less sensitive to pressure measurement noise.

Chapter 10

White Noise, Flow Integration Smoothing Techniques, 5 and 6 Models.

All pressure measurements taken from gas networks are subject to white noise, which is assumed to have a Gaussian distribution with mean 0 bar and standard deviation 0.1 bar [11], [38]. Due to the sensitivity of small flow demand estimates to pressure measuremen

N.B. Up un

biases of 1 bar, -1 bar and 1 bar respectively. These corrupted pressures were then fed into the $\mathcal{M}1$ and $\mathcal{M}2$ models, and $\mathcal{M}3$ and $\mathcal{M}4$ model based observers. The flo

Experiment 10.1

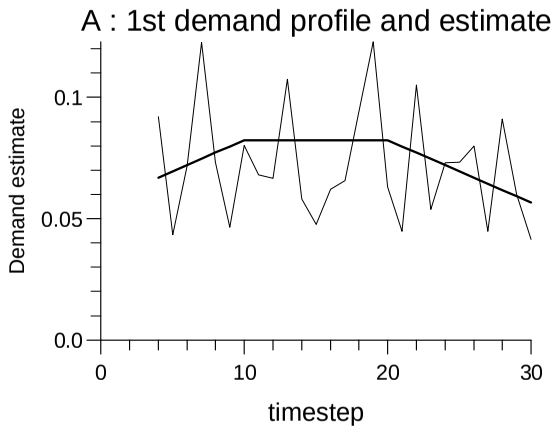

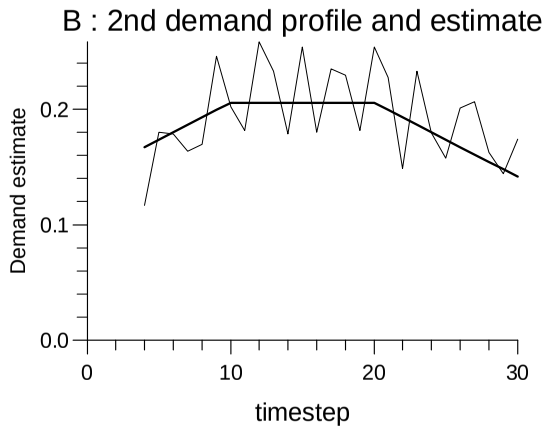

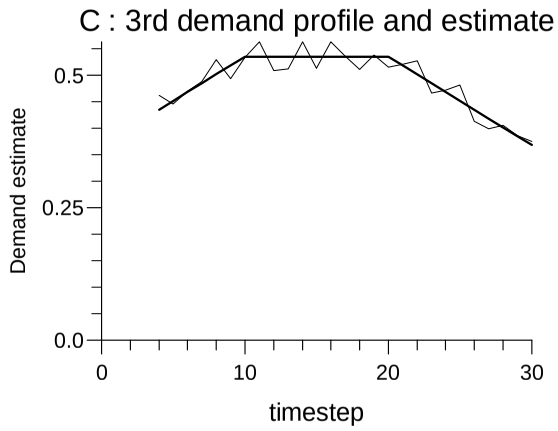

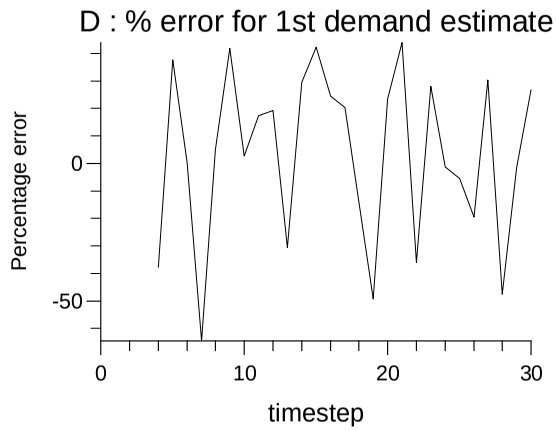

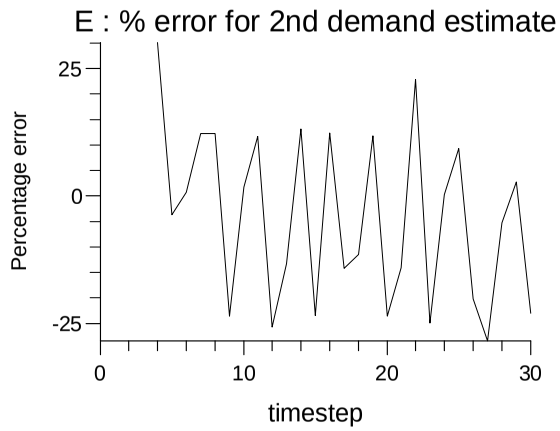

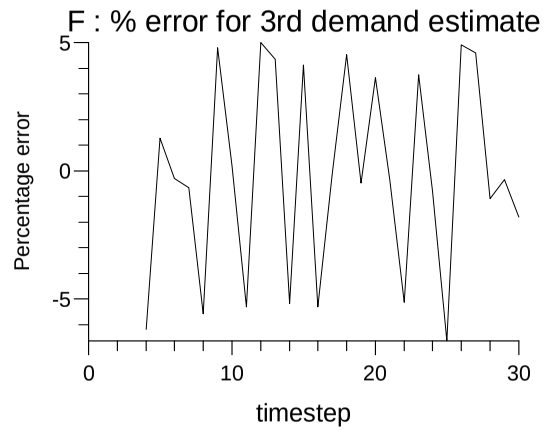

Experiment 10.2

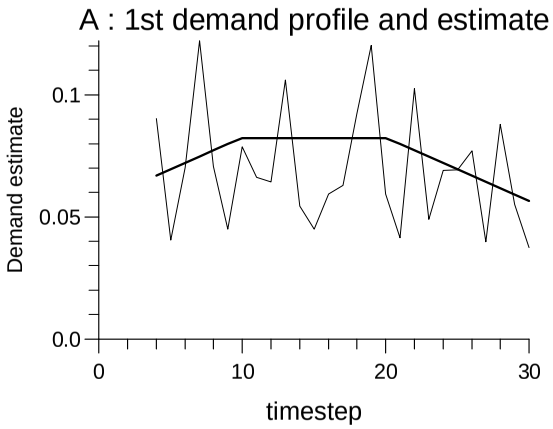

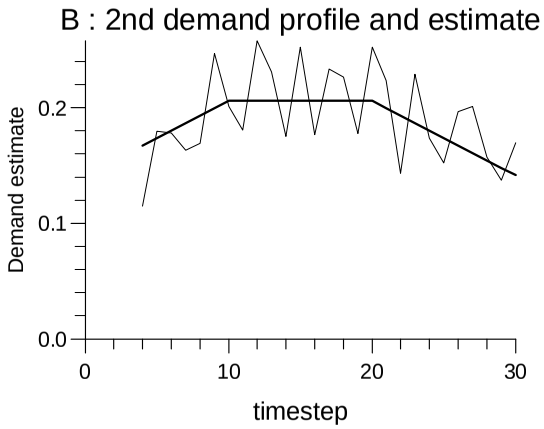

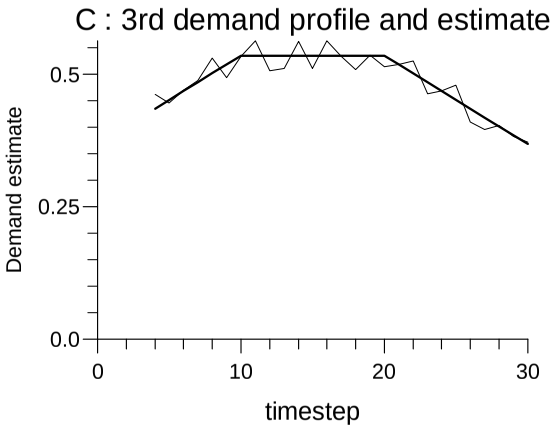

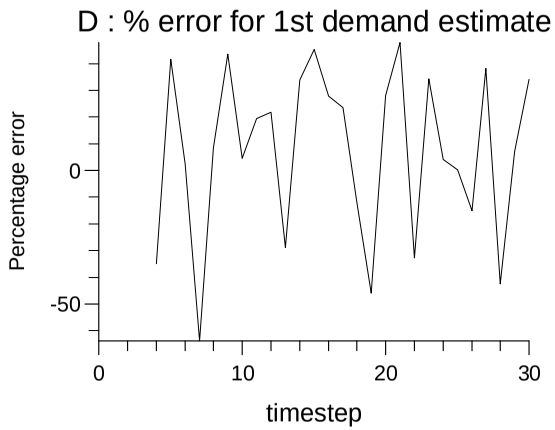

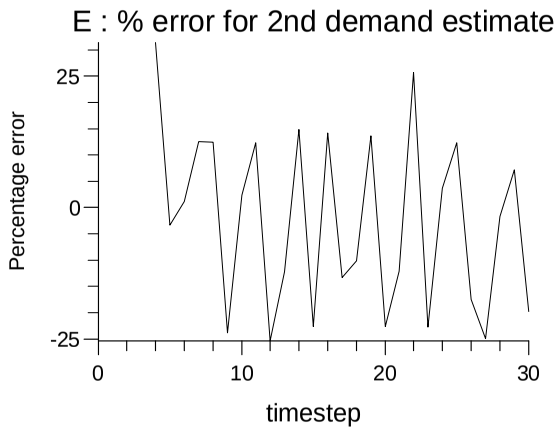

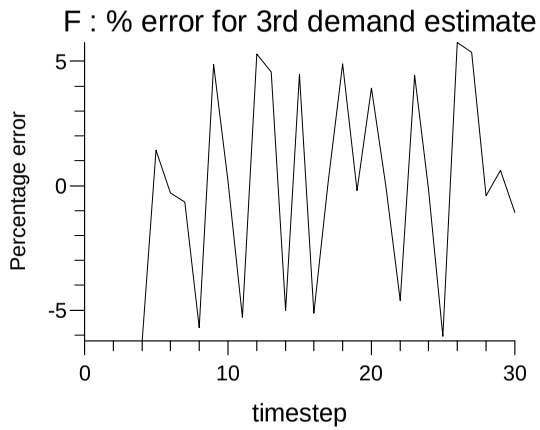

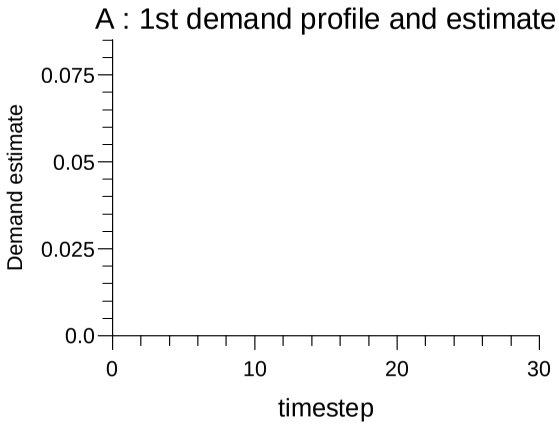
A : 1st demand profile and estimate
Demand estimate
0.075
0.05
0.025
0.0
0
10
20
30
timestep

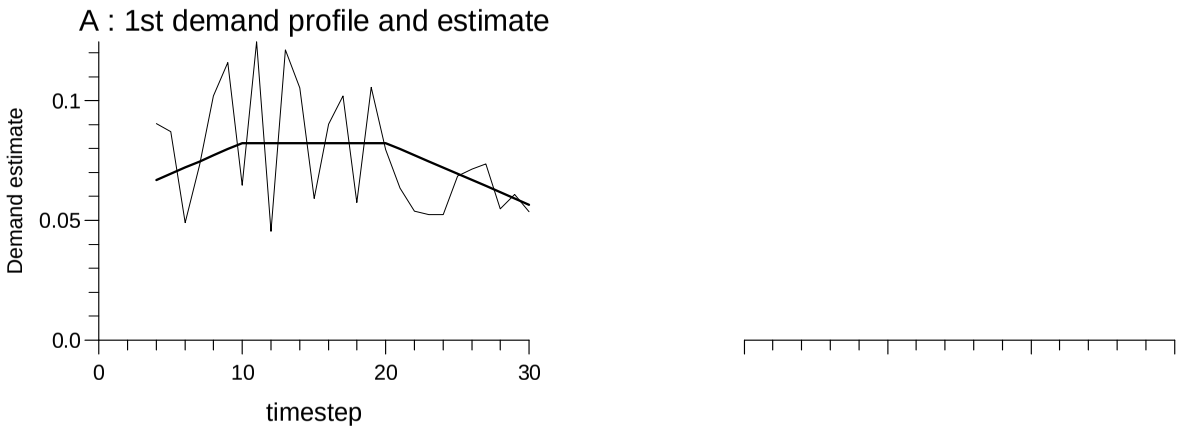
A : 1st demand profile and estimate
Demand estimate
0.0
0.05
0.1
0
10
20
30
timestep

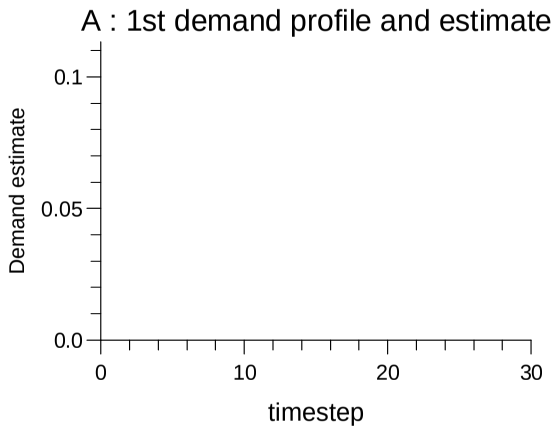
A : 1st demand profile and estimate
Demand estimate
0.1
0.05
0.0
0
10
20
30
timestep

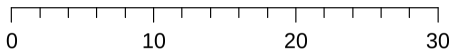
0
10
20
30

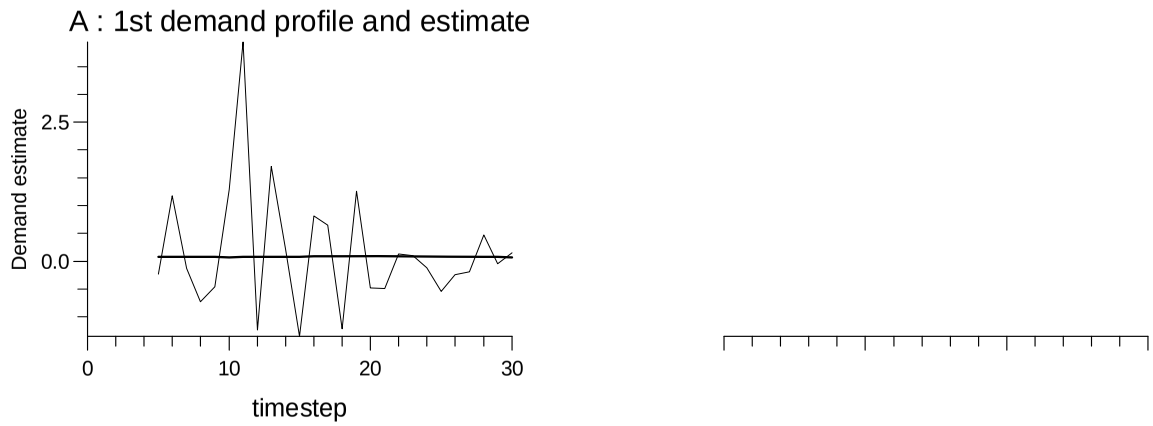
A : 1st demand profile and estimate
Demand estimate
2.5
0.0
0
10
20
30
timestep

10.1.2 Discussion

Since the assigned observer eigenvalues are asymptotically stable, we would expect that in the sum $\sum_{k=r}^{s} e_k$, the individual e_k cancel out to some extent, and that

$$\frac{\sum_{k=r}^{s} \widehat{d}_k^{demand\ site}}{\sum_{k=r}^{s} d_k^{demand\ site}} \longrightarrow 1 \quad as\ s-r \longrightarrow \infty. \tag{10.1}$$

Some attempt was made to provide a statistical proof of equation (10.1), but this was not achieved. Future theoretical investigation of the validity of equation (10.1), would be worthwhile, and a useful reference for this would be [12] p.30. Assuming equation (10.1) holds, if the time period $k = r, ..., s$ is large enough, $\sum_{k=r}^{s} \widehat{d}_k^{demand\ site}$ is a good estimate of $\sum_{k=r}^{s} d_k^{demand\ site}$.

If, after a large time period, $k = r, ..., s$, we assume we have a good estimate of $\sum_{k=r}^{s} d_k^{demand\ site}$, then we can find $d_r^{demand\ site}$ from the following.

From the definition of the flow demand profile jumps, $\tilde{f}_k^{demand\ site}$, it can be seen that for any timestep k

$$d_k^{demand\ site} = d_r^{demand\ site} + \sum_{j=r}^{k-1} \tilde{f}_j^{demand\ site} \qquad if\ k > r$$

from which we can derive

$$\sum_{k=r}^{s} d_k^{demand\ site} = (s-r+1) d_r^{demand\ site} + \sum_{k=r+1}^{s} (\sum_{j=r}^{k-1} \tilde{f}_j^{demand\ site}),$$

i.e.

$$d_r^{demand\ site} = \frac{(\sum_{k=r}^{s} d_k^{demand\ site}) - \sum_{k=r+1}^{s} (\sum_{j=r}^{k-1} \tilde{f}_j^{demand\ site})}{(s-r+1)}.$$

Once $\sum_{k=r}^{s} \widehat{d}_k^{demand\ site}$ is calculated, it may be used as an estimate for $\sum_{k=r}^{s} d_k^{demand\ site}$. $d_r^{demand\ site}$ may then be estimated from the above equation. From $d_r^{demand\ site}$, w

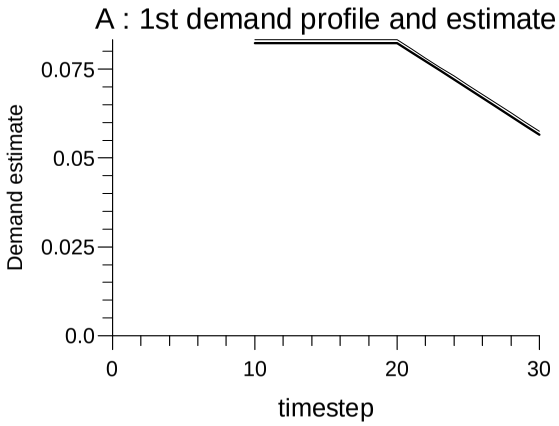
A : 1st demand profile and estimate
Demand estimate
0.075
0.05
0.025
0.0
0
10
20
30
timestep

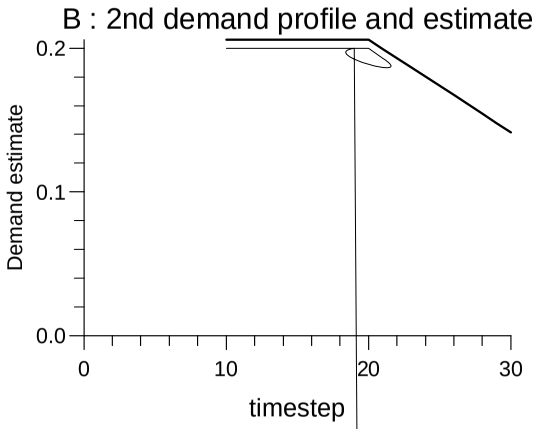
B : 2nd demand profile and estimate
Demand estimate
0.2
0.1
0.0
0
10
20
30
timestep

10.2.2 Discussion

It can be readily seen that the $\mathcal{M}3$ flow integration smoothing technique significantly reduces the error, due to pressure measurement noise, in the flow demand estimates of $\mathcal{M}3$ model based dynamic observers. Also, the smoothing technique maintains the true 'shapes' of the profiles, but with the measurement noise causing such estimated profiles to be shifted up or down the flow demand axis.

Although it was not investigated experimentally, the $\mathcal{M}3$ flow integration smoothing technique could be implemented as a filtering technique for each current time-level. At each new timestep, s, the smoothing process would be carried out over some timesteps, $k = r, ..., s$, to give a filtered estimate for the current time-level s. This would be a more useful approach, and the effectiveness of such an $\mathcal{M}3$ flow integration filtering technique would be worth exploring.

10.3 The $\mathcal{M}4$ Flow Integr tion Smoothing Technique

For the $\mathcal{M}4$ flow integration smoothing technique, we use trivial difference equations for the flow demand perturbations of the form (9.3). An $\mathcal{M}4$ model based observer is run continuously. Over some time interval, $k = r, ..., s$, (say one hour), for each demand the estimated flow perturbation at each time step is integrated, that is, for each flow demand, we find $\sum_{k=r}^{s} \widehat{d}_k^{demand\ site}$, where $\widehat{d}_k^{demand\ site}$ is our noise contaminated estimate of $d_k^{demand\ site}$. As explained previously, we expect that if the time period $k = r, ..., s$ is large enough, then $\sum_{k=r}^{s} \widehat{d}_k^{demand\ site}$ will be a good estimate of $\sum_{k=r}^{s} d_k^{demand\ site}$.

Firstly, it is obvious that

$$\begin{aligned} Total\ normalised\ integrated\ flow &= \sum_{k=r}^{s} (d_k^{demand\ site} + \mathcal{Q}^{demand\ site}) \\ &= (s - r + 1)\mathcal{Q}^{demand\ site} + \sum_{k=r}^{s} d_k^{demand\ site}. \end{aligned} \tag{10.2}$$

Secondly, from equation (9.3) it can be seen that

$$Total\ normalised\ integrated\ flow = (d_r^{demand\ site} + \mathcal{Q}^{demand\ site})$$

$$\times(1 + w_r^{demand\ site} + w_r^{demand\ site} w_{r+1}^{demand\ site} + ... + \prod_{k'=r}^{s-1} w_{k'}^{demand\ site})$$

$$= (d_r^{demand\ site} + \mathcal{Q}^{demand\ site})(1 + \sum_{k=r}^{s-1}(\prod_{k'=r}^{k} w_{k'}^{demand\ site}))$$

$$= d_r^{demand\ site}(1+\sum_{k=r}^{s-1}(\prod_{k'=r}^{k} w_{k'}^{demand\ site})) + \mathcal{Q}^{demand\ site}(1+\sum_{k=r}^{s-1}(\prod_{k'=r}^{k} w_{k}^{demand\ site}$$

10.3.2 Discussion

For Figs. D and F, the graphs coincide with the axes.

It can be readily seen that the $\mathcal{M}4$ flow integration smoothing technique significantly reduces the error, due to pressure measurement noise, in the flow demand estimates of $\mathcal{M}4$ model based dynamic observers. However, the error is still very large indeed.

In a similar way to the $\mathcal{M}3$ flow integration smoothing technique, the $\mathcal{M}4$ flow integration smoothing technique may be implemented as a filter for each current time-level. Although an $\mathcal{M}4$ flow integration filtering technique was not investigated experimentally, the performance of such a technique would be worth exploring.

The $\mathcal{M}3$ and $\mathcal{M}4$ models still contain the underlying sensitivity of the small flow demands to pressure measurement perturbations. For this reason we next examine two new model variations, $\mathcal{M}5$ and $\mathcal{M}6$ models, for which the estimates of small flow demands from observers constructed upon such models are significantly less sensitive.

10.4 The $\mathcal{M}5$ odel

Due to the sensitivity of the previous models to pressure measurement noise, we now investigate a new model variation, denoted by $\mathcal{M}5$, which has only a single total flow demand perturbation state variable that is the sum of all the individual demand flow perturbation variables. We consider the g scalar equations of the form (6.22). If we add these g equations together we can derive

$$d_{k+1}^{tot}$$

$$+\begin{bmatrix} \underline{v}(k+1) \\ 0 \end{bmatrix} + \begin{bmatrix} \underline{v}(k) \\ \tilde{f}_k^{tot} \end{bmatrix} \tag{10.6}$$

where the vectors $\underline{e}(k+1)$ and $\underline{a}(k)$ contain only the time-varying coefficients linking the total flow variable, d_k^{tot}, with the new forms of the $g-1$ connectivity equations and the single downstream flow boundary equation. Likewise, the vectors $\underline{v}(k+1)$ and $\underline{v}(k)$ contain only elements associated with the g flow equations. These elements of $\underline{e}(k+1)$, $\underline{a}(k)$, $\underline{v}(k+1)$ and $\underline{v}(k)$ are now determined by considering the new forms of the flow equations in $\mathcal{M}5$ models.

The original general 'connectivity equation' between two pipe sections z and $z+1$ is given by (2.23). For an $\mathcal{M}5$ model, equation (10.5) is substituted into equation (2.23) to give

$$\begin{aligned}
&-(\Phi^{z/z+1}\epsilon_3^z\Gamma^z_{s^z-1}\theta/\delta x^z)p^z_{s^z-1,k+1} + (1+\Phi^{z/z+1}\epsilon_3^z\Gamma^{z/z+1}\theta/\delta x^z + \Phi^{z/z+1}\epsilon_3^{z+1}\Gamma^{z/z+1}\theta/\delta x^{z+1})p^{z/z+1}_{k+1} \\
&-(\Phi^{z/z+1}\epsilon_3^{z+1}\Gamma_1^{z+1}\theta/\delta x^{z+1})p^{z+1}_{1,k+1} + \Phi^{z/z+1}\theta(\alpha^{z/z+1}_{k+1}d^{tot}_{k+1} + \alpha^{z/z+1}_{k+1}\mathcal{Q}^{tot} - \mathcal{Q}^{z/z+1}) = \\
&(\Phi^{z/z+1}\epsilon_3^z\Gamma^z_{s^z-1}(1-\theta)/\delta x^z)p^z_{s^z-1,k} + (1-\Phi^{z/z+1}\epsilon_3^z\Gamma^{z/z+1}(1-\theta)/\delta x^z - \Phi^{z/z+1}\epsilon_3^{z+1}\Gamma^{z/z+1}(1-\theta)/\delta x^{z+1})p^{z/z+1}_k \\
&+(\Phi^{z/z+1}\epsilon_3^{z+1}\Gamma_1^{z+1}(1-\theta)/\delta x^{z+1})p^{z+1}_{1,k} - \Phi^{z/z+1}(1-\theta)(\alpha^{z/z+1}_k d^{tot}_k + \alpha^{z/z+1}_k\mathcal{Q}^{tot} - \mathcal{Q}^{z/z+1})
\end{aligned} \tag{10.7}$$

which can be rearranged to

$$\begin{aligned}
&-(\Phi^{z/z+1}\epsilon_3^z\Gamma^z_{s^z-1}\theta/\delta x^z)p^z_{s^z-1,k+1} + (1+\Phi^{z/z+1}\epsilon_3^z\Gamma^{z/z+1}\theta/\delta x^z + \Phi^{z/z+1}\epsilon_3^{z+1}\Gamma^{z/z+1}\theta/\delta x^{z+1})p^{z/z+1}_{k+1} \\
&-(\Phi^{z/z+1}\epsilon_3^{z+1}\Gamma_1^{z+1}\theta/\delta x^{z+1})p^{z+1}_{1,k+1} + \Phi^{z/z+1}\theta\alpha^{z/z+1}_{k+1}d^{tot}_{k+1} = \\
&(\Phi^{z/z+1}\epsilon_3^z\Gamma^z_{s^z-1}(1-\theta)/\delta x^z)p^z_{s^z-1,k} + (1-\Phi^{z/z+1}\epsilon_3^z\Gamma^{z/z+1}(1-\theta)/\delta x^z - \Phi^{z/z+1}\epsilon_3^{z+1}\Gamma^{z/z+1}(1-\theta)/\delta x^{z+1})p^{z/z+1}_k \\
&+(\Phi^{z/z+1}\epsilon_3^{z+1}\Gamma_1^{z+1}(1-\theta)/\delta x^{z+1})p^{z+1}_{1,k} - \Phi^{z/z+1}(1-\theta)\alpha^{z/z+1}_k d^{tot}_k \\
&-\Phi^{z/z+1}\theta(\alpha^{z/z+1}_{k+1}\mathcal{Q}^{tot} - \mathcal{Q}^{z/z+1}) - \Phi^{z/z+1}(1-\theta)(\alpha^{z/z+1}_k\mathcal{Q}^{tot} - \mathcal{Q}^{z/z+1}).
\end{aligned} \tag{10.8}$$

Equation (10.8) represents the new form of the connectivity equation for pipe sections z and $z+1$ used in $\mathcal{M}5$ models. The last two terms of equation (10.8), $-\Phi^{z/z+1}\theta(\alpha^{z/z+1}_{k+1}\mathcal{Q}^{tot} - \mathcal{Q}^{z/z+1})$ and $-\Phi^{z/z+1}(1-\theta)(\alpha^{z/z+1}_k\mathcal{Q}^{tot} - \mathcal{Q}^{z/z+1})$, are contained in the the vectors $\underline{v}(k+1)$ and $\underline{v}(k)$ respectively. The coefficients $\Phi^{z/z+1}\theta\alpha^{z/z+1}_{k+1}$, $-\Phi^{z/z+1}(1-\theta)\alpha^{z/z+1}_k$ of the total flow perturbation variable, $d^{tot}_{timestep}$, are contained in the vectors $\underline{e}(k+1)$ and $\underline{a}(k)$ respectively.

A similar procedure is carried out to obtain the new form of the downstream flow boundary equation. The original downstream flow boundary equation is giv

For such an $\mathcal{M}$

Proof

By inspection, the eigenvalues of an $\mathcal{M}5$ system consist of the n eigenvalues of the base $\mathcal{M}0$ system, and 1 eigenvalue equal to 1. Hence, the eigenvalues of the $\mathcal{M}5$ system are real.

We have the Hautus condition for the $\mathcal{M}5$ system if and only if for all $\mu \in \mathbf{R}$

$$(A_5(k) - \mu E_5(k+1))\underline{v} = \underline{0} \tag{10.13}$$

$$C_5\underline{v} = \underline{0} \tag{10.14}$$

$$\Longleftrightarrow$$

$$\underline{v} = \underline{0} \tag{10.15}$$

where $\underline{v} \in \mathbf{R}^{n+1}$.

Equation (10.15) $\Longrightarrow$ equations (10.13), (10.14) trivially.

Equations (10.13), (10.14) and (10.15) can be expressed in the following way. We have the Hautus condition for the $\mathcal{M}5$ system if and only if for all $\mu \in \mathbf{R}$

$$(A_0 - \mu E_0)\underline{v}_n + (\underline{a}(k) - \mu \underline{e}(k+1))\underline{v}_1 = \underline{0} \tag{10.16}$$

$$(1-\mu)\underline{v}_1 = \underline{0} \tag{10.17}$$

$$C_0\underline{v}_n = \underline{0} \tag{10.18}$$

$$\Longleftrightarrow$$

$$\underline{v}_n = \underline{0}\ ,\ \underline{v}_1 = \underline{0} \tag{10.19}$$

where $\underline{v} = [\underline{v}_n^T, \underline{v}_1^T]^T$, and $\underline{v}_n \in \mathbf{R}^n$, $\underline{v}_1 \in \mathbf{R}^1$.

We firstly consider the case where $\mu \neq 1$.

Equation (10.17) implies $\underline{v}_1 = \underline{0}$.

form $-(2(1-\theta)\Omega^g_{sg} r^g \delta x^g/\epsilon^g_3)\alpha^{downstream}_k - (2\theta\Omega^g_{sg} r^g \delta x^g/\epsilon^g_3)\alpha^{downstream}_{k+1}$ which results from the downstream flo

The following two experiments do have measurement noise added.

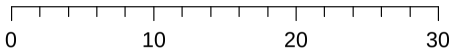
0
10
20
30

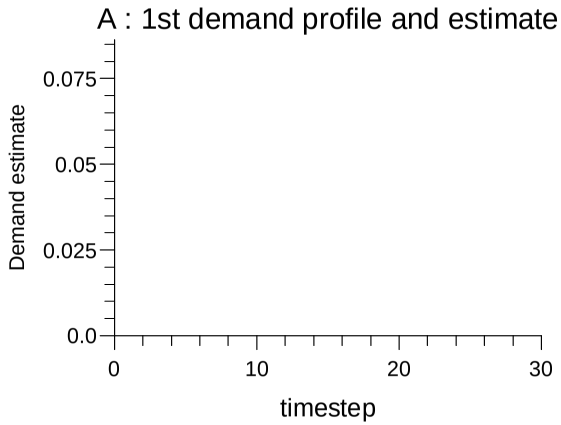
A : 1st demand profile and estimate
Demand estimate
0.075
0.05
0.025
0.0
0
10
20
30
timestep

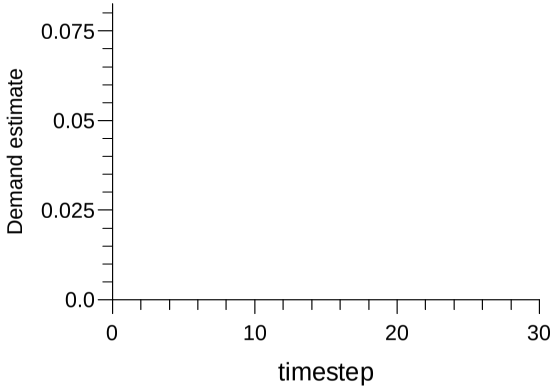
0.075
0.05
0.025
0.0
Demand estimate
0
10
20
30
timestep

Experiment 10.16

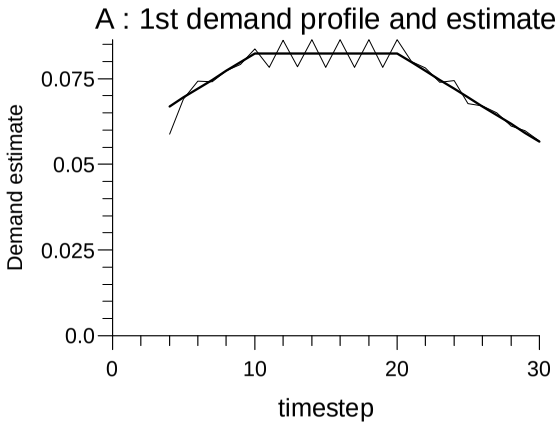

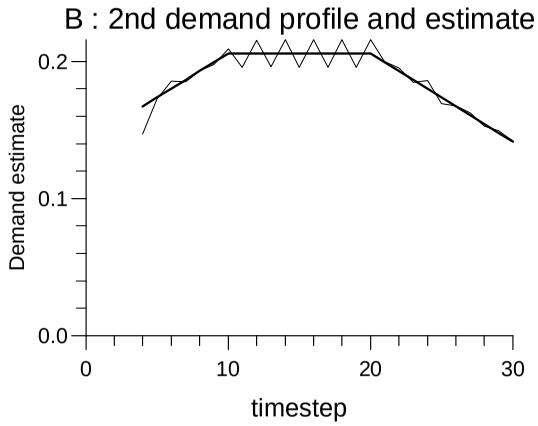

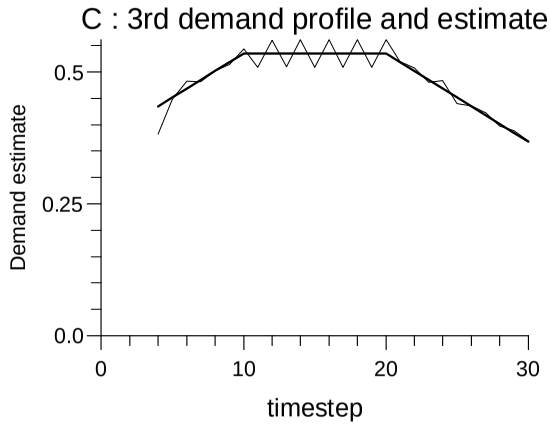

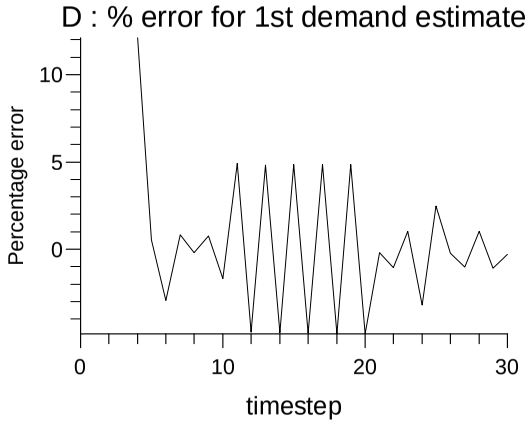

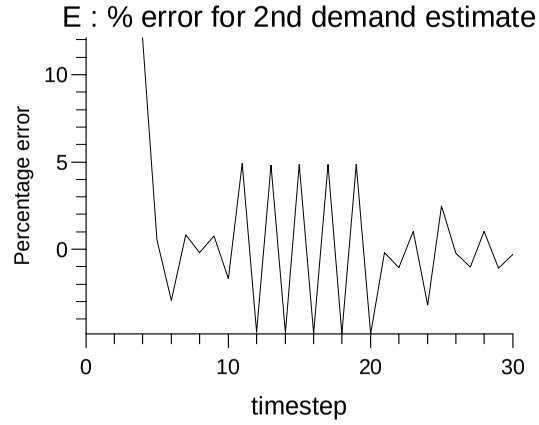

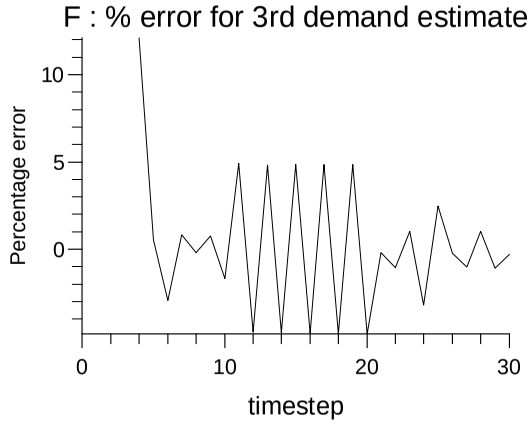

Experiment 10.17

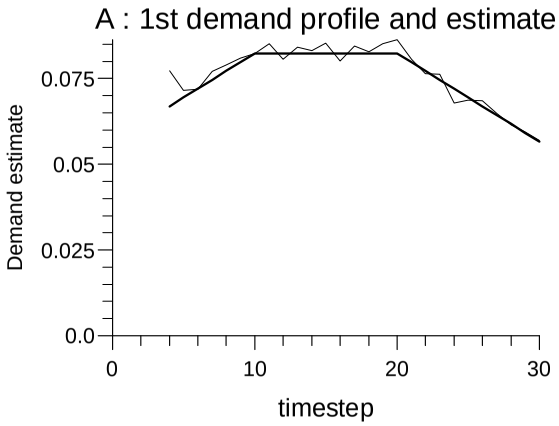

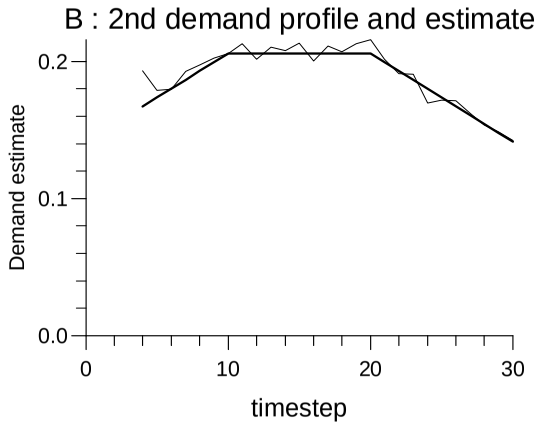

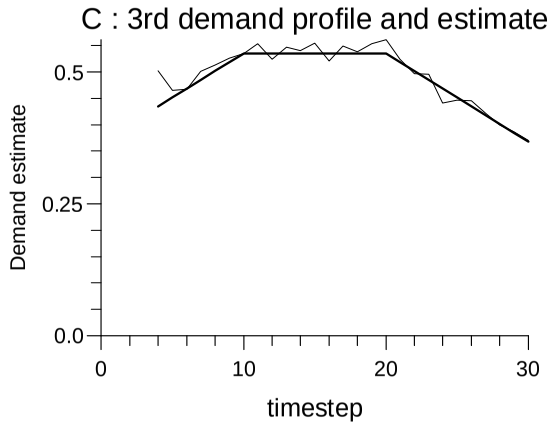

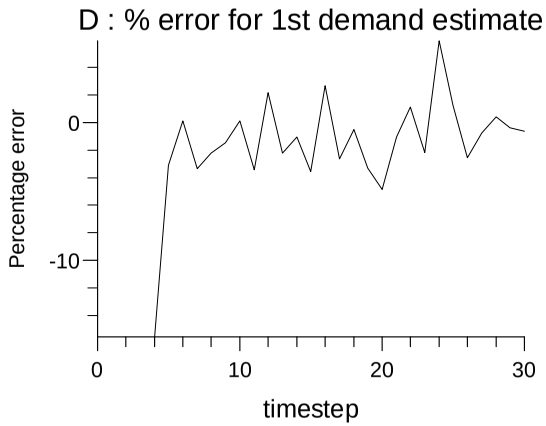

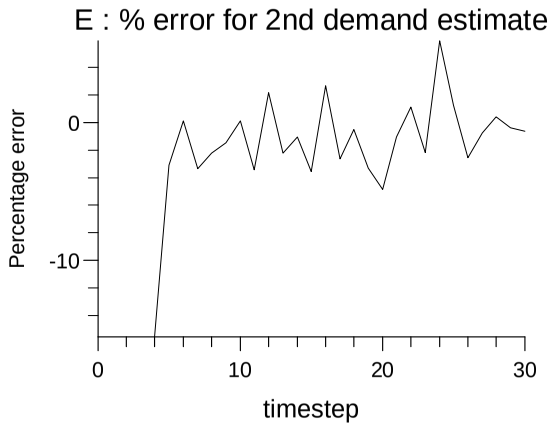

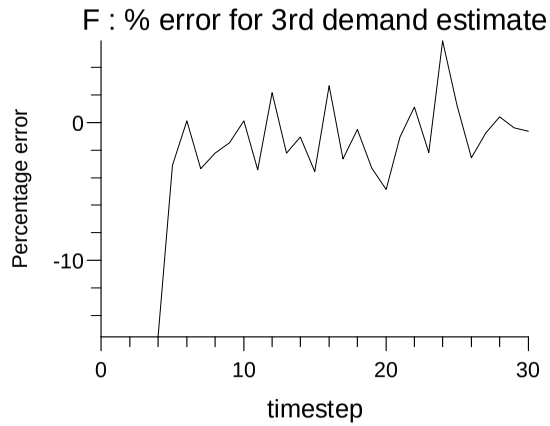

Experiment 10.18

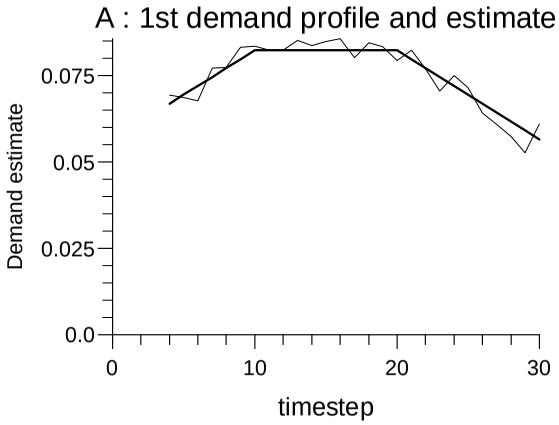

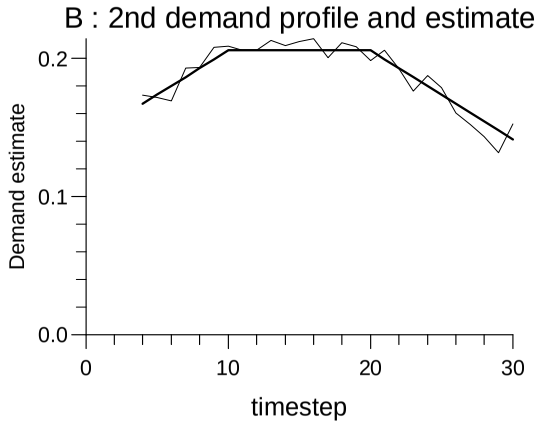

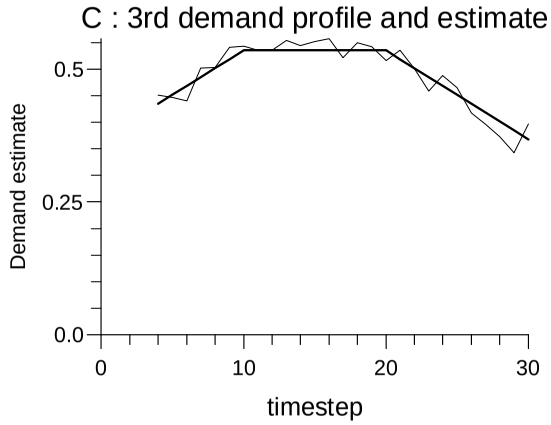

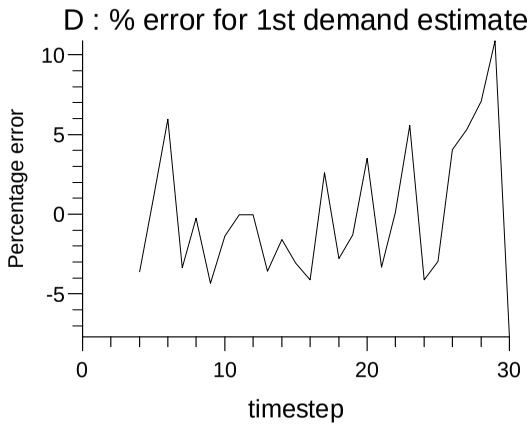

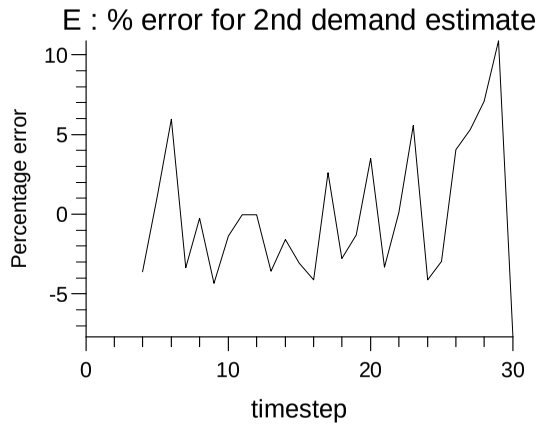

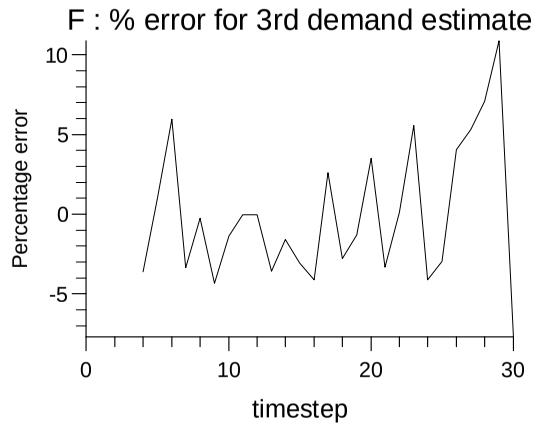

Experiment 10.19

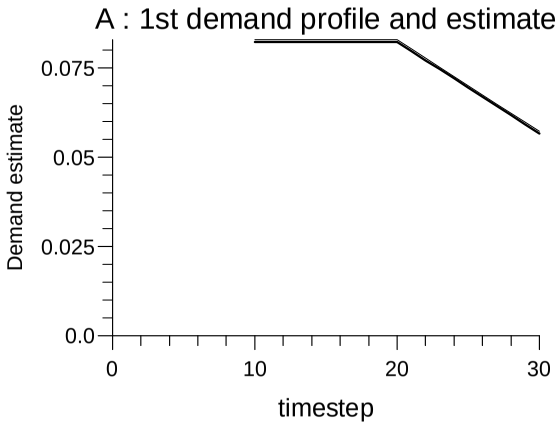

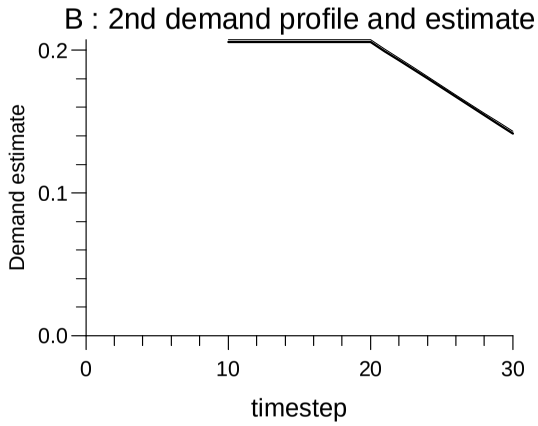

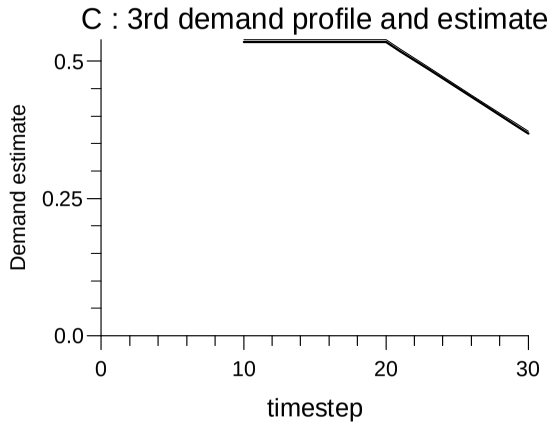

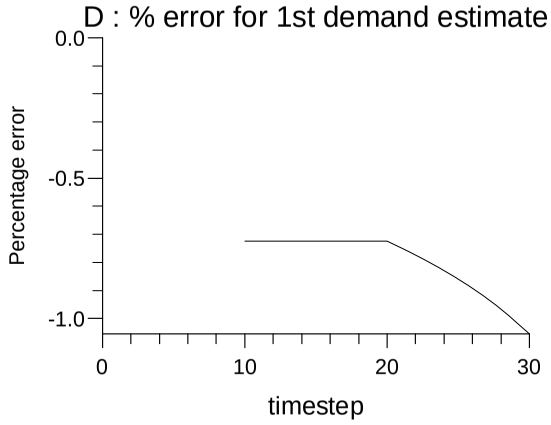

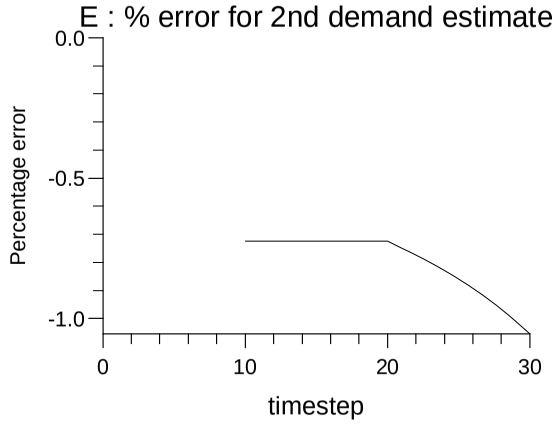

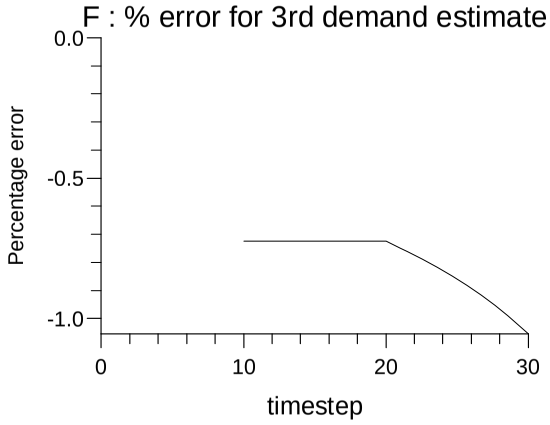

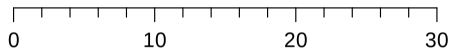
0
10
20
30

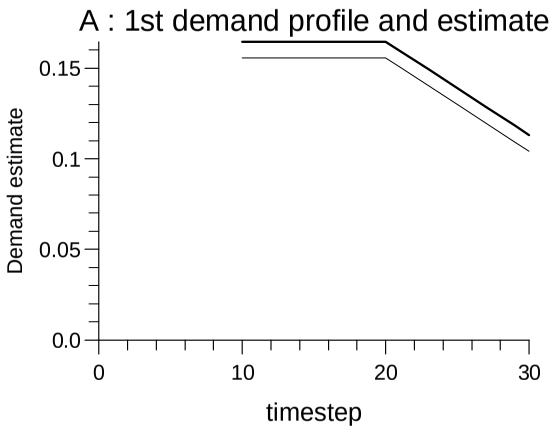
A : 1st demand profile and estimate
Demand estimate
0.15
0.1
0.05
0.0
0
10
20
30
timestep

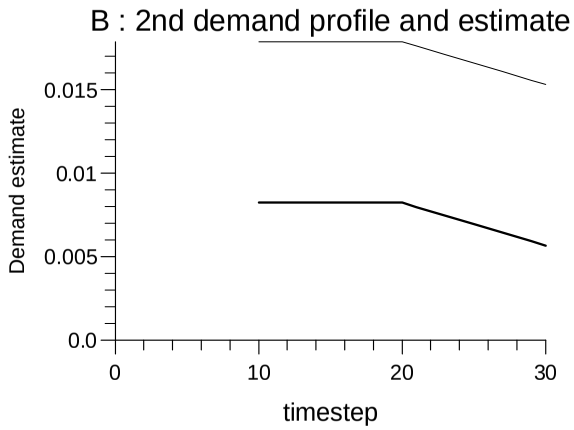
B : 2nd demand profile and estimate
Demand estimate
0.015
0.01
0.005
0.0
0
10
20
30
timestep

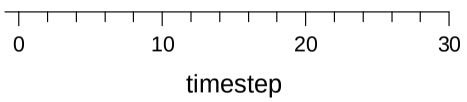
0
10
20
30
timestep

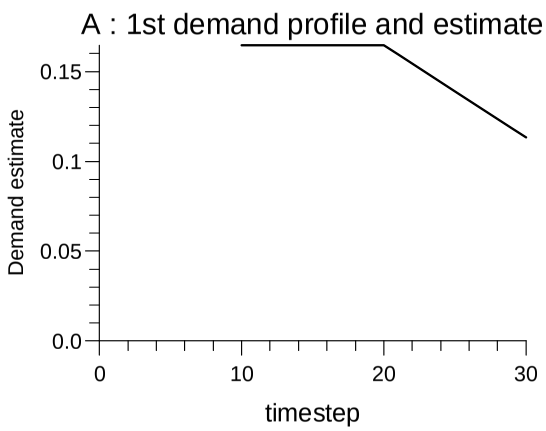
A : 1st demand profile and estimate
Demand estimate
0.15
0.1
0.05
0.0
0
10
20
30
timestep

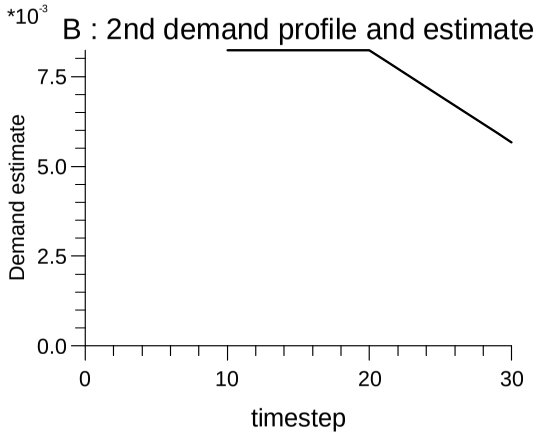
*10-3
B : 2nd demand profile and estimate
Demand estimate
7.5
5.0
2.5
0.0
0
10
20
30
timestep

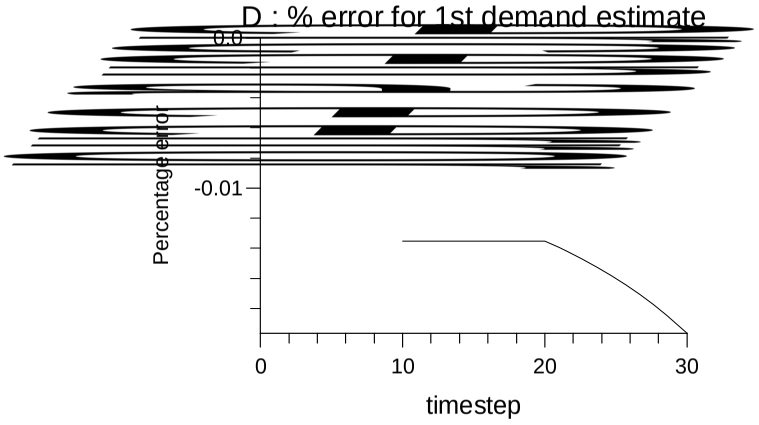
D : % error for 1st demand estimate
Percentage error
0.0
-0.01
0
10
20
30
timestep

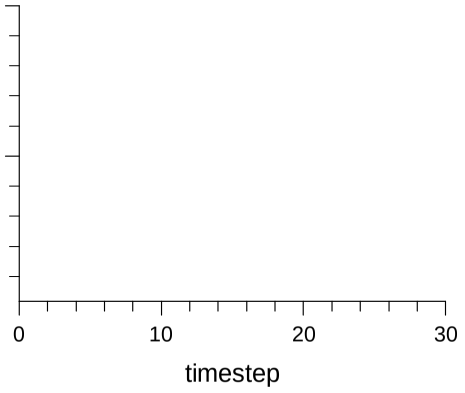
0
10
20
30
timestep

10.4.3 Discussion

When pressure data was taken from an $\mathcal{M}$

scalar equations of the form (9.4). If we add these g equations together we can derive

$$d_{k+1}^{tot} = \sum_{demand\ site=1}^{g} w_k^{demand\ site} d_k^{demand\ site} + \sum_{demand\ site=1}^{g} (w_k^{demand\ site} - 1)\mathcal{Q}^{demand\ site} \tag{10.25}$$

where $d_k^{tot} = \sum_{demand\ site=1}^{g} d_k^{demand\ site}$ for all k, as before. We can now use equation (10.5) to substitute for each term, $d_k^{demand\ site}$, on the right hand side of equation (10.25) to give

$$d_{k+1}^{tot} = \sum_{demand\ site=1}^{g} w_k^{demand\ site} (\alpha_k^{demand\ site} d_k^{tot} + \alpha_k^{demand\ site} \mathcal{Q}^{tot} - \mathcal{Q}^{demand\ site})$$

$$+ \sum_{demand\ site=1}^{g} (w_k^{demand\ site} - 1)\mathcal{Q}^{demand\ site} \tag{10.26}$$

and rearranging gives

$$d_{k+1}^{tot} = c_k d_k^{tot} + (c_k - 1)\mathcal{Q}^{tot} \tag{10.27}$$

where $c_k = \sum_{demand\ site=1}^{g} w_k^{demand\ site} \alpha_k^{demand\ site}$. The $\mathcal{M}6$ models now contain the single state flow variable, d_k^{tot}, with a difference equation of the form (10.27) where the term $(c_k - 1)\mathcal{Q}^{tot}$ is contained in a vector on the right hand side of the system as shown later.

To form an $\mathcal{M}6$ model, we start from a base $\mathcal{M}0$ model and initially proceed in a similar way to the formation of an $\mathcal{M}5$ model. All the basic difference equations of the form (2.17) remain unchanged in an $\mathcal{M}6$ model. However, the $g-1$ connectivity equations and the single downstream flow boundary equation are altered by the following. The g flow demand perturbation variables are removed from the input vector, summed into a single total flow demand perturbation variable, and then incorporated into the new $\mathcal{M}6$ state vector. The new trivial difference equation (10.27) is then added to form the $\mathcal{M}6$ system.

However, with $\mathcal{M}6$ models we now assume, as we have assumed with $\mathcal{M}4$ models, that the pressure measurements at the sites of flow demand are now subject to a constant bias described by equation (9.1)

$$\underline{y}(k) = \underline{p}_2(k) + \underline{b}(k).$$

The g measurement biases are assumed to obey equation (9.2)

$$\underline{b}(k+1) = \underline{b}(k).$$

The last step in the construction of an $\mathcal{M}$

Proof

By inspection, at any particular timestep k, the eigenvalues of an $\mathcal{M}6$ system consist of the n eigenvalues of the base $\mathcal{M}0$ system, 1 eigenvalue equal to c_k, and g eigenvalues equal to 1. Hence, the eigenvalues of the $\mathcal{M}6$ system are real.

We have the Hautus condition for the $\mathcal{M}6$ system if and only if for all $\mu \in \mathbf{R}$

$$(A_6(k) - \mu E_6(k+1))\underline{v} = \underline{0} \tag{10.31}$$

$$C_6\underline{v} = \underline{0} \tag{10.32}$$

$$\Longleftrightarrow$$

$$\underline{v} = \underline{0} \tag{10.33}$$

where $\underline{v} \in \mathbf{R}^{n+1+g}$.

Equation (10.33) $\Longrightarrow$ equations (10.31), (10.32) trivially.

Equations (10.31), (10.32) and (10.33) can be expressed in the following way. We have the Hautus condition for the $\mathcal{M}6$ system if and only if for all $\mu \in \mathbf{R}$

$$(A_0 - \mu E_0)\underline{v}_n + (\underline{a}(k) - \mu \underline{e}(k+1))\underline{v}_1 = \underline{0} \tag{10.34}$$

$$(c_k - \mu)\underline{v}_1 = \underline{0} \tag{10.35}$$

$$(1 - \mu)\underline{v}_g = \underline{0} \tag{10.36}$$

$$C_0\underline{v}_n + \underline{v}_g = \underline{0} \tag{10.37}$$

$$\Longleftrightarrow$$

$$\underline{v}_n = \underline{0}\ ,\ \underline{v}_1 = \underline{0}\ ,\ \underline{v}_g = \underline{0} \tag{10.38}$$

where $\underline{v} = [\underline{v}_n^T, \underline{v}_1^T, \underline{v}_g^T]^T$, and $\underline{v}_n \in \mathbf{R}^n$, $\underline{v}_1 \in \mathbf{R}^1$, v

If we assume the $\mathcal{M}0$ model is partitioned according to equation (3.1), then equation (10.42) may be written as

$$\begin{bmatrix} (\mathcal{A}_{1,1} - c_k\mathcal{E}_{1,1}) & (\mathcal{A}_{1,2} - c_k\mathcal{E}_{1,2}) & \underline{0} \\ (\mathcal{A}_{2,1} - c_k\mathcal{E}_{2,1}) & (\mathcal{A}_{2,2} - c_k\mathcal{E}_{2,2}) & \underline{\tilde{h}}(k) \end{bmatrix} \begin{bmatrix} \underline{v}_{n-g} \\ \underline{\tilde{v}}_g \\ \underline{v}_1 \end{bmatrix} = \underline{0} \tag{10.43}$$

where the vector $\underline{\tilde{h}}(k) \in \mathbf{R}^g$ now contains the g elements of $(\underline{a}(k) - c_k\underline{e}(k+1))$ that correspond to coefficients from the flow equations. Also, $\underline{v}_n = [\underline{v}_{n-g}^T, \underline{\tilde{v}}_g^T]^T$ where $\underline{v}_{n-g} \in \mathbf{R}^{n-g}$ and $\underline{\tilde{v}}_g \in \mathbf{R}^g$.

Equation (10.39) zeros the g elements of $\underline{v}_n$ corresponding to the measured pressures at the sites of flow demand. Hence $\underline{\tilde{v}}_g = \underline{0}$.

Removing $\underline{\tilde{v}}_g$ from system (10.43) gives

$$\begin{bmatrix} (\mathcal{A}_{1,1} - c_k\mathcal{E}_{1,1}) & \underline{0} \\ (\mathcal{A}_{2,1} - c_k\mathcal{E}_{2,1}) & \underline{\tilde{h}}(k) \end{bmatrix} \begin{bmatrix} \underline{v}_{n-g} \\ \underline{v}_1 \end{bmatrix} = \underline{0}. \tag{10.44}$$

If c_k is not an eigenvalue of the corresponding $\mathcal{M}1$ system, then $(\mathcal{A}_{1,1} - c_k\mathcal{E}_{1,1})$ is full rank. Hence equation (10.44) implies $\underline{v}_{n-g} = \underline{0}$.

The vector $(\underline{a}(k) - c_k\underline{e}(k+1))$ contains $g-1$ elements of the form $-\Phi^{z/z+1}(1-\theta)\alpha$

From the above theorem, we expect the Hautus condition to hold for the $\mathcal{M}6$ model almost always. However, in an equivalent way to $\mathcal{M}4$ models, it is interesting to note that θ may be chosen to exert some control over the discrete values of the coefficients, c_k, for which the theorem does not guarantee the Hautus condition to hold for the $\mathcal{M}6$ system.

10.5.2 Experiments

As the $\mathcal{M}0$ model was run, the pressures at the upstream end and the sites of flow demand were recorded at each timestep. For experiments 10.23 to 10.25, there was no pressure measurement noise added. However, for experiments 10.26 to 10.31, the pressure measurements at the three flow demand sites, A/B, B/C and C, were corrupted by white noise with a Gaussian distribution with mressfiGaussiΩΩTffldelerimenTflDfltttheo.tiamΩΩTflΩΩ

estimates of $D_k^{A/B}$, $D_k^{B/C}$ and D_k^C and their true values are shown in Figs. D, E and F respectively.

The following three experiments do not have measurement noise added.

Data taken from $\mathcal{M}0$ model with identical mesh

Experiment 10.23) ($\mathcal{M}6$ model) Observer Design B with $\theta = 1$

Experiment 10.24) ($\mathcal{M}6$ model) Observer Design B with $\theta = 0.5$

Data taken from $\mathcal{M}0$ model with much finer mesh

Experiment 10.25) ($\mathcal{M}6$ model) Observer Design B with $\theta = 1$

The following two experiments do have measurement noise added.

Data taken from $\mathcal{M}0$ model with identical mesh

Experiment 10.26) ($\mathcal{M}6$ model) Observer Design B with $\theta = 1$

Data taken from $\mathcal{M}0$ model with much finer mesh

Experiment 10.27) ($\mathcal{M}6$ model) Observer Design B with $\theta = 1$

The following four experiments do have measurement noise added, but the $\mathcal{M}4$ flow integration smoothing technique is then applied.

Data taken from $\mathcal{M}0$ model with identical mesh

Experiment 10.28) ($\mathcal{M}6$ model) Observer Design B with $\theta = 1$

Data taken from $\mathcal{M}0$ model with much finer mesh

Experiment 10.29) ($\mathcal{M}6$ model) Observer Design B with $\theta = 1$

Experiment 10.30) ($\mathcal{M}4$ model) Observer Design B with $\theta = 1$ *(New flow ratio 20:1:79)*

Experiment 10.31) ($\mathcal{M}6$ model) Observer Design B with $\theta = 1$ *(New flow ratio 20:1:79)*

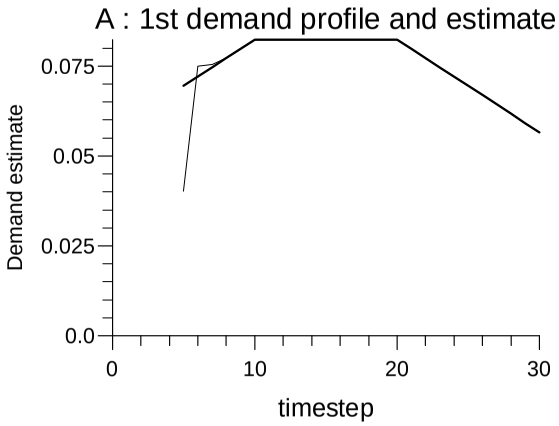
A : 1st demand profile and estimate
Demand estimate
0.075
0.05
0.025
0.0
0
10
20
30
timestep

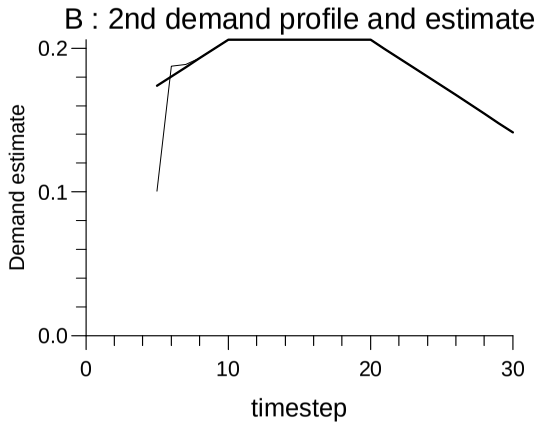
B : 2nd demand profile and estimate
Demand estimate
0.2
0.1
0.0
0
10
20
30
timestep

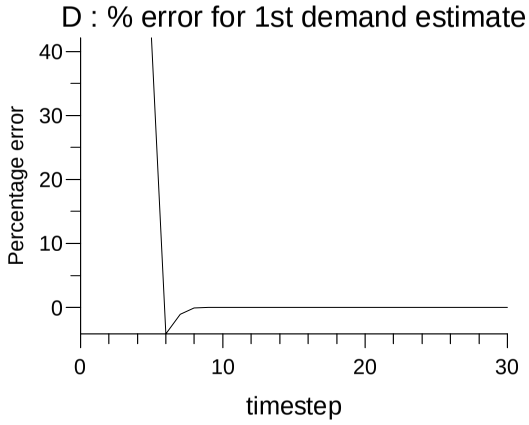
D : % error for 1st demand estimate
Percentage error
40
30
20
10
0
0
10
20
30
timestep

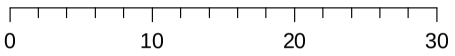
0
10
20
30

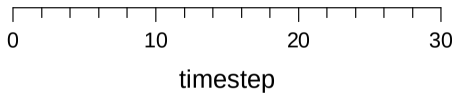
0
10
20
30
timestep

Experiment 10.25

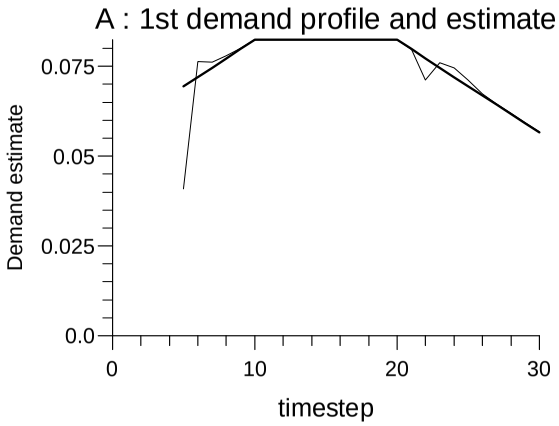

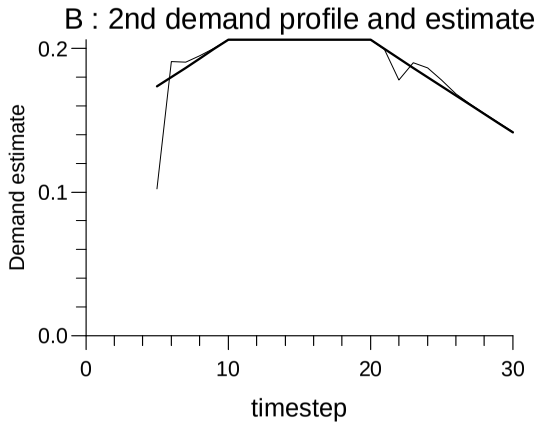

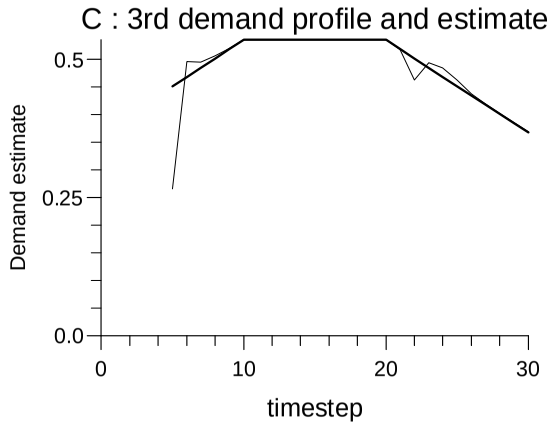

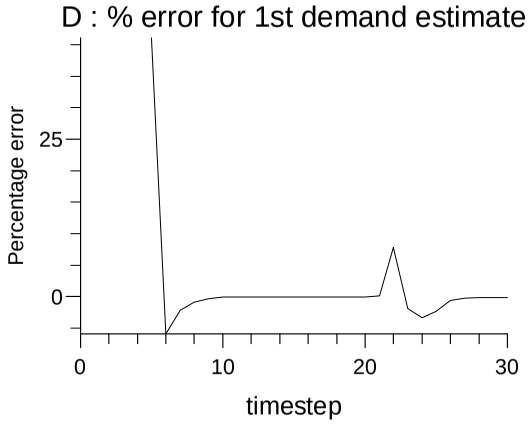

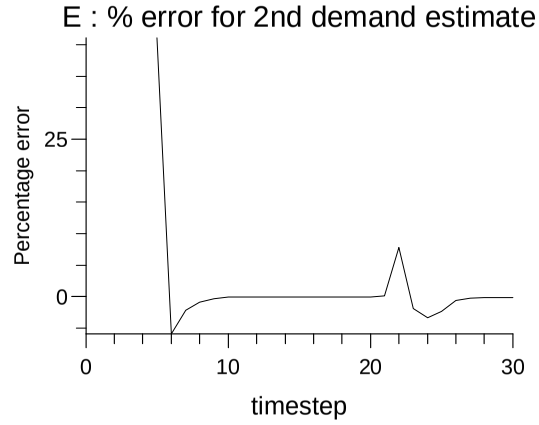

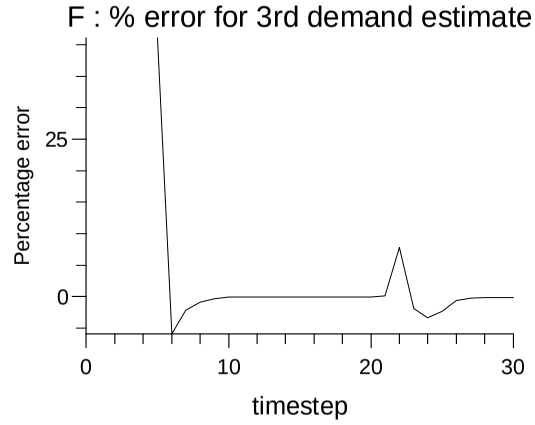

Experiment 10.26

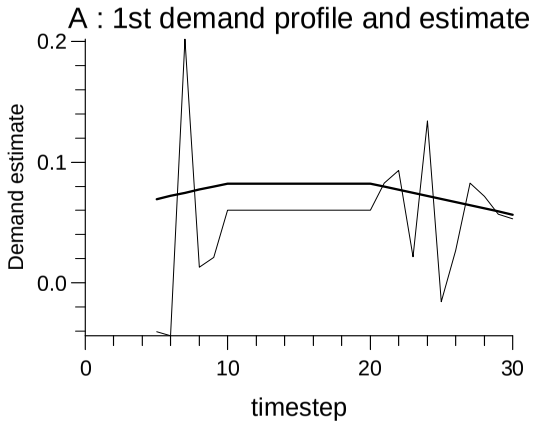

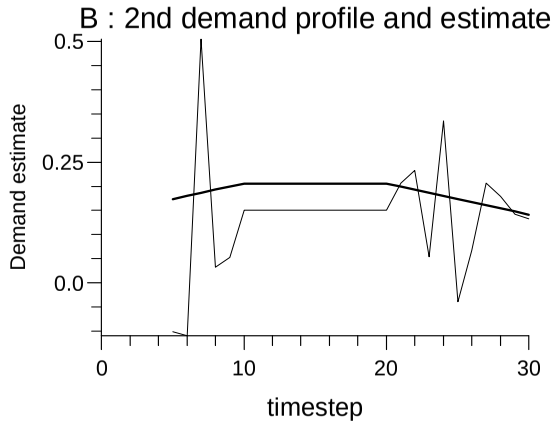

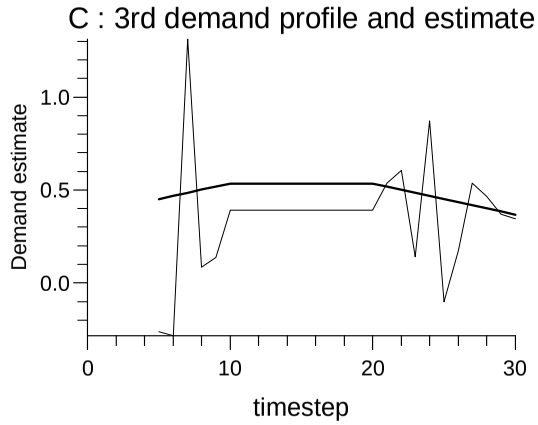

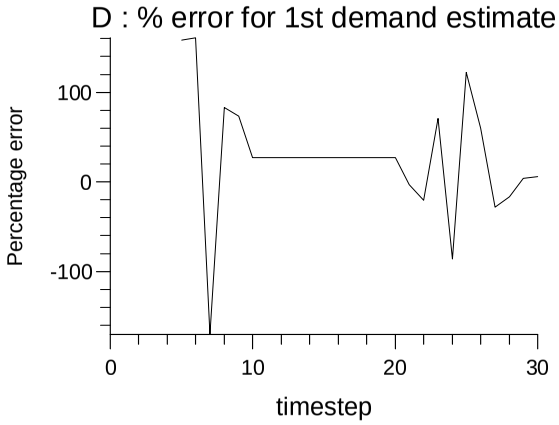

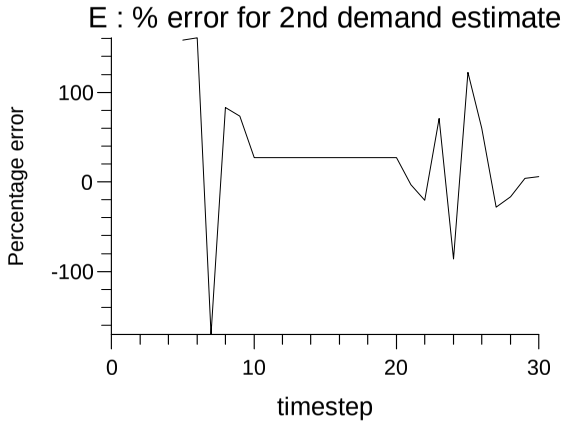

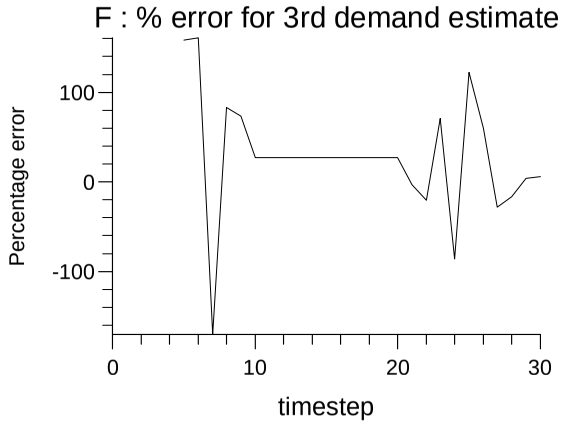

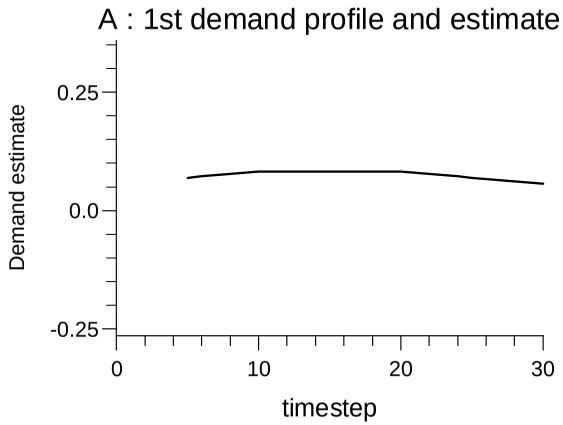
A : 1st demand profile and estimate
Demand estimate
0.25
0.0
-0.25
0
10
20
30
timestep

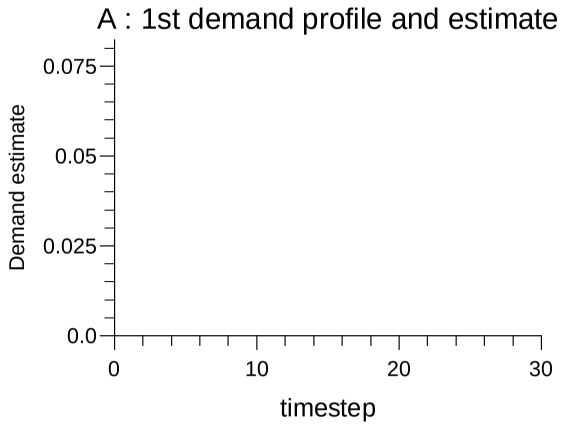
A : 1st demand profile and estimate
Demand estimate
0.075
0.05
0.025
0.0
0
10
20
30
timestep

Experiment 10.30

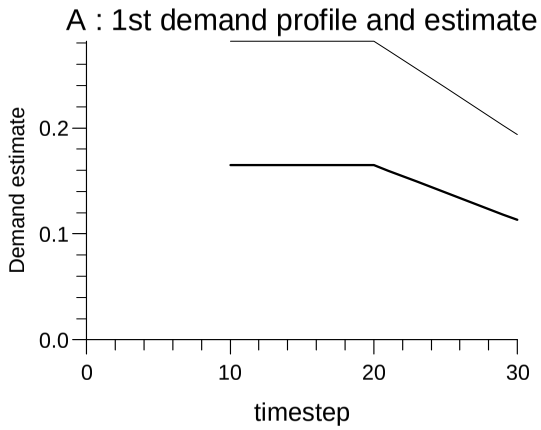

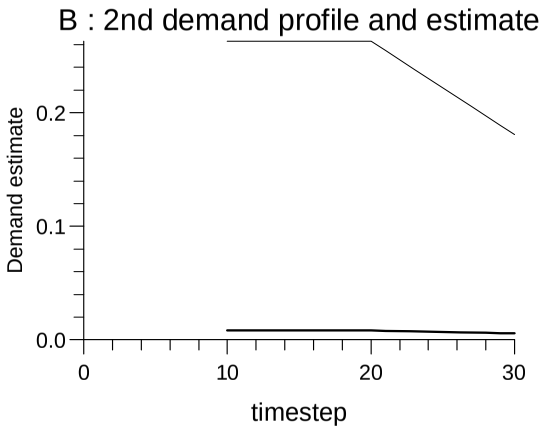

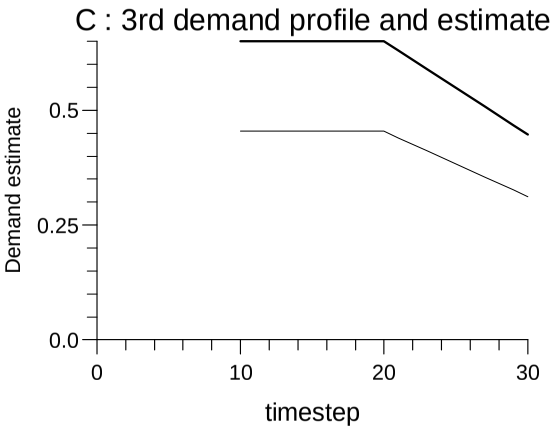

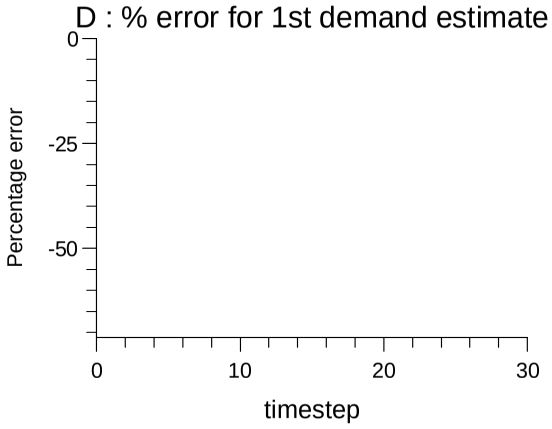

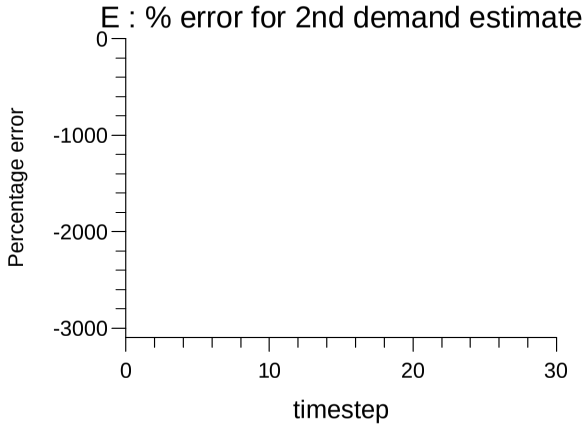

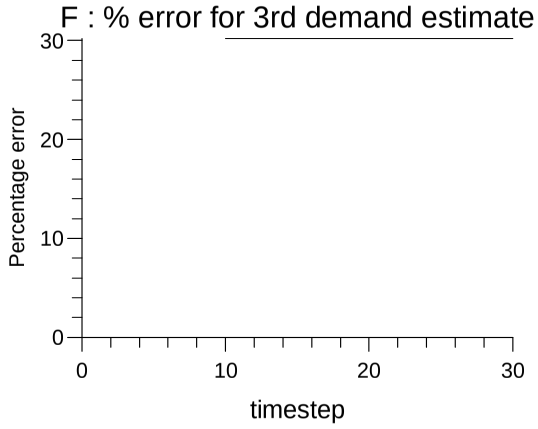

10.5.3 Discussion

The performance of $\mathcal{M}6$ model based dynamic observers showed the same dependency on θ as dynamic observers based upon previous flow estimation models. The dynamic observer based on an $\mathcal{M}6$ model converged perfectly for $\theta = 1$ when the $\mathcal{M}0$ model used to generate the pressure data was constructed on an identical mesh. However, as θ moved close to $1/2$, the observer completely failed to converge. Similarly to dynamic observers based upon previous flow estimation models, the assigned observer eigenvalues became more sensitive as θ moved from 1 to $1/2$, and a theoretical study of whether the Hautus condition is near to failing for $\theta = 1/2$ would be useful. As with $\mathcal{M}4$ systems, $\mathcal{M}6$ systems have time-varying system matrices. As with $\mathcal{M}4$ systems, the theoretical analysis of firstly, the observability of $\mathcal{M}6$ systems, and secondly, the convergence of dynamic observers constructed upon $\mathcal{M}6$ systems, would be worthwhile future research.

When data was taken from an $\mathcal{M}0$ model with a much finer discretisation, the $\mathcal{M}6$ model based dynamic observer did not perform so well. The same super-sensitivity that existed with $\mathcal{M}4$ systems exists for $\mathcal{M}6$ systems. As was suggested for $\mathcal{M}4$ systems, perhaps some further investigation into modelling strategies and different observer designs may help to remedy this. For example, perhaps an observer that switched between the different models, $\mathcal{M}5$ and $\mathcal{M}6$, at certain times of day could be designed to estimate the biases, where the $\mathcal{M}6$ model based observer would run over certain 'favourable' timesteps only. Then these estimates of the biases may be kept while an $\mathcal{M}5$ model based observer is run over periods where an $\mathcal{M}6$ model based observer would fail.

When pressure measurement noise was added, but no smoothing technique applied, it could be seen that the estimates of the first two small demands contained less error than with the previous $\mathcal{M}4$ model based dynamic observer designs. When the $\mathcal{M}4$ flow integration smoothing technique was also applied, the estimates of the flow demands improved further. However, the last two experiments, 10.30 and 10.31, clearly demonstrate the considerable benefit of using $\mathcal{M}6$ models to estimate very small flow demands. Unfortunately, the error due to measurement noise and modelling error is still unacceptably large.

Although we do not yet have a viable technique for estimating flow demands from

pressure telemetry in the presence of *both* measurement bias and noise, some proposals for future research are presented in the next chapter.

Ch pter 11

Fin l Conclusions nd ropos ls for Future Work

The fundamental problem in estimating flow demands from pressure telemetry is the sensitivity of the flow demands, especially small flow demands, to modelling and measurement error. When the pressure measurements fed into 1/ 2 models and observers constructed upon 3/ 4 models, were corrupted by noise, the flow demand estimates were swamped by the resulting error. The 5/ 6 modelling approach of summing all the flow demand variables into a single total flow variable seemed to reduce greatly the sensitivity. The flow integration smoothing techniques were also particularly effectided theHIw[9V

[12], [9], [8], [10]. Some references [17], [40], [35], have suggested little gain from the extra computational expense involved with Kalman filters. However, in these experiments, the Kalman filter was compared with an observer design with a built in filter. The filtering technique used in this comparison observer relied on the availability of both flow demand and pressure measurements at the sites of gas inflow/outflow. Hence, such a filtering technique cannot be used for our purpose, where flow measurement is not available.

Various theoretical questions raised in the thesis should also be explored. Can the solutions to the numerical models be shown to converge to the solutions to the governing differential equations as the compuational mesh is refined? What are the conditions necessary to guarantee the observability of the time-varying models? When do dynamic observers based upon time-varying models converge?

In conclusion, we have investigated a series of models and made some progress in tackling the practical problems of flow demand estimation from pressure telemetry. However, more research is required, perhaps involving Kalman filters, to find a technique that gives acceptably accurate flow estimates from pressure data from a *real* gas network.

Bibliography

[1] Anderson, B.D.O. and Moore, J.B., . Prentice Hall, 1990.

[2] Barnett, S. and Cameron, R.G. (2nd dition). Clarendon Press, Oxford, 1985.

[3] Benkherouf, A. and Allidina, A.Y., Leak Detection and Location in Gas Pipelines, , vol.135, Pt.D, No.2, March 1988.

[4] Bunse-Gerstner, A., Mehrmann, V. and Nichols, N.K., Regularisation of descriptor systems by derivative and proportional state feedback, , , 1992, 46-67.

[5] Burden, R.L. and Faires, J.D., , PWS-Kent, 1989.

[6] Campbell, S.L. and Terrell, W.J., Observability of linear time-varying de-

[11] Clarke, G.M. and Cooke, D., , dward Arnold, 1983.

[12] Davis, M.H.A. and Vinter, R.B., , Chapman and Hall, 1985.

[13] Fletcher, L. R., Kautsky, J. and Nichols, N.K. igenstructure assignment in descriptor systems, , , 1986, 1138-1141.

[14] Fraleigh, J.B. and Beauregard, R.A. . Addison Wesley, 1987.

[15] , edited by Arthur Gelb. M.I.T. Press, 1989.

[16] Gladwell, I. and Wait, R., , Oxford University Press, 1979.

[17] Goldfinch, M.C., , British Gas technical report LRS T 678. (1984)

[18] Goldwater, M.H., , British Gas technical report LRS T112. (1972)

[19] Goldwater, M.H. and Fincham, A. ., Modelling of Gas Supply Systems, . dited by H. Nicholson. Peter Peregrinus, 1981.

[20] Golub, G.H., and Van Loan, C.F., , Johns Hopkins University Press, 1983.

[21] Goodwin, N.H., , British Gas technical report LRS T511. (1982)

[22] Horn, R.A. and Johnson, C.R., ,CeA1In,Nt7644dgeg7p63J[vk-bp-3e6ypK3

[25] Kautsky, J., Nichols, N.K. and Chu, .K.W., Robust pole assignment in singular control systems, , , 1989, 9-37.

[26] Kuo, B.C., , Holt, Rinehart and Winston, 1981.

[27] Lipschutz, S., , McGraw-Hill, 1981.

[28] Mitchell, A.R. and Griffiths, D.F., , John Wiley and Sons, 1987.

[29] O'Reilly, J., . Academic Press, 1983.

[30] Osiadacz, A.J., , . and F.N. Spon, 1987.

[39] Stewart, G.W. Gerschgorin theory for the generalised eigenvalue problem $Ax = \lambda Bx$. *Math. Comp.*, 1975, **29**, 600-606.

[40] Whitley, A. and John, R.I., *The Use of Kalman Filtering to Estimate rid Conditions from Telemetry Data - Results of Tests on Simulated Data*, British Gas technical report LRS T 538. (1982)

[41] Wiberg, D.M., *State Space and Linear Systems*, McGraw-Hill, 1971.

[42] Yip, .L. and Sincovec, R.F. Solvability, controllability and observability of continuous descriptor systems. *IEEE Trans. Aut. Control*, 1981, **AC-26**, 702-707.